TIME-DEPENDENT DAMAGE EVOLUTION IN MULTIDIRECTIONAL POLYMER COMPOSITE LAMINATES

BY

ANAND BIRUR

A Thesis submitted to the Faculty of Graduate Studies of

The University of Manitoba

in partial fulfilment of the requirements of the degree of

MASTER OF SCIENCE

Department of Mechanical and Manufacturing Engineering

University of Manitoba

Winnipeg, Manitoba, Canada

ABSTRACT

Multi-directional polymer matrix composite materials are increasingly used in load-bearing structural applications ranging from primary aircraft structures and automotive parts to rehabilitation of bridges. Long-term durability, characterized by time-dependent degradation in strength (known as creep-rupture) and modulus (known as creep), is an important concern in these applications. Despite the experimental evidence on the influence of time-dependent damage on creep and creep rupture of multi-directional composites, current level of understanding of this is very limited. Hence, the focus of this thesis is to develop a clear understanding of the time dependent evolution of various damage modes and their influence on creep rupture of polymer matrix composite laminates. Hexcel Corporation's F263/T300 unidirectional composite prepreg was used in this study. Three laminates [0/90/0], $[\pm 45/90_2]_s$, and $[0/90_2]_s$ were subjected to a wide range of constant stresses at various test temperatures and creep rupture time was recorded. Additionally, the time for appearance of first damage in [90] layer (known as First Ply Failure which influences design) as well as the various damage modes and their time-dependent evolution until fracture were monitored. While the first two laminates were used to understand the effect of stacking sequence, the third laminate, $[0/90_2]_s$, was compared with the other two laminates to delineate the effect of outer-ply constraint ([90] versus [45]) and thickness of [90] layers on time-dependent progressive damage in the [90] ply. The various damage modes that developed, with stress during tensile testing, and with time during constant stress creep rupture testing were transverse cracking, vertical cracking, delamination, vertical splitting and fiber fracture. While

transverse cracking was the first damage mode in $[\pm 45/90_2]_s$, vertical cracking was the first damage mode in [0/90/0]. The appearance of these damages were time dependent confirming that the FPF stress is time-dependent, while the conventional wisdom is to consider it to be time-independent in design. Beyond FPF, the above single modes of damage continued to evolve for a certain period of time beyond which additional damage modes started to evolve influencing the evolution rate of one-another. The % of creep rupture time during which a single mode of damage was evolving decreased with increase in applied stress and test temperature. Based on these results it is concluded that creep rupture of multidirectional laminates is influenced by contributions from a complex interaction of various damage modes that evolve with time, suggesting that creep rupture predictions could be good approximations only.

Acknowledgement

I take this opportunity to express my sincere appreciation to **Prof. R. Jayaraman** for his guidance throughout the course of this work.

I would like to thank **M.A.Balachander** for training me on the instruments at the composite lab. I would also like to thank **John VanDorp** and **Mike Boskwick** for their assistance during the experimental trials.

Thanks to my lab mates for having made my stay at the U of M a memorable one. Special thanks to **Yang Zhang** and **Abhishek Gupta** for their valuable suggestions at various times throughout my association with the composite lab.

This work would not have been possible with the constant support and encouragement from my **wife** and **parents**. **A very special thanks to them**.

TABLE OF CONTENTS

LIST OF FIGURES

LIST OF TABLES

1. INTRODUCTION

The engineering fraternity has always had a focused goal to develop structures and materials that are lighter, stronger and tougher than those that already exist. The use of advanced structural composites has helped to achieve that goal. Composite materials are those that consist of two or more different materials that are combined to form a structural unit. Polymer composites have a unique combination of light weight, high specific strength, high specific stiffness, corrosion resistance and ease of manufacturing.

The use of advanced composite materials has expanded into a wide variety of areas. Products that have been fabricated from composites include military and commercial aircrafts, space vehicles, rocket motor cases, automobile components, turbine blades and a range of sporting goods. These applications have made composite materials attractive candidates for replacing structural materials like steel and aluminum.

The two basic constituents of advanced polymer matrix composite (PMC) are fiber and matrix. Based on the type, geometry and orientation of reinforcement phase (fiber), composites can be broadly classified into particulate, discontinuous and continuous fiber. A schematic of the classification of composite is shown in Figure 1.1 Continuous fiber composite can be further classified based on the orientation of the prepregs during the lay-up sequence.

- Unidirectional composites – fibers are parallel to each other
- Multidirectional composites – fiber orientation varies from layer to layer
- Textile composites – fibers are woven like cloth

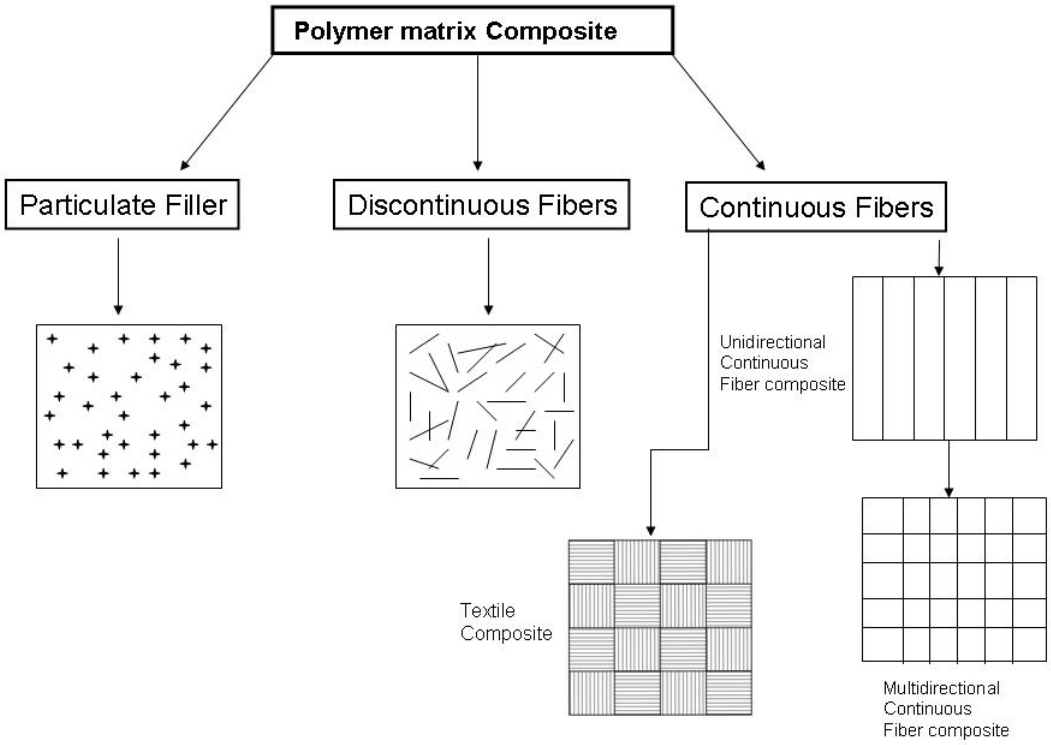

Figure 1.1: Classification of the polymer matrix composite system

Polymer matrices in PMC structures can display the properties of both elastic solids and viscous fluids, depending on the temperature or test time scale. The fibers in a PMC are essentially elastic in nature, while the epoxy matrix shows significant viscoelastic response. Since changes in composites stiffness, strength and fatigue life can all be related to changes in mechanical properties of polymer matrix, it is reasonable to consider the laminate also to be a viscoelastic material. Owing to the viscoelastic nature PMC exhibits time dependent degradation in modulus and strength while in service, under load. The time dependent degradation in modulus is known as creep, while time dependent degradation in strength is known as creep rupture. This time dependent degradation is one of the major limitations when PMC's are being considered for potential applications.

Unidirectional composites shown in Figure 1.2 are not preferred since the properties are anisotropic. Composites used in structural applications are multidirectional as shown in Figure 1.3. In order to obtain quasi-isotropic properties the fibers are oriented at various angles. Depending on the lay-up design, the fiber orientation in a multidirectional composite varies from layer to layer. To characterize each laminate for time dependent strength and modulus is not practical, hence researchers have used data from unidirectional composites with appropriate models to predict creep and creep rupture properties in multidirectional composites.

In one of the earliest studies on creep and creep rupture of multidirectional PMCs, Dillard [1] found extensive damage in creep ruptured composite specimens. An attempt was made to predict the creep rupture time and compare it with the experimental results.

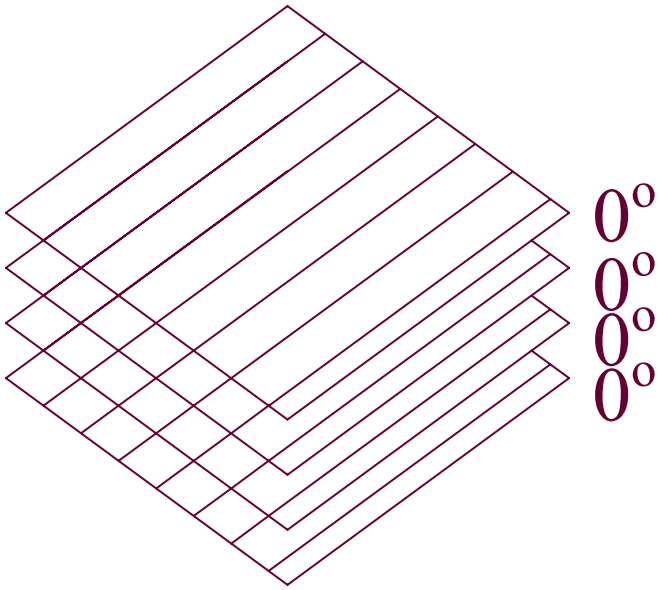

Figure1.2: Schematic illustration of unidirectional laminate

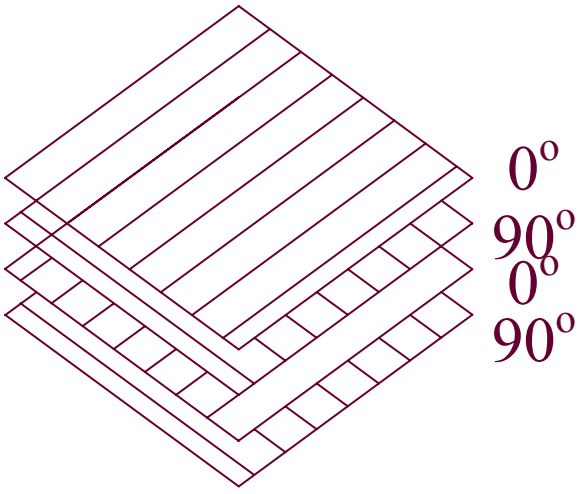

Figure 1.3: Schematic illustration of multidirectional laminate

The outcome of this exercise proved futile and the reason identified at that point was the influence of time dependent damage that was not considered in the modeling. Despite the significance of the results, which pointed towards a need for more research on the issue of time dependent damage, very little attention has been devoted to the study of damage during creep and creep rupture of multidirectional polymer composite and its influence on creep and creep rupture. As indicated before, test temperature and stress levels higher than service temperature are normally used to accelerate creep and creep rupture and obtain data on them beyond experimental time window. Since the evolution of damages is likely to be accelerated too, understanding this evolution and the impact of damage on accelerated testing procedure is very crucial and are lacking currently.

To bridge this knowledge gap, the present research was pursued The work involved the experimental study of evolution of various damage modes with time in a multidirectional composite (Hexcel Corporation's F263 reinforced with continuous carbon fiber T300) subjected to constant load. Creep rupture data obtained during the course of the tests were correlated with the various damage modes observed. Influence of various parameters such as stress, temperature, thickness of inner ply and outer ply constraint on damage evolution was evaluated.

ORGANIZATION OF THESIS

Chapter 2 will be a brief overview of the composites, creep and creep rupture of uni-directional composites. This will be followed by a discussion on the creep and creep rupture of multi-directional composites. Work done on time dependent damage will be

another aspect of chapter 2. Chapter 3 will comprise of the experimental work and the materials used. Presentation of the results and the discussion associated with it will be covered in chapter 4. Chapter 5 will have conclusions on the research.

2. LITERATURE REVIEW

2.1 INTRODUCTION

Load bearing engineering structures are designed to last many years. While using a PMC in theses structures its creep and creep rupture behavior is an important consideration. This thesis is focused on creep rupture of a specific class of polymer matrix composite (PMC), multi-directional composite. This chapter is thus dedicated to a thorough review of the published literature pertinent to this topic. The first section deals with the background information on creep and creep rupture as well as the factors that influence them. An overview of the creep and creep rupture in unidirectional composite is presented next. Section 2.3 deals with the creep and creep rupture of multidirectional composites. Damage (time independent and time dependent) is reviewed in the next section. Shortcomings of the present work available in the literature are summarized in section 2.5, which sets the context for the objectives of this thesis.

2.2 BACKGROUND

In today's world there is a need for high strength, light weight materials for a wide range of applications such as aerospace, automotive, civil infrastructure, sporting goods, etc. As a result, fiber reinforced composites such as graphite/epoxy systems, is currently used due to their superior mechanical properties and light weight. Composite is a material system consisting of two or more phases whose mechanical performance and properties are designed to be superior to those of the constituent material acting

independently. One of the phases is usually stiffer and stronger called the reinforcement. The less stiff and weaker phase is called matrix. In a high performance composite (like the one used in this study), the continuous fiber reinforcement is the backbone of the material that determines its stiffness and strength in the direction of fiber. The matrix phase provides protection and support to the fibers and local stress transfer from one fiber to another. The interphase can play a significant role in controlling the failure mechanisms and the mechanical behavior of the material.

Since the fibers are much stiffer than the matrix, the fiber properties tend to control the response of a lamina in the fiber direction, thus the compliance in the fiber direction is said to be fiber dominated. On the other hand, the compliances in the shear and transverse to the fiber direction are referred to as matrix dominated properties because they are closely tied to matrix response. The basis of the superior performance of composites lie in the high specific strength (strength to density ratio) and high specific stiffness (modulus to density ratio). These two properties are controlled by the fibers.

The coordinate system convention used for the fiber reinforced lamina is illustrated in Figure 2.1, with X-Y-Z corresponding to global laminate coordinate reference system and 1-2-3 corresponding to principal coordinate system for a ply. θ is the angle of orientation of the fibers in a ply with respect to loading axis, which is coincidental with the global X-axis.

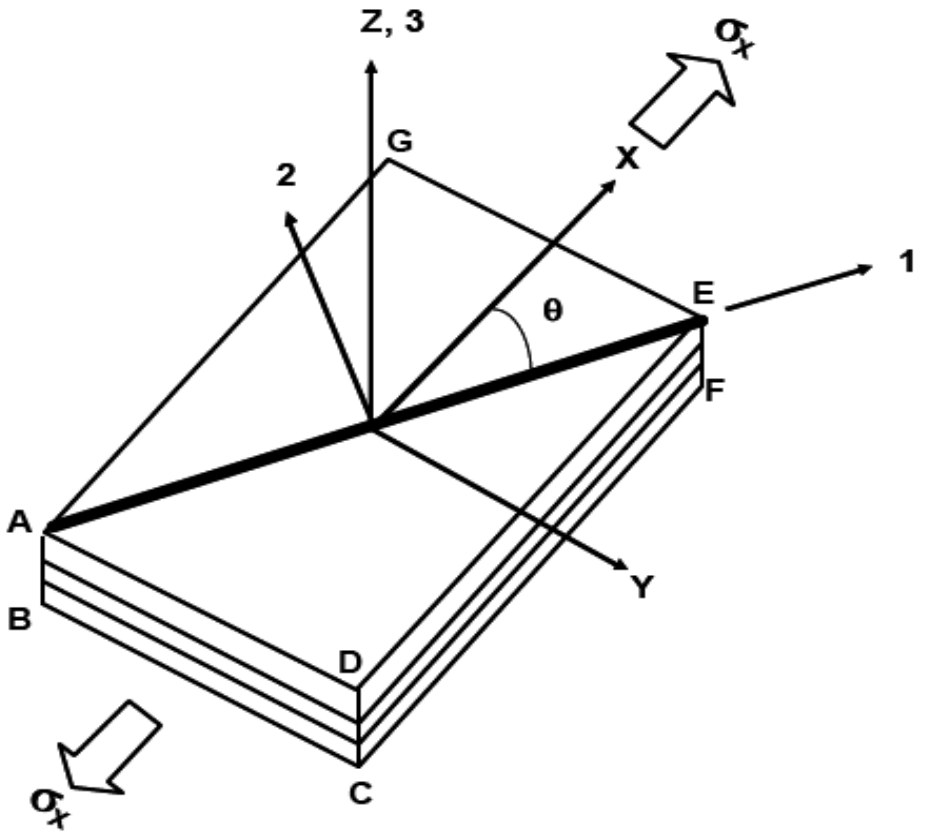

Figure 2.1: Schematic illustration of global and principal coordinate system

The configuration of the laminate indicating its ply orientation is called lay-up, while the exact location or sequence of the various plies is denoted by the stacking sequence.

Following are some examples of laminate designations:

Unidirectional 4 ply: $[0/0/0/0] = [0]_6$

Cross-ply: $[0/90/90/0] = [0/90]_s$

Angle-ply: $[+45/-45/-45/+45] = [\pm 45]_s$

Multi-directional: $[0/+45/-45/-45/+45/0] = [0/\pm 45]_s$

Subscript 's' corresponds to symmetric laminate in which the orientation of the plies forms a mirror image about the laminate mid-plane.

In order to thoroughly utilize polymer matrix composites for structural applications every aspect of their behavior in a service environment must be understood. One such aspect is the creep and creep rupture.

2.2.1 Creep

Creep is defined as the time dependent deformation of the material. A schematic of the creep curve is shown in Figure 2.2. The polymer in a PMC exhibits a viscoelastic response, while the fibers are elastic. Creep is characterized by applying a constant tensile load to a tensile specimen and measuring the strain obtained as a function of time.

2.2.2 Creep Rupture

Time dependent failure of a specimen under constant load is known as creep rupture. The creep rupture data is obtained by applying a constant load to the specimen and recording the time to failure. The time at which the fracture occurs is termed as creep

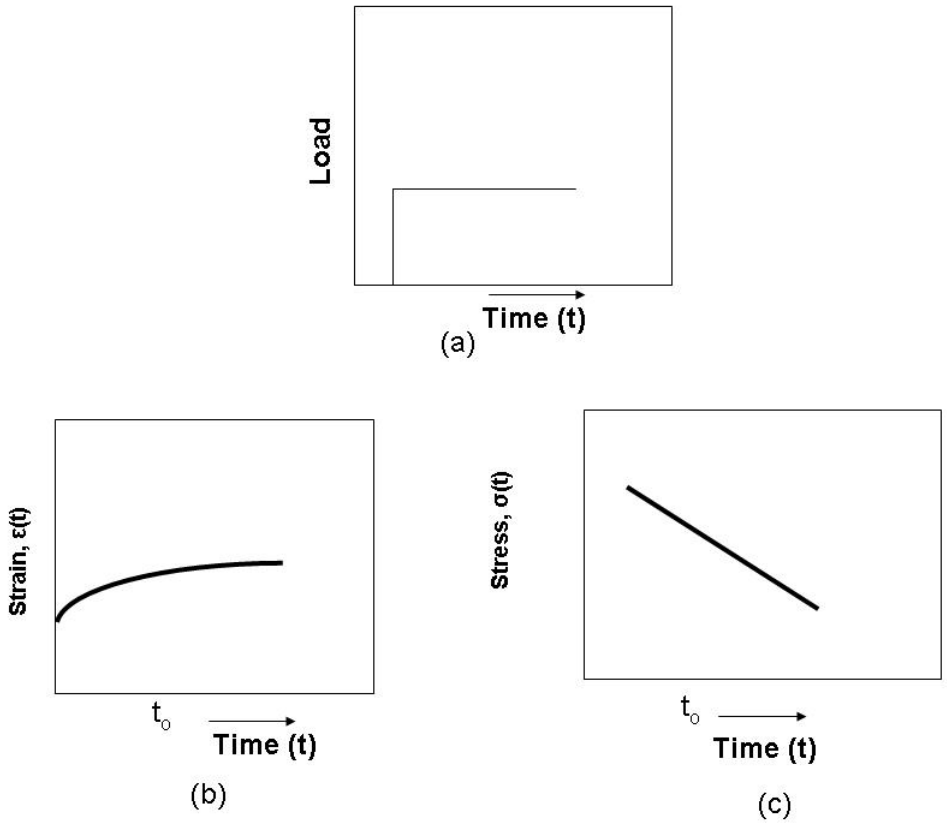

Figure 2.2 Schematic illustration of (a) Loading during creep and creep rupture (b) Creep and (c) Creep rupture

rupture time. In a PMC, creep rupture of a material leads to sudden failure of the specimen without any macroscopic yielding.

The various factors that influence creep and creep rupture are stress, temperature, moisture and physical aging. A review of the literature pertinent to this section can be found in the Appendix. Details on the creep and creep rupture of unidirectional composite can be obtained from the literature listed in the reference [1-6, 8-12, 16-24, 43] Stress, temperature, moisture and physical aging influence the creep compliance and the creep rupture time.

2.3 Creep and Creep Rupture of Multidirectional Composites

Early research on creep of multidirectional composites was carried out by Dillard [9]. Some of the laminates he studied include, $[90/60/-60/90]_{2s}$, $[75/45/-75/75]_{2s}$, $[10/55/-35/10]_{2s}$, $[90/45/-45/90]_{2s}$, $[75/30/-60/75]_{2s}$, $[20/60/-25/20]_{2s}$, $[15/-75]_{4s}$, $[60/15/-75/60]_{2s}$ and $[30/-60]_{4s}$. He developed a numerical model, based on classical lamination theory and creep data of unidirectional lamina to predict the creep of laminates. It was observed that the predictions fell below the experimental data for laminates with two ply orientations, while the predictions were in good agreement with the experimental data for laminates with three ply orientations. The reason for the good agreement in a three or more ply orientation laminate according to Dillard, was due to the formation of large number of triangular trusses by the fiber which led to the strain being accrued.

Dillard [9] also studied the creep rupture strength of multidirectional composites. He predicted the rupture strength based on the strength properties of the unidirectional material and were found to be low for all multidirectional laminates. The failure model

was considered responsible for the discrepancies because of the supposition that a ply ceases to support any σ_2 or τ_2 stresses once ply matrix failure had occurred.

Woo [18] carried out creep experiments on $[\pm 45]_{2s}$ specimens in dry and wet (0.9% moisture content) conditions over a temperature range of 25^0C – 160^0C. He found that the compliance was 20% greater for the wet laminates at 26^0C, but the difference increased to 120% at higher temperatures (82 – 138^0 C).

Corum et al. [44] carried out creep and creep rupture tests on [0/90] and $[\pm 45]_{3s}$ specimens. For the cross-ply [0/90] specimen, room temperature tests were carried out in the stress range from 100 to 470 MPa. The duration of the tests ranged from approx. 5000 hrs to 8000 hrs. Creep curves indicated that the creep behavior beyond 1000 hrs was approximately a linear function of the applied stress. Best fit curve derived from the power law equation was plotted with the experimental values and were found to be in good agreement below 400 MPa stress. Tests on the $[\pm 45]_{3s}$ specimens were carried out in the stress range of 25 to 107 MPa at room temperature. Test durations ranged from 2000 to 6000 hrs.

Corum et al. [45] carried out another set of creep rupture tests on [0/90] and $[\pm 45]_{3s}$ specimens at room temperature, 70^0 C and 120^0 C. Room temperature tests were carried out to test the repeatability of the earlier experiments. Tests were carried out on [0/90] specimens at 70^0C in the stress range of 200 – 400 MPa. One specimen fractured at 400 MPa while loading, while at the other stress range the creep rupture time was around 4000 hrs. At 120^0 C, tests were carried out at 200 and 300 MPa. The specimen failed immediately on loading at 300 MPa, while at 200 MPa the creep rupture time was around 1800 hrs. For the $[\pm 45]_{3s}$ specimens, tests were carried out between 50 - 88 MPa

stress range at 70^0 C. These specimens did not fracture but cracked or delaminated towards the end of the test. The creep resistance decreased by a factor of 4 in terms of creep strain.

Guedes [46] modified the energy failure criterion and developed an algorithm (LAMFLU) to predict the long term behavior of multidirectional composite laminates. He compared the theoretical methodology to the experimental results obtained by Dillard [9]. Predictions for laminates with three ply orientations ($[0/30/-30/0]_{2s}$ and $[0/45/-45/0]_{2s}$) were found to be in reasonably good agreement with the experimental results. Predictions for laminaes with only two fiber orientations ($[0/90]_{4s}$) did not correlate well with the experimental data. This is explained to be due to the inability of the energy criterion to predict the correct stress rupture level and the capacity of these laminaes to carry the load even after all plies cracked through the thickness.

Balachander [22] carried out creep and creep rupture tests on $[0/\pm45/90]_s$ laminates. The stress levels ranged from 12.5 MPa to 330 MPa, while the temperature range was between 100^0C to 160^0C. The duration of the creep tests ranged between 2 -3 hrs. Creep rupture tests were done at the above mentioned stress and temperature range until final fracture. He found that at lower stress (12.5 MPa) the experimental results agreed well with the simulated results for creep (based on lamination theory) at all test temperatures. For higher stresses the model creep predictions were conservative, due to time-dependent cracking of the [90] plies causing a reduction in modulus.

2.4 Damage

2.4.1 Introduction

Damage in a polymer matrix composite plays a vital role in determining the life span of a load bearing structure. Damage can be classified as intrinsic or extrinsic. Intrinsic damage mode consists of damage within lamina layer, such as fiber fracture, fiber debonding and matrix yielding, as well as delamination between layers. These damage modes may or may not influence one another. A brief overview of some of the damage that may occur during service is presented in the first part of this section, followed by a review of time dependent damage and its impact on creep and creep rupture of polymer composites is presented.

Transverse cracking also known as matrix cracking is shown in Figure 2.3. It occurs due to the stresses generated by mechanical and/or thermal loading. Residual stresses arise due to the difference in coefficients of thermal expansion between adjacent plies and resin cure shrinkage. High temperature curing fiber/epoxy systems are highly susceptible to micro-cracking. Matrix crack develop in the weaker laminae of a multidirectional laminate. The failure in the weaker laminae would be constrained by the outlying stronger laminae, thus preventing the crack from spanning the entire laminate. These constrained cracks are termed as matrix cracks, since they are observed in the matrix. When these matrix cracks reach an upper bound for the density (number of cracks per unit length), the saturation state is termed as Characteristic Damage State (CDS) [40].

Fiber fracture shown in Figure 2.4, is another damage sustained in-service. This occurs when the stress on the fiber exceeds the fiber strength.

Delamination shown in Figure 2.5 is one of the principal damages that can occur during the service life of a composite structure. This type of damage has a detrimental effect on the strength and life expectancy of composite components.

Fiber pull-out typically occurs subsequent to fiber breakage and debonding of the fiber from the matrix.

The stress at which a damage appears first in the weakest laminae of the laminate is termed as the First-ply Failure Stress (FPF). Observed FPF stress will be much less than the ultimate laminate failure (ULF) stress and is often used in service.

The influence of manufacturing process on the mechanical behavior of the material is an important aspect in studies related to polymer composites. Many of these materials require high temperature cure causing residual stress to be present in the final structure. These stresses are caused by thermal expansion mismatch of the constituents and from chemical shrinkage of the polymers. Thermal mismatch between the laminate and the tool on which it is processed also induces residual stress. A review of the literature on process induced damage can be found in Appendix-B.

2.4.2 Time Independent Damage

Many theoretical and experimental research have been carried out on damage evolution during tensile testing of composite laminates and its influence on time independent properties.

The focus of this section as well as the present study is on cracking in 90^0 plies with the predominant loading direction normal to those cracking plies. Researchers prefer to study the matrix cracking in the 90^0 plies because cracks that form in the 90^0 plies typically span the entire width of the 90^0 plies.

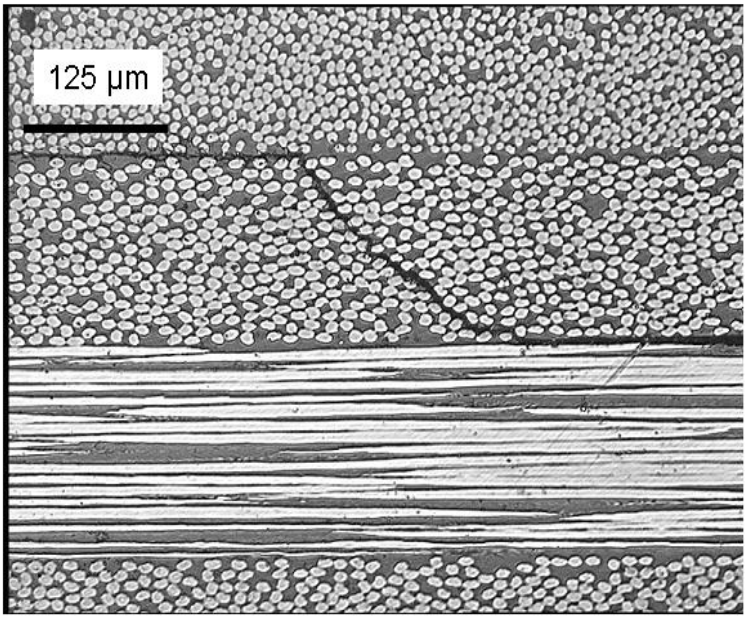

Figure 2.3 Micrograph of matrix micro-cracking in multidirectional laminate [26]

(Printed with permission from National Physical Laboratory, Crown copyright 2006)

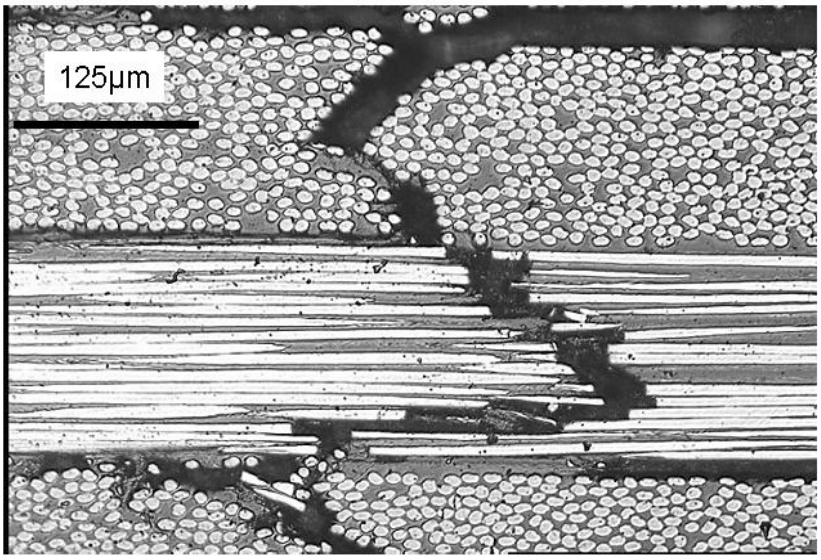

Figure 2.4 Micrograph of fiber fracture in multidirectional laminate [26]

(Printed with permission from National Physical Laboratory, Crown copyright 2006)

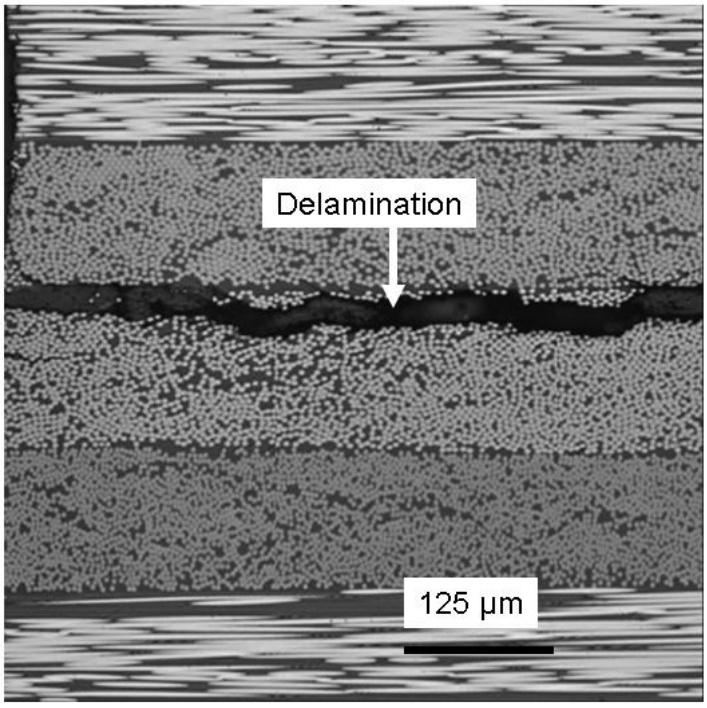

Figure 2.5 Micrograph of delamination in a multidirectional laminate [26]

(Printed with permission from National Physical Laboratory, Crown copyright 2006)

After the formation of first transverse crack, continued loading leads to additional microcracks and continued degradation in thermo-mechanical properties. Nairn et al.[41] characterized the laminate property by recording the microcrack density as a function of applied load. They carried out tests on 21 different lay-ups for a carbon-epoxy laminate. For the [0/90] laminates with different [90] thickness, the crack density increased rapidly during initial stages but decreased as it approached CDS. It was also observed that the FPF stress decreased as the thickness of [90] ply increased. This led to the observation that transverse cracks formed more easily in thicker [90] plies and that its formation was suppressed in thin [90] ply groups. However, thinner [90] plies developed more cracks than thicker [90] ply group. Thus, the CDS for transverse cracks was inversely related to the thickness of [90] ply.

They also carried out tests on [90/0] laminates with varying [0] ply thickness. Comparing the results for the [0/90] laminates with that for [90/0] laminates they concluded that the microcracking was dependent on the outer plies. It was also observed that the cracks started sooner in [90/0] laminates, but [0/90] laminates develop more cracks at saturation.

The experiments done by Nairn et al. also showed that the tip of the crack at [0] – [90] ply interface provided a site for initiation of delamination between [0] and [90] plies. The likelihood for the delamination to occur from the tip increased as the thickness of the [90] plies increased. Once delamination began to form, they propagated on continued loading while additional transverse cracks slowed down or stopped.

Kobayashi et al.[47] studied the effect of stacking sequence on transverse crack behavior in [90] plies. Laminate configurations studied were $[0/\pm45/90]_s$, $[45/0/-45/90]_s$,

$[\pm 45/0/90]_s$, $[0/90/\pm 45]_s$, $[0/45/90/-45]_s$, $[45/0/90/-45]_s$ and $[90/45/0/-45]_s$. Tensile tests were carried out at room temperature. They found that for the group of laminates with [90] plies at the center, the distance of [0] plies from the neutral plane are closely related to the transverse crack onset strain. Transverse crack density at final fracture for this group was less than that of $[90/45/0/-45]_s$ laminates.

2.4.3 Time Dependent Damage

Due to time constraints accelerating testing and modeling is required to predict creep and creep rupture beyond the experimental time window to predict creep and creep rupture behavior of multidirectional laminates during the entire service window. Dillard et al. [4] was the first one to study the accelerated testing of multidirectional laminates for their creep and creep rupture behavior. They found extensive damage in creep ruptured multidirectional composite and concluded that time dependent damage was the reason for the difference between experimental and predicted creep rupture results. Despite this important finding, no follow-up work was pursued during the subsequent 10 years in studying these damages that develop under constant load with and their impact on creep and creep rupture of multidirectional composite.

One of the first studies on time dependent damage progression was carried out by Moore and Dillard [40]. They carried out creep tests on $[0/90_3]_s$ cross-ply laminates and measured a time dependent increase in crack density in the [90] layer of the laminate at 30% of ultimate tensile strength. The average duration for each test was around two weeks. Edge replication technique and light transmission technique was used to inspect the damage state. They found that the stress in the transverse layer decreased with time when the laminate was subject to sustained loads. They observed that the crack formed

under creep loading did not span the entire width of the specimen. Based on the quasi-static loading they concluded that the matrix cracking process was dependent on loading rate. The study also concluded that the composites displayed unique and complex damage development and that each layer of composites has its own stress history which was not proportional to the applied stress.

Raghavan and Meshii [30] also investigated experimentally the time dependent behavior of transverse cracking. Tests were conducted on $[0/90_4]_s$ cross-ply laminates at room temperature. The crack density in the inner [90] laminae was measured by viewing the specimen edge using a traveling microscope. When tensile tests were carried out at constant strain rates, the strain rate was found to affect the first ply failure stress and progressive cracking. Creep tests carried out at 300 MPa and 286 MPa showed an increase in the crack density with time, which increased rapidly at the start and leveled off towards the end. They observed a strain rate dependence of cracking during creep load, which led to the increase in crack density. They also observed a dependence of progressive cracking on strain rate, i.e. the stress or strain at a given crack density varied with strain rate. The lower the rate of loading, higher was the compliance of the transverse lamina and lesser was the stress needed for further cracking. They observed creep rates for the cracked laminates to be much higher than that of the laminate with no cracks. The investigation showed that the matrix crack density and its rate of increase depended on the strain rate and stress respectively.

Ogi, K. and Takao,Y. [38] studied creep of $[0/90_3]_s$ and $[90_8]$ specimens at 110^0C. They formulated a creep model in which the transverse crack density increased and the model was based on viscoelasticity theory and shear lag analysis. They found two

different stages of evolution of transverse cracking. In the first case the crack density gradually increased as the strain increased during the period between 0-5000 seconds. Most of the transverse cracks during the first stage were generated by the increase in strain due to viscoelastic deformation. In the second stage when the time period was greater than 5000s, the crack density continued to increase although the creep strain was very small. They termed the transverse cracking in the latter as delayed fracture. They concluded that transverse cracking occurred both during and after significant amount of viscoelastic deformation. The creep strains predicted agreed very well the experimental results.

Ogi and Shiraishi [39] studied the effect of shear lag parameter and transverse crack density on the creep behavior of carbon fiber/epoxy $[0/90_3]_s$ laminate. Creep tests were carried out on specimens with and without transverse cracking at 110^0C. They observed the mechanical strain during creep to increase with increase in transverse crack density from 0 to 0.35 mm^{-1}. The theoretical strain values obtained by inverse Laplace transform also showed a similar trend. Although they obtained good results with predicting the creep strain no attempt was made to predict the creep rupture time based on transverse crack density.

Ogi and Smith [28] carried out studies on the quasi-isotropic $[0^0/90^0/-45^0/45^0]_s$ laminate with transverse cracking in the transverse layer at room temperature. Creep tests were done on unidirectional $[0^0]$, $[10^0]$, $[90^0]$ and $[\pm 45^0]$ coupons to obtain the viscoelastic constants required for the predictive model for creep strain. The quasi-isotropic specimen was initially loaded so that transverse cracks could be generated only in the [90] layers. Creep tests were carried out on specimens with three different crack

densities; 0.0/mm (no cracks), 0.25/mm and 0.5/mm. Creep tests were performed at low stress (58 MPa) such that there was no initiation of new cracks during the test. Experimental results on cracked laminates showed that the initial creep strain increased with transverse crack density; but the total creep strain remained almost the same for the three different transverse crack densities. They also found the predicted creep strain increments to be comparable with the experimental results. They concluded that the creep behavior was affected by the time dependent transverse and shear relaxation moduli.

Ogi and Kim [27] investigated the creep deformation for laminates with constant transverse crack density. They carried out analysis on unidirectional [0^0], [10^0] and [90^0] as well as cross-ply [0^0 /90^0 $_3$]$_s$ laminates in the temperature range of 110^0 C to 150^0 C. Some of the cross-ply specimens were initially loaded to introduce transverse cracks before the creep tests. At 250 MPa stress the creep strain increment for specimens with initial cracks was higher than those without initial cracks. It was also seen that the strain was higher at 150^0 C when compared to that at 110^0 C. A prediction based on the viscoelastic shear model was made and the creep strain predicted was less than that obtained experimentally. The underestimation was highly pronounced in the initial creep portion with the reason being attributed to the wrong choice of relaxation moduli during modeling.

The combined effect of microcracks and physical aging on creep was investigated by Akshantala and Brinson [29]. Tests were carried out on [$\pm45^0$ /$90^0{}_3$]$_s$ laminate at 225^0 C. Isothermal aging of the specimens were carried out at 225^0 C for aging times ranging from 0.375 hrs to 48 hrs. Prior to the aging process the specimens were damaged at room temperature. The creep curves for all the aging times obtained at 20.47 MPa were shifted

horizontally to obtain a master curve at a reference aging time of 48 hrs. A comparison of the master curves for the damaged and undamaged showed a slight increase in the initial compliance due to damage, while there was no significant change in the shape of the creep curve. These results imply that moderate levels of damage affected the initial compliance slightly and that linear viscoelastic behavior was not affected.

The mechanism of time dependent evolution of damage can be explained as follows. Since fibers are elastic, time-dependent damage in multi-directional polymer composites is owing to the viscoelasticity of the polymer matrix. Time dependence of intrinsic damages is due to this viscoelasticity. However, in the case of extrinsic damages, both viscoelasticity and outer-ply constraint contribute to their time dependence. For example, let us consider the case of transverse cracking. Due to viscoelasticity of the matrix, when a weaker inner ply fractures with time, the crack would not span the entire thickness to cause laminate failure due to stronger outer plies. Due to this, undamaged portions of the weaker ply would continue to sustain load until it fails again. This process continues until the crack density increases with time and reaches a CDS. During this time-dependent damage evolution in the weaker ply, the load shared by this ply will be gradually transferred to other relatively stronger plies, which subsequently develop damage with time and fracture. The final fracture of the laminate occurs when the strongest ply in the laminate fails. Time-dependent evolution of other damage modes is possible, independently or triggered by the transverse cracking. For example, delamination can originate from transverse cracking; vertical cracking can develop instead of transverse cracking depending on the lay-up.

2.5 Motivation for this thesis

In summary, time-independent damage during tensile loading of multidirectional laminates at room temperature has been studied well in the past. The main focus of these studies was transverse cracking of weaker [90] plies sandwiched between other stronger plies in a laminate. Early studies by Dillard [40] indicated the possibility of damage in multidirectional laminates being time-dependent. Two previous studies (Dillard [9] and Raghavan [20]) have proven this possibility during creep of multi-directional laminates at room temperature. Balachander [22] has shown that prediction of creep without accounting for this time-dependent damage will be erroneous. Ogi and researchers [27], and Akshantala and Brinson [29] have studied the effect of pre-existing damage on creep of composites. Few studies have focused on generating creep rupture data for multidirectional laminates.

Even though above studies indicate that time-dependent damage is a reality in polymer matrix composites, it has not been given the importance it deserves. Moreover, accelerated testing is often used to predict creep and creep rupture during the service period of a polymer matrix composite structure. Without data on time-dependent evolution of damage, any prediction would be erroneous. Additionally, while most of the previous studies focused on one type of damage mode (transverse cracking in weaker [90] plies), existence of other damage modes, their time –dependent evolution during service of a composite structure, interaction among them, and their impact on creep and creep rupture of a composite structure is currently unknown. These unknowns are the motivation for this study.

2.6 Thesis Objective

Hence, the overall thesis objective, formulated based on the above literature review, is to study experimentally the time-dependent evolution of damage in polymer matrix composites. Specific objectives are

1. Identify the various types of damage that can develop in a polymer matrix composite under constant load and quantify their dependence on time, stress, and temperature
2. Develop a qualitative understanding of any interaction among these damage modes and their impact on behavior of a polymer composite under constant load
3. Develop a qualitative understanding of the effect of laminate-related factors such as ply thickness and outer-ply constraint on the type of initiated damage and its evolution with time in a composite under constant load.

In order to accomplish this, constant load tests were pursued. Since samples were frequently unloaded to examine for damage, creep strain was not measured. Instead, time to failure was recorded resulting in creep rupture data. It is envisaged that the data and knowledge generated through this thesis will be used by this author's successor to develop a predictive model for creep and creep rupture of polymer composites that exhibit time-dependent damage.

3. EXPERIMENTAL PROCEDURE

The objectives outlined in the previous chapter were realized by carrying out an extensive experimental work on creep rupture of multi-directional laminates. Constant load tests were carried out to obtain creep rupture data as well as time dependent evolution of damage for laminates with different laminate sequence.

3.1 Materials

The material used in the present work was the F263-7 epoxy resin reinforced with T300 carbon fiber procured from Hexcel Corporation. The pre-impregnated resin (prepreg) was in the form of a roll, with a width of 12" and a thickness of 0.01".

3.2 Composite Manufacturing

Manufacturing of composite panels consisted of an initial preparatory and lay-up process. This was followed by vacuum bagging. Autoclave curing the panel was the next step in the manufacturing process. Finally the cured panels were post cured.

3.2.1 Preparatory and Lay-up Process

The as-received uncured prepreg was sealed in a vacuum tight bag and stored at -25^0 C in a freezer to prevent the curing during storage. Prior to the actual panel preparation, the lay-up area and the tools being used for the manufacturing were thoroughly cleaned to ensure a composite with no embedded foreign objects. The prepreg

was removed from the freezer and allowed to thaw to room temperature, while still sealed in the evacuated bag.

The next part of the preparatory step involved applying a non-stick coating by means of an aerosol spray on the two aluminum tool plates to prevent sticking of resin from the prepreg to the plates. The non-stick coating was allowed to dry in air.The thawed prepreg was removed from the vacuum bag and 12" X 12" square pieces were cut. These pieces were then stacked one over another to get the desired lay-up sequence. While laying up the air between the plies were squeezed out using a plastic tool to prevent any entrapped air in the cured composite. Next the bagging film, the breather cloth and the release film were cut to size of the prepreg.

3.2.2 Bagging Procedure

This step involved arrangement of prepreg along with the films and the breather cloth to ensure a defect free composite panel. As shown in the Figure 3.1, a peel-ply (release film) was placed on top of the tool that was coated with a non-stick coating. The peel-ply prevents the sticking of the resin from the prepreg to stick to the tool. The cut prepreg layers were laid on the release film. Another peel ply was placed over the prepreg. This peel-ply does not allow the resin to soak the breather cloth. Above the release film was a breather cloth, which provides a path to the vacuum system for the gases evolved during curing. The breather cloth was in direct contact with a aluminum plate, which was placed below another breather cloth. Using a sealing tape, the cut prepreg along with the peel-ply and the breather cloth were encapsulated in a bagging film which can withstand high pressure and temperature. The whole system was evacuated using a vacuum pump connected through the vacuum port.

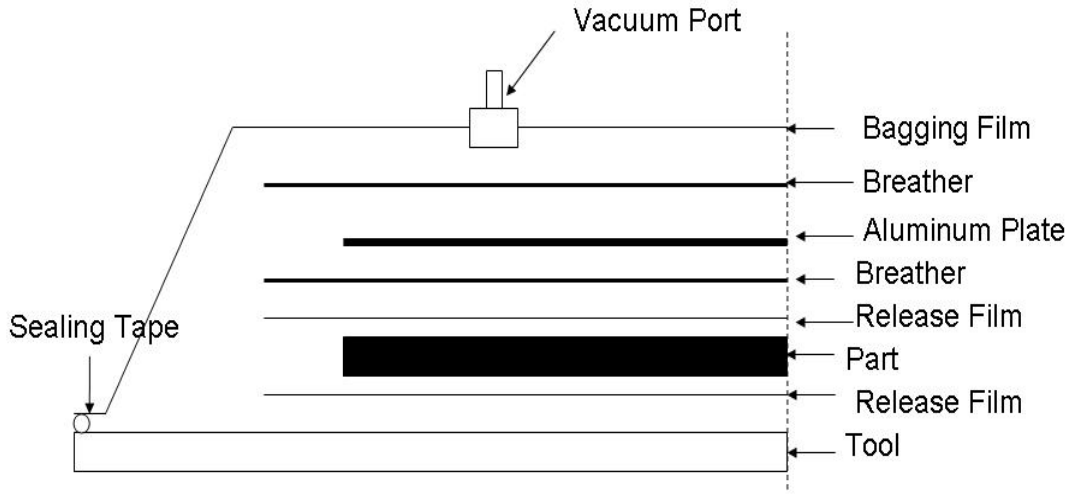

Figure 3.1: Schematic illustration of vacuum bag assembly

3.2.3 Curing Sequence

The panels were cured using the in-house hot press facility and a mold in a simulated autoclave environment. A photograph of the facility is shown in Figure 3.2 A schematic of the cure cycle is shown in Figure 3.3. At the start of the cycle, the vacuum bag was evacuated by vacuum and the temperature was ramped up to 80^0 C. When the temperature reached 80^0 C the vacuum was cut off and the vacuum bag was vented to the atmospheric pressure. The mold was then pressurized to 85 ± 15 psi using nitrogen. The temperature was increased to cure temperature, 180 ± 6°C, at a rate of 3^0 C/min. The temperature and pressure was held constant for 120 min. After this point the mold was allowed to cool down at a rate of 3^0 C/min till the temperature reached 60^0 C. The N_2 pressure was cut-off. The cured panel was allowed to cool down to room temperature while in the hot press.

3.2.4 Post Cure

The final step in the manufacturing process was the post curing of the laminates. This step was carried out to make sure that there was complete polymerization and cross linking of any unreacted monomer. Post curing was carried out at 240°C for 4 hrs in an air-circulated oven.

3.2.5 Fiber Volume Fraction

The post cured panels were tested for the volume of fiber using water displacement and acid digestion methods.

In the water displacement method the specimen was initially weighed in air. A wire was weighed when it was partially submerged in water. The wire suspended

Figure 3.2: Photograph of the hot press facility

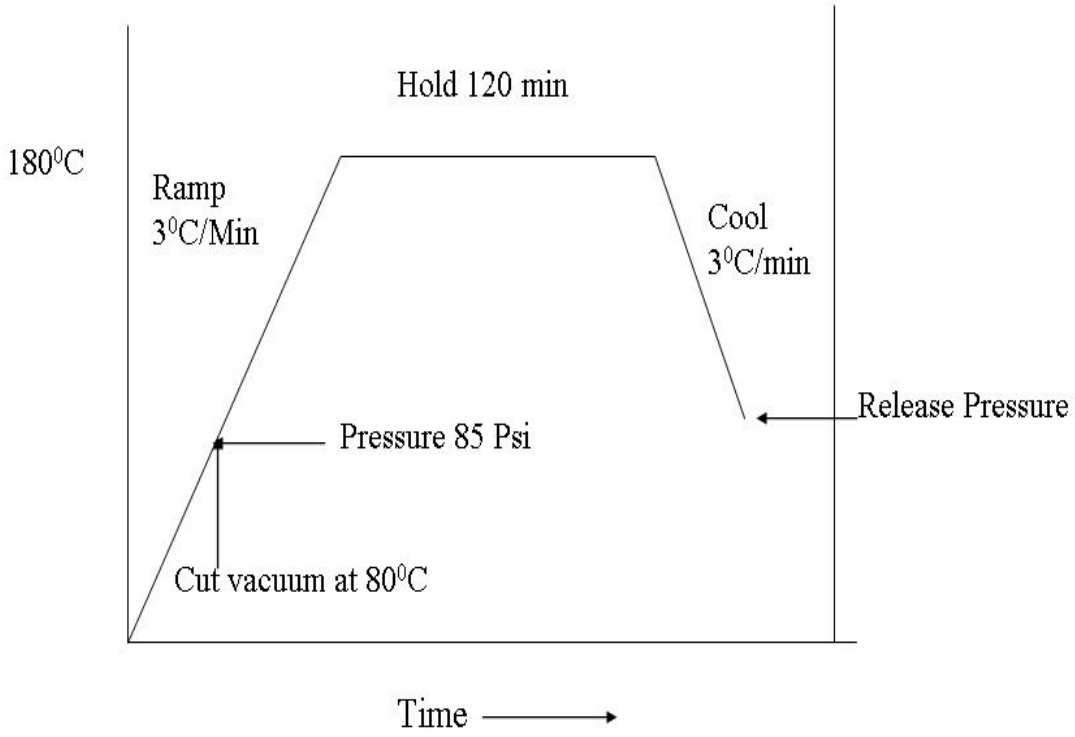

Figure 3.3: Schematic illustration of the cure cycle

specimen was subsequently weighed when fully submerged in water, and with the wire partially submerged.

The density of the material was obtained using the following formula:

$$\rho = a \times \frac{0.9975}{(a + w - b)} \qquad \text{(Eq. 3.1)}$$

Where,

ρ = Density (g/cm^3)

a = Weight of specimen in air (g)

b = Weight of fully immersed specimen with partially immersed wire in water (g)

w = Weight of partially immersed wire in water (g)

Acid digestion method, described in ASTM D3171-76 was used to determine the volume fraction. A sample of composite material was dried and weighed. The sample was then heated in conical flask with 30ml of 70% nitric acid in a water bath at 75^{o}C. A reflex condenser was connected to the conical flask to condense and recirculate the acid back to the flask. The digestion of the matrix was carried out for 5 hrs. Undissolved fibers were filtered onto a sintered glass filter crucible under a vacuum of 16.9 Pa. The undissolved fibers in the filter were thoroughly washed with water and subsequently with acetone. The washed fibers were dried at 100^{o}C for one hour in an air circulated oven. The dried fibers were cooled to room temperature in a desiccator to prevent any moisture absorption. The cooled fibers were weighed to the nearest 0.1 mg. The average volume fraction of all the panels was approximately 54% V_f and was calculated based on the following equation:

Fiber volume % = $[(W/\rho_f) / (w/\rho_c)]$ X 100

Where W = Weight of fiber in composite (measured after digestion)

w = Weight of composite specimen (measured before digestion)

ρ_f = Fiber density

ρ_c = Composite density

3.3 Laminate Lay-up Selection and Process Induced Damage

A number of laminates were initially considered for the study. Cross-ply $[0/90_m]_s$ laminate with m varying from 0.5 to 3, and quasi isotropic/angle ply laminates, ($[0/ \pm 45/ 90]_s$, $[0/ 45/ 90/ -45]_s$, and $[\pm 45/ 90_2]_s$), were studied. The edges of the above configurations were examined after manufacturing which revealed process induced damage in the following laminates $[90/ 0_m]_s$ (m = 0.5 to 3), $[90/ \pm 45/ 0]_s$, and $[90/ 45/ 0/ -45]_s$.

Two modes of damage were observed in all cured laminates: (a) Transverse cracks in [90] layers due to in-plane transverse stress (σ_{22}) as shown in Figure 3.4. (b) vertical cracks due to out-of-plane normal stress (σ_{33}) as shown in Figure 3.5. Polishing of the edges of the laminate resulted in disappearance of vertical cracks as shown in Figure 3.6, suggesting that the vertical cracks did not propagate along the entire width. This is to be expected since the out-of-plane normal stress reduces to zero away from the edge. Appearance of these damage modes depend on the laminate type as well as lay-up sequence, which can be inferred from Tables 3.1 and 3.2.

In $[0/\ 90_m]_s$, both transverse and vertical cracks were observed for m =1 or more, while only transverse cracks were observed for $[90/\ 0_m]_s$. For m = 0.5, no cracking was observed.

Transverse and vertical cracks were observed in $[90^0]$ ply while only transverse cracks were observed in $[\pm\ 45^0]$ plies. However, the cracks in both plies of $(0/\pm45/90)_s$ were staggered as shown in Figure 3.7. The cracking behavior of $[90/\ \pm\ 45/\ 0]_s$ was similar except for the lack of vertical cracks in outer $[90^0]$ ply. When $[45^0]$ plies were dispersed (instead of being together), as in $[0/\ 45/\ 90/\ -45]_s$, cracking was observed only in $[90^0]$ and $[-45^0]$ plies as shown in Figure 3.8. In addition, no vertical cracking was observed in $[90^0]$ ply. The cracking behavior of $[90/\ 45/\ 0/\ -45]_s$ was similar. Finally, no cracking was observed in $[\pm\ 45/\ 90_2]_s$.

Cracking behavior of outer $[90^0]$ plies in $[90/0_m]_s$ and $[90/\pm\ 45/0]_s$ was observed to be different from that of $[90^0]$ plies in $[0/90_m]_s$ and $[0/\pm\ 45/90]_s$. Figures 3.9 and 3.10 illustrates the cracking pattern in the $[90/0_2]_s$ and $[90/\pm\ 45/0]_s$ laminate.

In summary, the residual stress induced during processing caused transverse as well as vertical cracking in most of the laminate configurations manufactured, except in the cross-ply $[0/90/0]_s$ and the angle-ply $[\pm\ 45/\ 90_2]_s$. Hence these were chosen to show the initiation and growth of time dependent damage and its impact on the creep rupture. Moreover $[0/90/0]_s$ provided an opportunity to study time dependent growth of vertical cracks in [90], while $[\pm\ 45/\ 90_2]_s$ provided an opportunity to study time dependent growth of transverse cracks. Additionally, to understand the effect of thickness of [90] ply, cross-ply $[0/90_2]_s$ laminate was selected for the present study. The $[0/90_2]_s$ laminate was compared with the other

Table 3.1: Process induced damage in Cross-ply laminates

Laminate type	Horizontal Crack Density across thickness (cracks/ cm)	Observation
$[0/\overline{90}]_s$	0	No cracks found
$[0/ 90]_s$	4.25	Transverse cracks with few vertical cracks
$[0/ 90_2]_s$	5.2	Transverse cracks with few vertical cracks

Table 3.2: Process Induced Damage in Quasi-isotropic laminates

Laminate type	Ply orientation	Horizontal Crack Density (cracks/ cm)	Experimental Observation
$[0/ \pm 45/ 90]_s$	$\pm 45^0$	5.50	Staggered transverse cracks with few vertical cracks in 90^0 ply
	90^0	7.33	
$[0/ 45/ 90/ -45]_s$	$\pm 45^0$	2.30	Staggered cracks only in -45^0 ply along with cracking in 90^0 ply
	90^0	2.30	
$[\pm 45/ 90_2]_s$	$\pm 45^0$	0	No cracks found
	90^0	0	

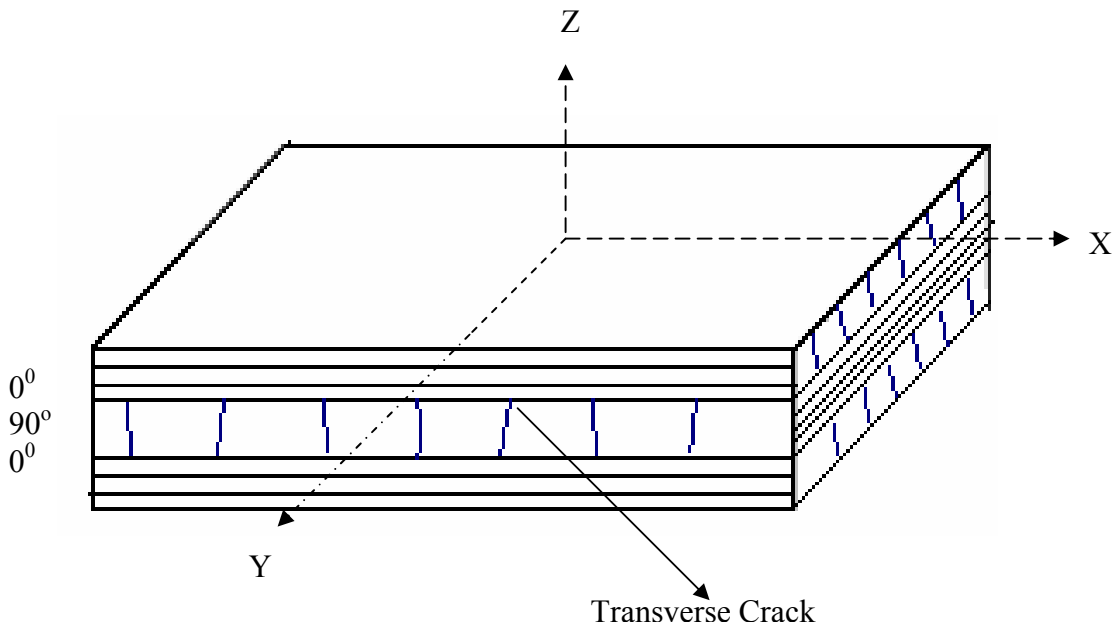

Figure 3.4: Schematic of damage in $[0/90_m]_s$

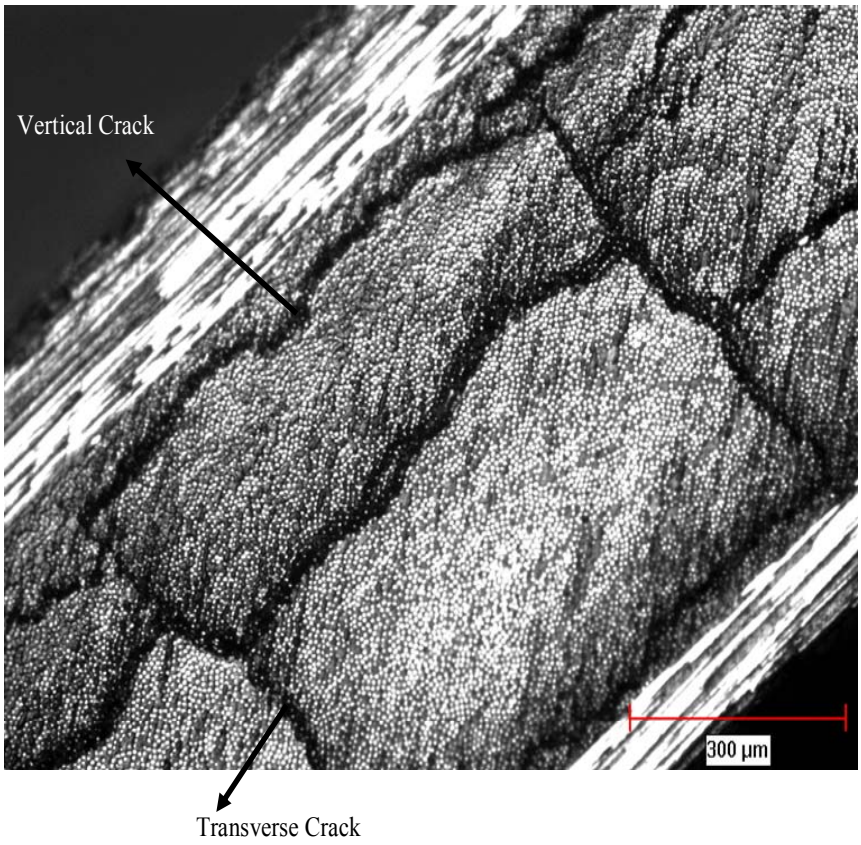

Figure 3.5: Damage in $[0/90_2]_s$ laminate, viewed along the edge

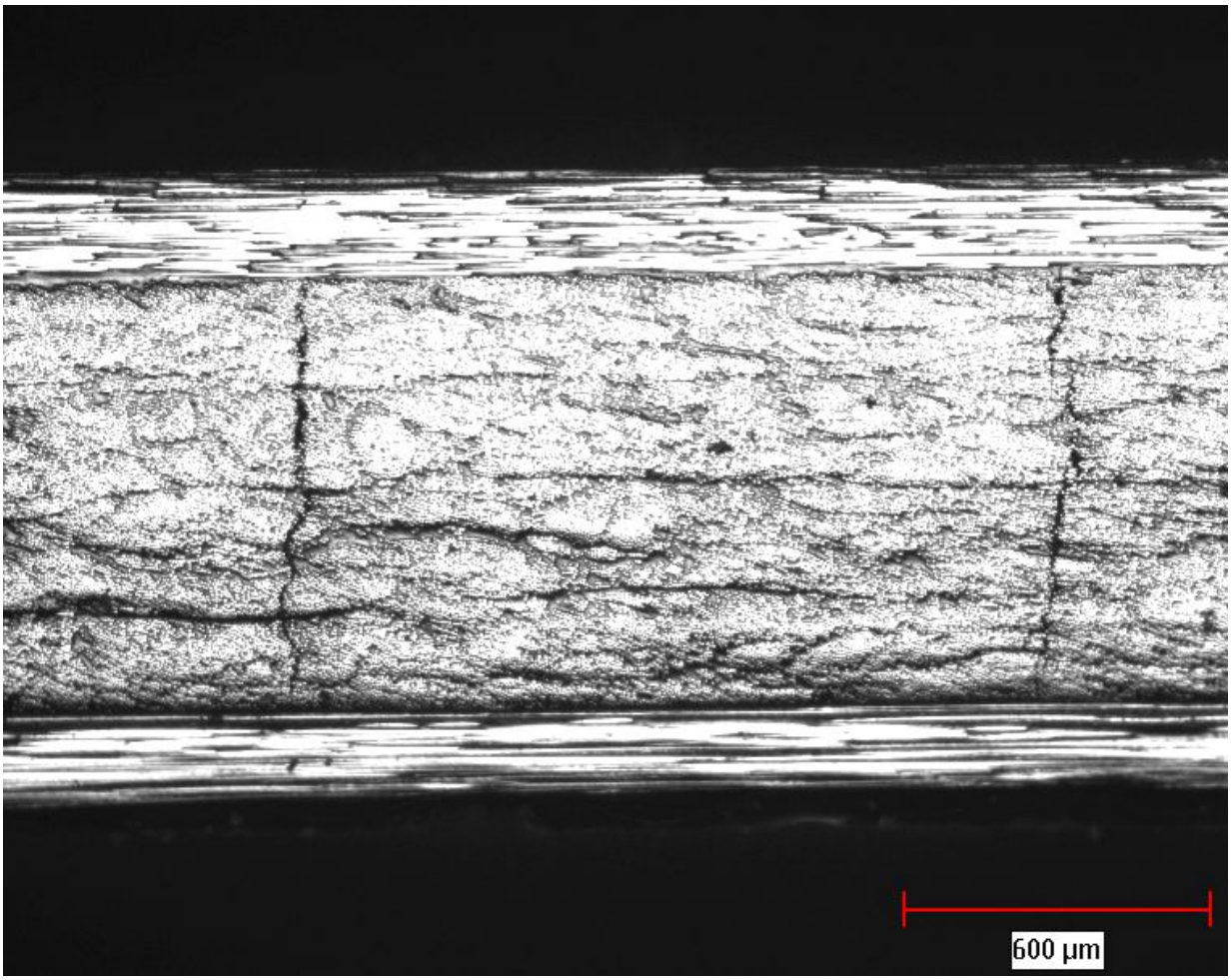

Figure 3.6: $[0/90_2]_s$ laminate after polishing

two laminates to study the effect of outer ply constraint and [90] thickness on time-dependent progressive damage in [90] ply.

3.4 Sample Preparation

3.4.1 Sawing

Edges of the post cured laminate panels were trimmed to a width of 1" from the boundary and discarded. The trimmed panels were held in position on a platform of a diamond saw using a double sided tape. The panels were cut using a precision diamond saw rotating at a speed of 500 RPM into coupons of size 152.4 mm X 12.7 mm (L X W). Table feed rate was kept to a minimum (10mm/min) to avoid overheating of the part. Water was used to cut the sample. Subsequently the samples were dried well.

3.4.2 Tabbing

Test specimens were tabbed at the ends to aid in gripping of the sample during testing. A woven glass epoxy composite was used as the tab material. This was laid-up and cured using a cure cycle similar to that discussed in section 3.2.3. One side of the tabbing was chamfered to 7^0 angle using a milling machine equipped with a carbide tipped end milling tool. This angle was selected to ensure uniform load transfer from the tab to the underlying test coupon.

The tab and panel surfaces were sanded using a 180 grit size silicon carbide paper to ensure good bonding. The two surfaces were cleaned using a wire brush to remove any loose particles. Using a slow speed precision diamond saw, tabs with dimension of 38.1 mm X 12.7 mm (L X W) were cut from the cured glass epoxy laminate. Ethyl alcohol was used to thoroughly clean the cut surface until all the loose particles were removed

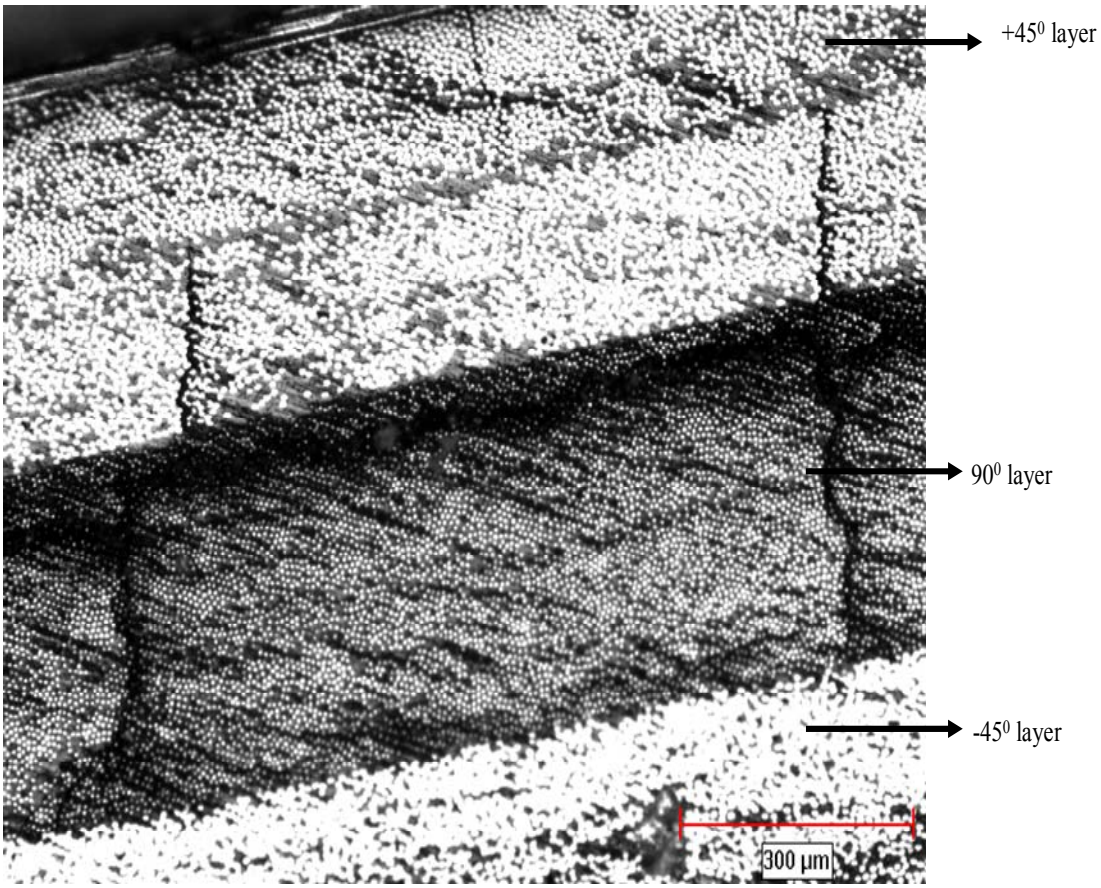

Figure 3.7: Damage in quasi-isotropic laminate $[0/\pm45/90]_s$, viewed along the edge

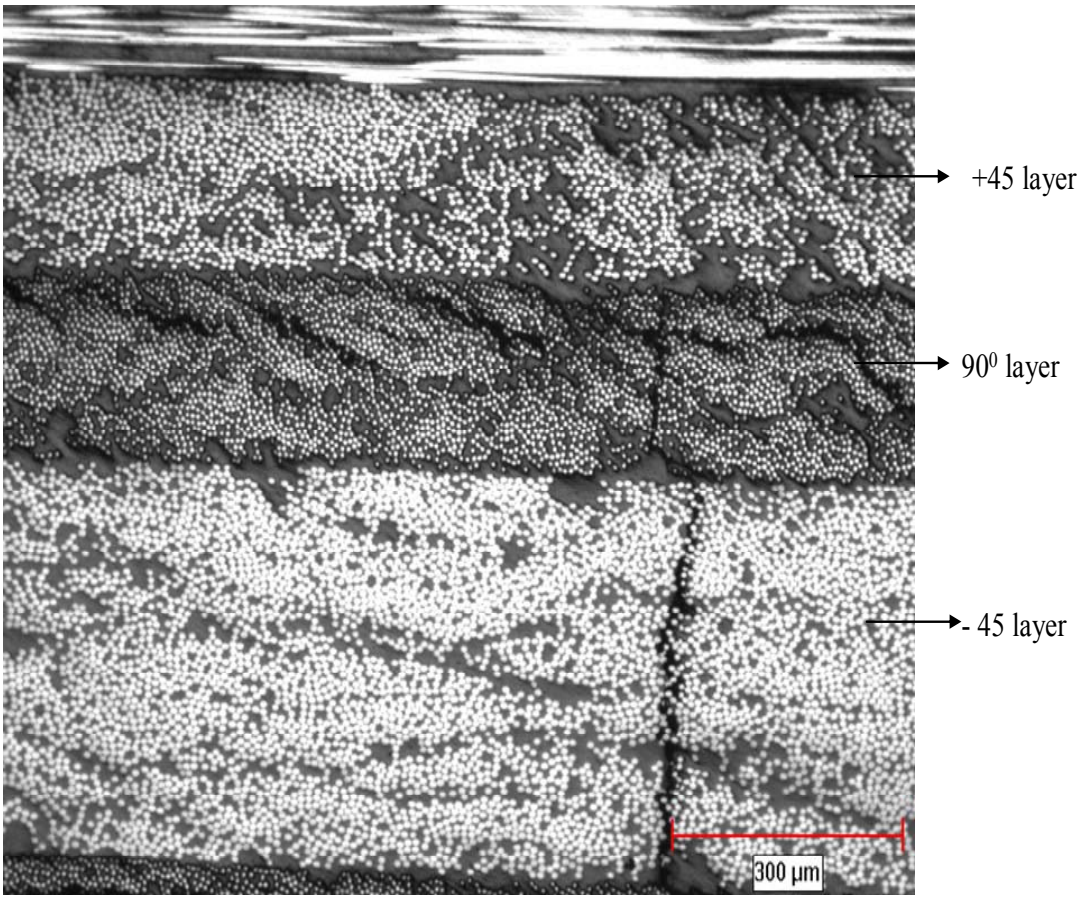

Figure 3.8: Damage in quasi-isotropic laminate $[0/+45/90/-45]_s$,viewed along the edge

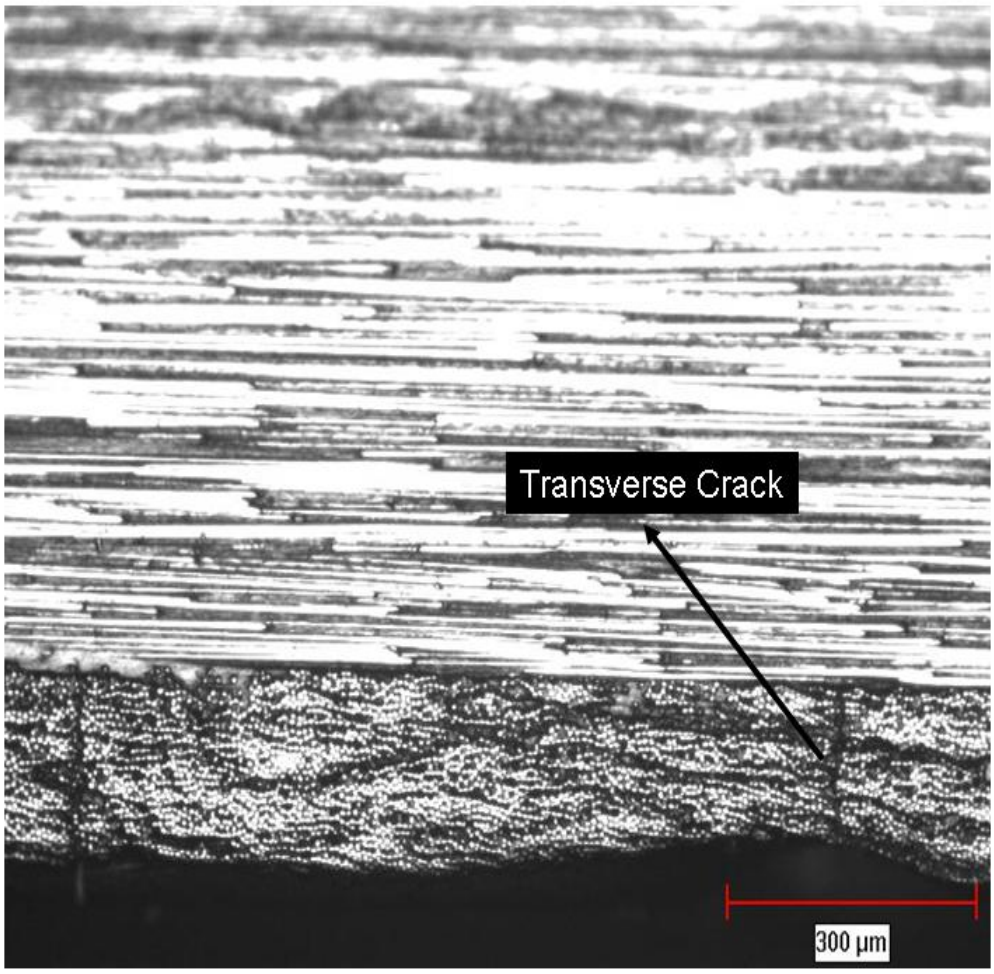

Figure 3.9: Damage in $[90/0_2]_s$ laminate viewed along the edge

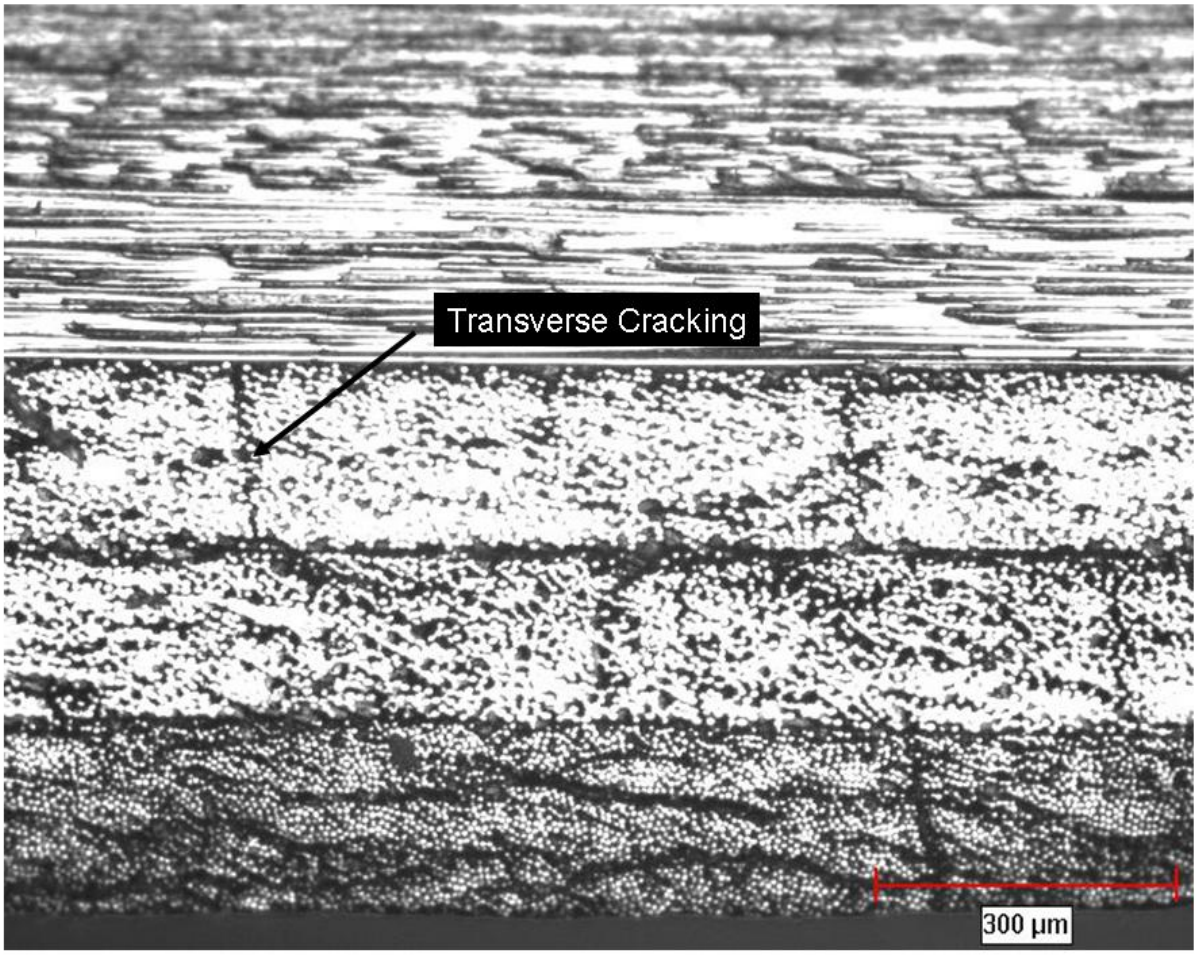

Figure 3.10: Damage in [90/$\pm$ 45/0]$_s$ laminate viewed along the edge

and to ensure that no adhesive from the double sided tape was present. Tabs were individually bonded to the cut composite test coupons using Dexter Corporation's BMI 9873 adhesive. Pre-cured adhesive was sandwiched between the tabs at either ends of the specimen to prevent movement of the tabs during adhesive curing, the tabs were held together using Mylar high temperature tape and spring clamp. This tape was also used to mask the entire gage length to prevent resin buildup and bleeding on the gage section. The test coupons were heated in an oven to 175^0C and held for 1 hour to allow the adhesive to cure. The coupons were then allowed to cool down to room temperature under spring clamp pressure.

3.4.3 Edge Preparation

The edge of the tabbed specimen was polished to get a scratch free surface. This was done by abrading the edge using silicon carbide papers, starting from a coarse grit paper (240) and progressing towards a finer grit paper (800). Subsequently they were thoroughly cleaned using ethyl alcohol to remove any traces of debris. The specimen were then polished using a 0.9 and 0.3 micron alumina slurry to obtain a scratch free surface.

3.4.4 Strain Gaging

WA-013-250BF-350 strain gages from Measurements Group, NC, USA, were used to measure the strain. The specimen surface was abraded using 240, 400, 600 grit papers. The abraded particles were removed using M prep conditioner A, and neutralized using M prep neutralizer B. This was done to ensure superior bonding between the strain gage and the specimen surface.

Strain gages were bonded to the coupons using M bond 610 adhesive at 180^0C for 90 minutes under spring loaded clamp pressure. The samples were allowed to cool to room temperature in the oven. The adhesive was post cured at 220^0C for 2 hrs without the spring clamp to ensure complete curing.

3.5 Test Conditions

3.5.1 Tensile Testing

Tensile tests were carried out to obtain the strength of the laminates which were later used to define the creep rupture test conditions. Tests were done on the chosen laminates at room temperature as well as at 80, 180 and 240^0 C using Instron's 8562 servo-electric test frame with Instron 8500 control system. The test frame was equipped with a ±125 KN load cell and high temperature oven capable of maintaining a set temperature within $\pm 1^0$C. The load and strain data were acquired using the National Instruments SCXI 1321 data acquisition system. A Lab-View based program was modified to allow data logging at different rates. The hardware was capable of acquiring four independent parameters simultaneously, which included strains, load and position.

Tensile tests were carried out at a constant strain rate of 10^{-4} s^{-1}. Prior to testing all samples were mechanically conditioned by loading and unloading few times to remove any slack in the load train and to ensure effective gripping of the samples with the wedge grips. The samples were also allowed to equilibrate to the set temperature before starting the tests.

3.5.2 Constant Load Rate Testing

The goal of this testing was to obtain FPF and CDS values. Tests were carried out at room temperature as well as at high temperatures (80, 180 and 240^0 C). Samples were subjected to constant load rate of 5kg/s in increments of 5% of the UTS (Ultimate Tensile Strength) till FPF (First Ply Failure) occurred. The samples were unloaded after every load increment and examined for appearance of cracks in various plies over the 50.8 mm gage length. For high temperature testing, the samples were removed from the testing machine and examined using a Carl-Zeiss digital microscope which could magnify images up to 1000 times.

At room temperature, damage was studied and characterized without removing the samples from the load train using a Nikon stereoscopic traveling microscope equipped with digital camera that was connected to a computer. A photograph of the setup is shown in Figure 3.11. This setup was later abandoned for testing at high temperature due to the inferior quality of pictures causing difficulties with crack density measurements. This was due to a combination of poor sample illumination and blurring of the image caused by the view window of the oven.

Beyond FPF stress the load was increased by 10% UTS to obtain the crack density data as a function of applied stress.

3.5.3 Creep Rupture Testing

Creep rupture tests were done to determine the time to fracture at a constant stress as well as to study time-dependent damage. Before testing, the specimens' cross-sectional area was determined and used to compute the stress level was measured. The specimen was mounted onto the grips and was allowed to equilibrate at the test temperature for at

least half-an-hour before the test began. Tests were carried out using Instron 8562 servo-electric tester as well as the SATEC lever arm tester. The test schedule is tabulated in Table 3.3. The SATEC machine had a lever arm ratio of 20:1. The two machines were equipped with high temperature ovens. In order to prevent the samples from slipping grips with serrated inserts were used. The time to fracture was recorded by built-in timer that automatically shut off the machine when test specimens fractured.

The various damage modes were observed at regular time intervals by unloading the samples and examining them using the Carl-Zeiss digital microscope. The increase in crack density in [90] layers with time was recorded. The vertical cracks appeared in different parts of the layer, grew in length with time and coalesced. Since it was difficult to quantify this, the growth of this damage mode was qualitatively studied. Similar reasoning is valid for the damage modes such as delamination and fiber fracture.

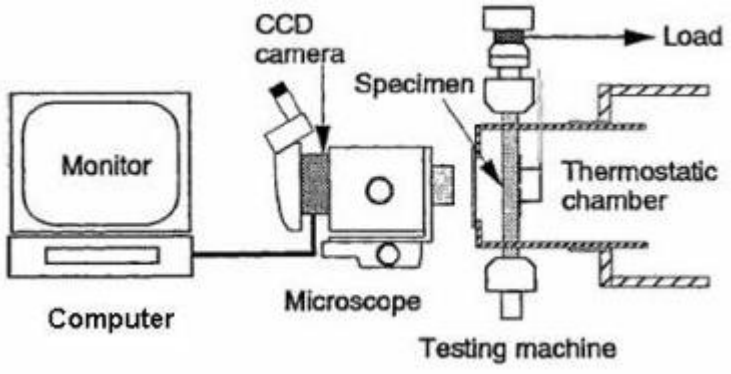

Figure 3.11: Setup for damage observation at room temperature

Table 3.3: Creep Rupture Test Matrix

Coupon Configuration	Temperature (^{0}C)	Stress (% UTS)
[0/90/0]	80	85, 90, 95
	180	85, 90, 95
	240	70, 80, 85, 90
$[0/90_2]_s$	80	75, 80, 85, 90
	180	40, 50, 70, 85, 90
	240	70, 75, 80, 85
$[\pm45/90_2]_s$	80	75, 80, 85, 90
	180	75, 80, 85, 90
	240	75, 80, 85, 90

4. RESULTS AND DISCUSSION

Experimental results obtained in the current study are presented in this chapter. The tensile test results along with the FPF results are presented and discussed in the first section. These results were required to select the creep rupture test conditions. The damage progression and CDS, observed during tensile testing were used in understanding damage progression during creep rupture testing. The second section deals with the results from creep rupture testing. Finally section 4.3 discusses the time dependent damage evolution.

4.1 TENSILE TEST RESULTS

4.1.1 [0/90/0] configuration

Tensile tests at a strain rate of 10^{-4} s^{-1} were carried out at 80, 180 and 240^{0}C to obtain the fracture strength of the specimen. The stress strain curves obtained from these tests are plotted in Figure 4.1and the properties calculated using these curves are tabulated in Table 4.1. The laminate exhibited a linear stress-strain relationship at all temperatures. The modulus decreased with increase in temperature. The strength apparently increased with temperature. This is believed to be due to the process induced residual stress, since the laminate was cured at 177 ^{0}C. The magnitude of the residual stress is proportional to ($T_{test} - T_{cure}$). Therefore the tensile residual stress in [90] layer will decrease with increase in temperature. This would result in lower UTS at 80 ^{0}C and relatively higher UTS at 180 ^{0}C.

First ply failure (FPF) stresses were obtained by carrying out tests at constant loading rate of 5 kg/s. The values are tabulated in Table 4.2. Transverse crack density in

[90] layer was measured within the gage length of 50.8 mm (defined as the number of cracks per millimeter). Micrograph of the as received, undamaged sample is shown in Figure 4.2. At room temperature, sample was loaded to 40 MPa (5% of UTS), unloaded from the Instron machine and observed using the Carl - Zeiss digital microscope for damage. This procedure was repeated till the first damage was observed, which occurred at 202 MPa. The first mode of damage observed was a vertical crack in the [90] ply. This type of damage mode was observed for the first time in any of the studies involving creep and creep rupture in multi-directional composites. Beyond FPF the load was increased in increments of 10% UTS without changing the loading rate and damage evolution was recorded. The vertical crack in the [90] layer ran the entire length of the sample. The micrograph of the damage is shown in Figure 4.3. With increase in load by 10% UTS there appeared no significant change in the width of the crack, while transverse cracks appeared for the first time as shown in Figure 4.4. The transverse crack density further increased with each additional load increment. At 50% UTS more than one vertical crack was observed. A new vertical crack appeared which ran parallel to the length of the specimen as shown in Figure 4.5. At 70% UTS the width of the vertical crack significantly increased while the transverse crack density also increased. The transverse cracks formed a bridge between the two vertical cracks as shown in Figure 4.6. The transverse crack density further increased with increase in load to reach CDS of around 15 cm^{-1} before the sample failed. A plot of the transverse crack density versus applied stress is shown in Figure 4.10.

FPF stresses were also determined at elevated temperatures using the procedure mentioned above. At 80^0C the FPF stress was found to be 239 MPa. Vertical cracking running along the entire gage length was the first mode of damage. With increase in load there was an increase in the transverse crack density; similar to the trend observed during the room temperature test. CDS was exhibited at this temperature as well. Constant load rate test at 180^0C produced a FPF of 265 MPa. Damage progression was very similar to that observed during the earlier tests (22^0C and 80^0C).

FPF stress at 240^0C was found to be 240 MPa with vertical cracking being the first mode of damage. The width of the vertical crack (Figure 4.7) appeared to be wider than those formed at lower temperatures. Increase in load caused an increase in the transverse crack density. At 65% UTS partial delamination between the [0] and [90] layer was observed for the first time, as shown in Figure 4.8. The micrograph shows the [0] layer out of focus and a vertical crack running along the [90] layer. The delaminated region is marked on both the sides and beyond that is the [0] layer. At 85% UTS, fracture of fiber in [0] layer, as shown in Figure 4.9, was observed. Further increase in load caused the sample to exhibit CDS and finally leading to failure. The evolution of transverse crack density in the [90] ply is plotted as a function of stress (%UTS) for the four temperature in Figure 4.10. It can be observed from the plot that the crack density reached a plateau at high stress levels, which corresponds to the CDS for [0/90/0] configuration. A marginal change in the CDS was observed for various test temperatures without any conclusive trend.

Table 4.1: UTS values at various temperatures for the three laminates

Laminate Type	**80^0 C**	**180^0 C**	**240^0 C**
[0/90/0]	823 MPa	1130 MPa	863 MPa
$[0/90_2]_s$	427 MPa	418 MPa	375 MPa
$[\pm45/90_2]_s$	64 MPa	54 MPa	30 MPa

Table 4.2: FPF stress at various temperatures for the three laminates

Laminate Type	**Damage Mode**	**80^0 C**	**180^0 C**	**240^0 C**
[0/90/0]	Vertical crack	239 MPa	265 MPa	240 MPa
$[0/90_2]_s$	----------	Process	Induced	Damage---------
$[\pm45/90_2]_s$	Transverse crack in [90] ply	29 MPa	26 MPa	9 MPa

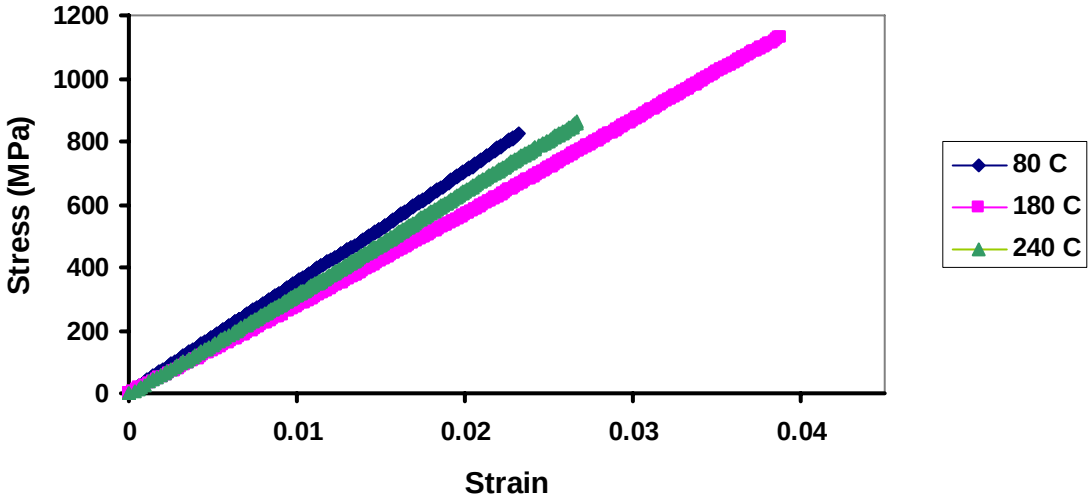

Figure 4.1 Stress-strain plot for [0/90/0] sample at various temperatures

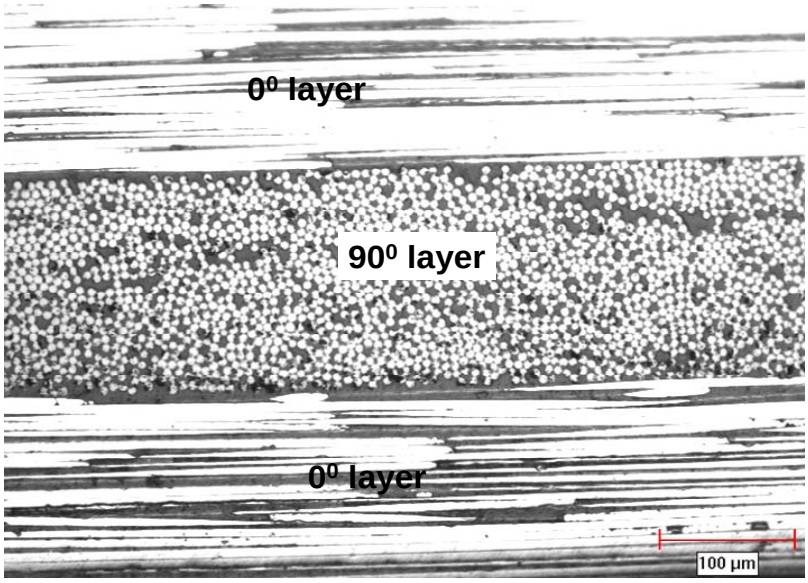

Figure 4.2: Micrograph of the undamaged [0/90/0] sample

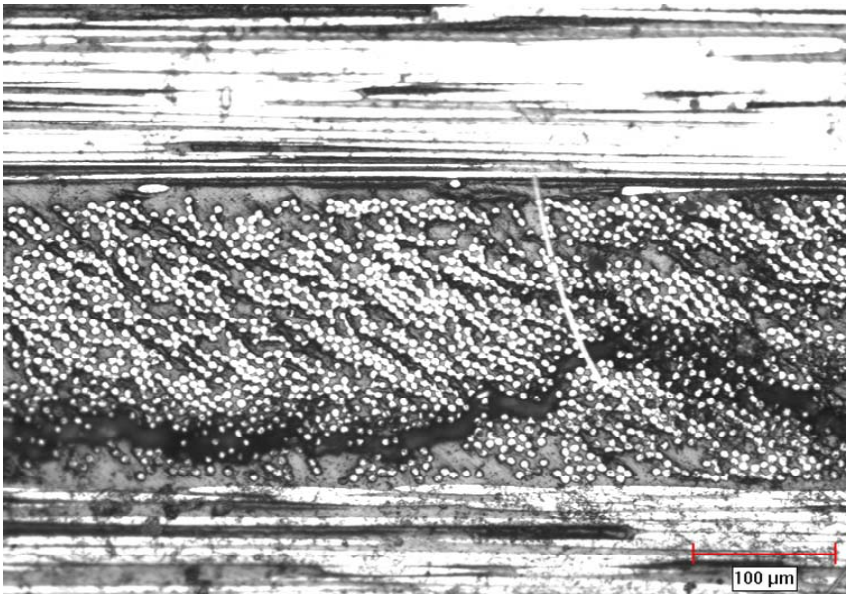

Figure 4.3: Micrograph of FPF damage in [90] layer

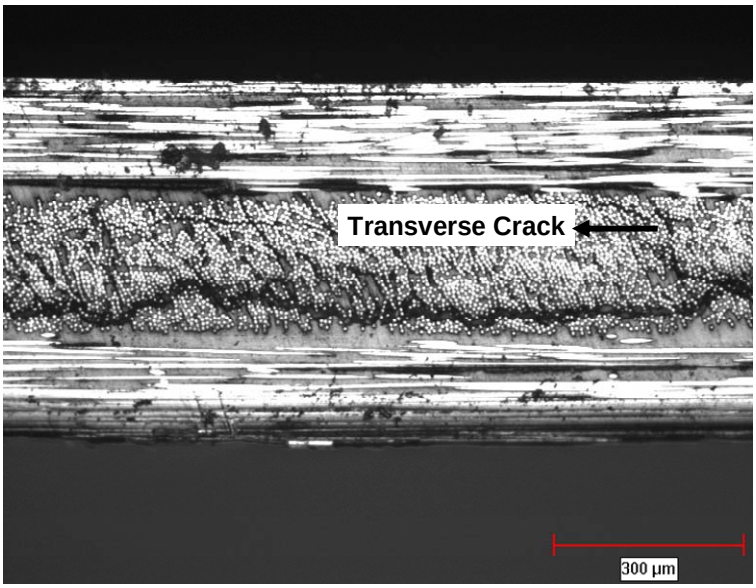

Figure 4.4: Micrograph of a transverse crack in the [90] layer of a $[0/90/0]_s$ sample

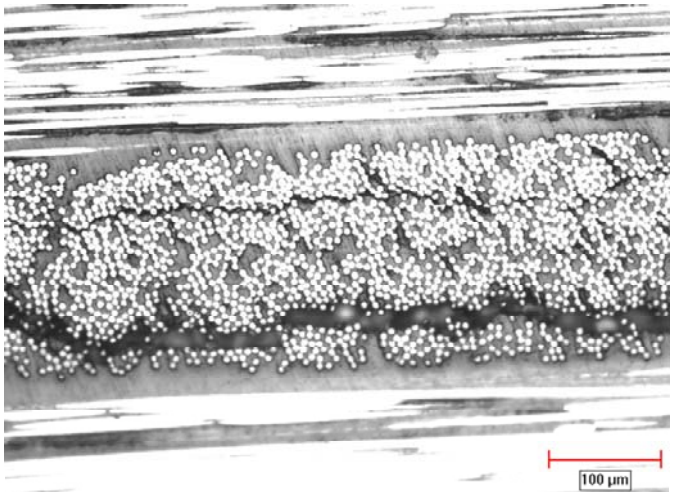

Figure 4.5: Micrograph of a second vertical crack in [90] layer of a $[0/90/0]_s$ sample

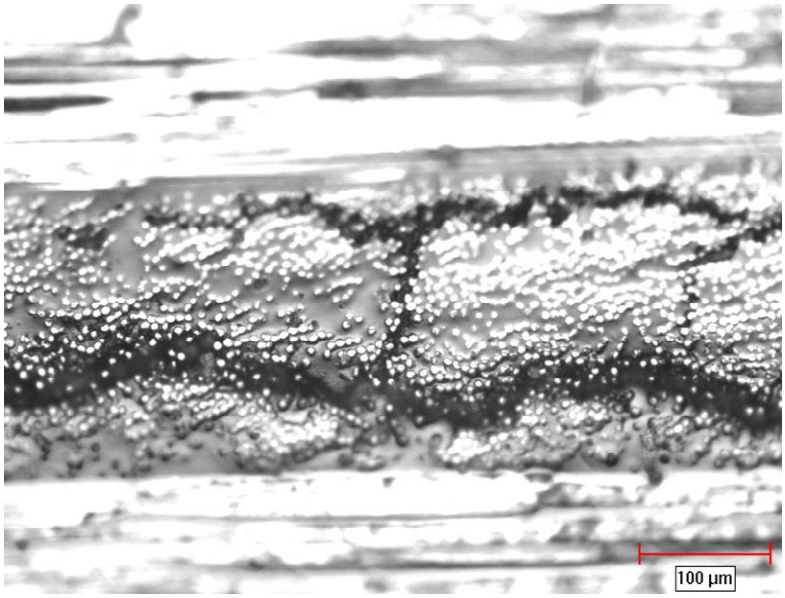

Figure 4.6: Micrograph showing transverse crack bridging vertical cracks in [90] layer of a $[0/90/0]_s$ sample

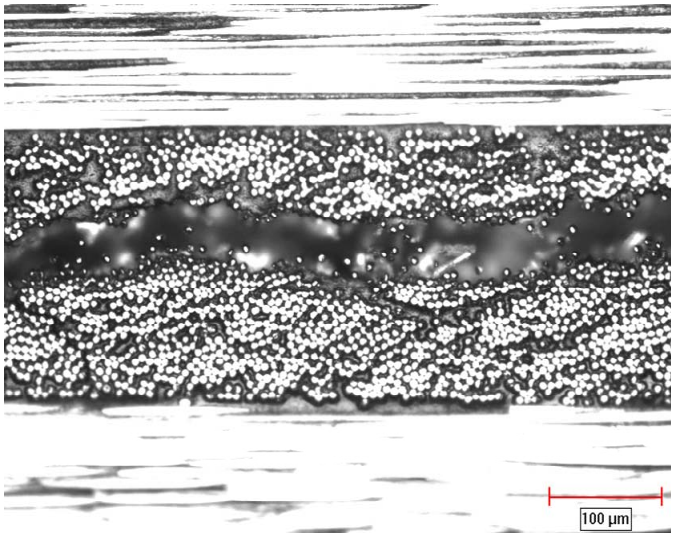

Figure 4.7: Micrograph of vertical crack in [90] layer at 240^0C in a $[0/90/0]_s$ sample

The [0] layers are out of focus on both sides of the delaminated region

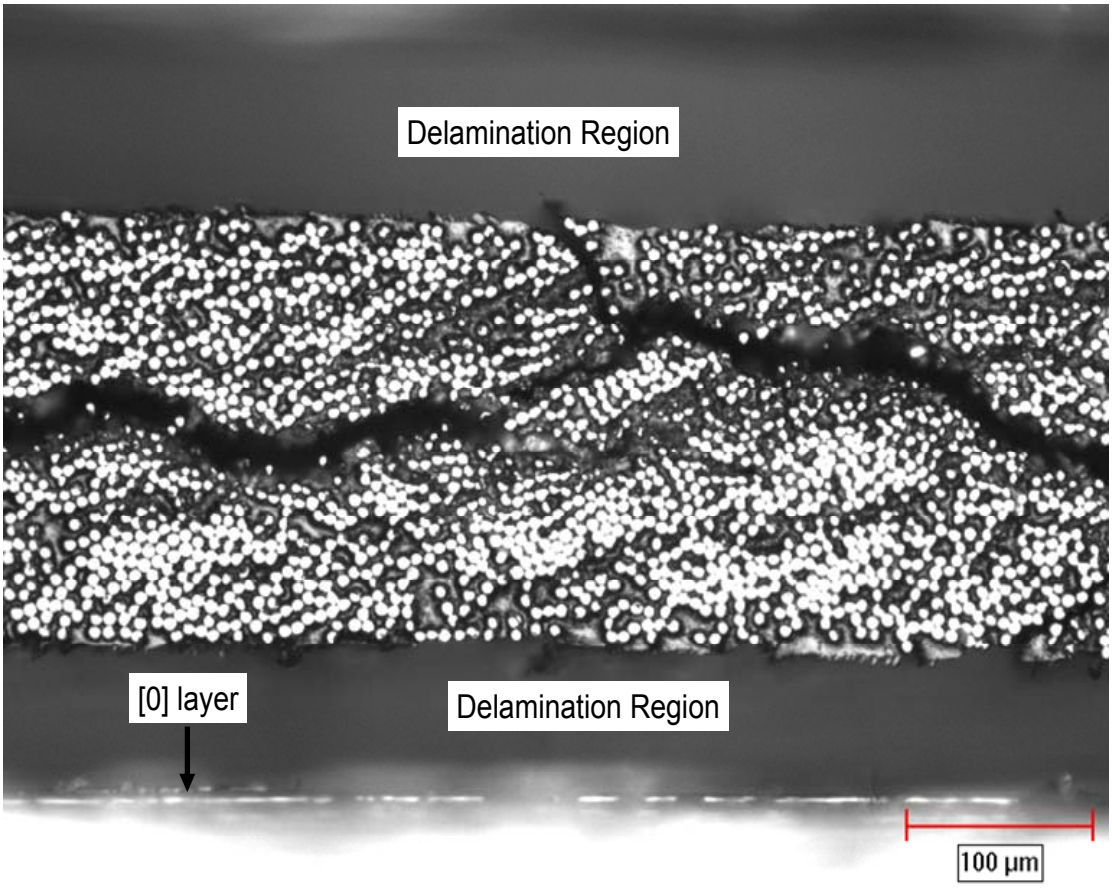

Figure 4.8: Delamination between [0] and [90] layer in a [0/90/0] sample at 240^0C

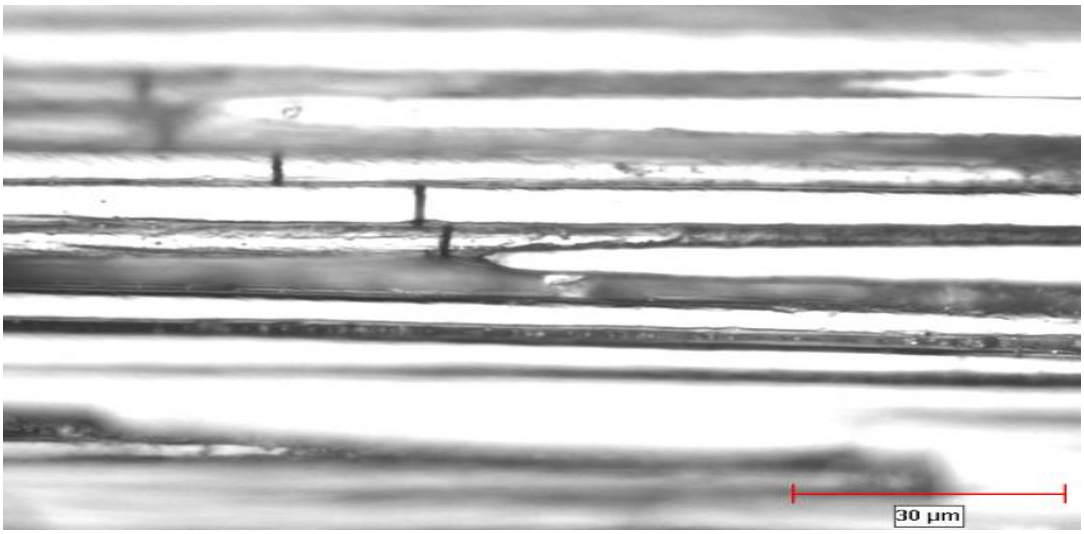

Figure 4.9: Fiber fracture in [0] ply [0/90/0] sample at 85% UTS and 240^{0}C

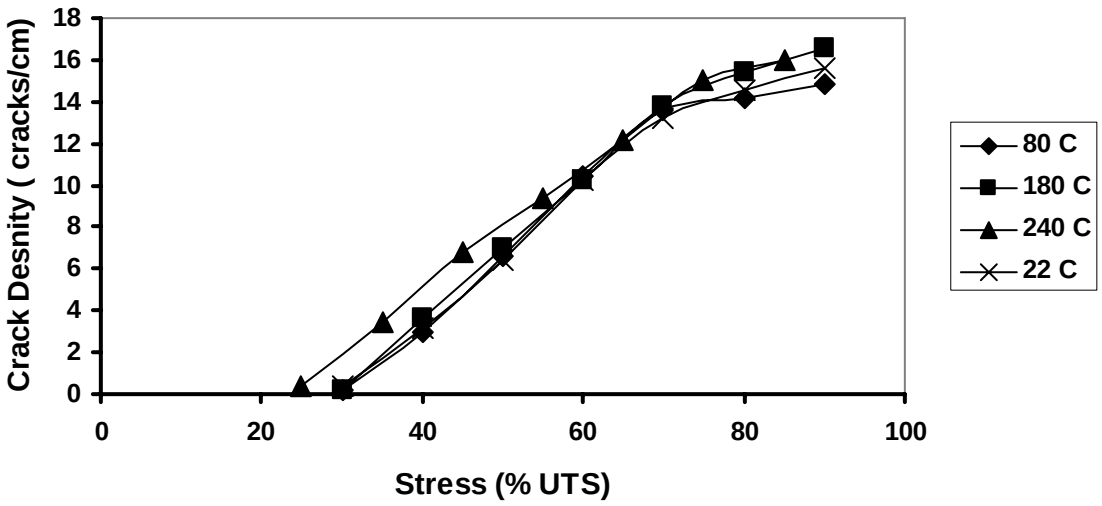

Figure 4.10: Crack density as a function of stress at various temperatures for [0/90/0] samples

4.1.2 $[0/90_2]_s$ Configuration

The as-received specimens had process induced damage, with vertical and horizontal cracks observed in all the samples. The vertical cracks did not span the entire gage length in contrast to $[0/90/0]_s$ laminate where the vertical crack observed at FPF spanned the entire gage length of the sample.

The transverse cracks spanned the entire width of [90] layer, as observed in Figure 3.2. Stresses in a cross-ply laminate include the out-of-plane normal stress (σ_{33}) and the interlaminar shear stress (σ_{23}). The out-of-plane normal stress reaches a maximum at the center of [90] plies, while the interlaminar shear stress attains a maximum at the interface between [0] and [90] plies. The vertical cracks, running parallel to the length of the specimen, were observed within [90] plies away from the interface. Hence, these cracks are believed to be due to the out-of-plane normal stress rather than the interlaminar shear stress.

The edge of the sample was polished by an amount equal to the thickness of [90] ply and observed under a microscope. The resultant sample had only transverse cracks, with no vertical cracks as shown in Figure 4.11.This suggests that the vertical crack did not extend across the entire width of the sample. This is to be expected since out of plane normal stress reduces to zero away from the edge. During the laminate selection process (refer to section 3.3) it was found that in $[0/ 90_m]_s$, both transverse and vertical cracks were observed for m = 0.5 or more. While transverse cracks were the first mode of damage for m = 1. Vertical crack was the first damage mode for m = 0.5. The transverse residual stress (σ_{22}) in the [90] ply of $[0/90_m]_s$ samples is calculated and tabulated in

Table 4.3. It can be inferred that the residual stress in the [90] plies decreases with increase in [90] plies due to the increase in laminate thermal expansion coefficient.

Specimens with process induced damage were tested at constant strain rate at different temperatures to obtain the UTS of $[0/90_2]_s$ cross ply configuration. Results obtained from this test are tabulated in Table 4.1 and plotted in Figure 4.12. FPF could not be determined since the specimens had developed transverse as well as vertical cracks prior to testing due to process induced residual stress. Constant load rate tensile tests were carried out to obtain data on the growth of transverse crack density in the [90] plies as a function of stress, as shown in Figure 4.13. Due to process induced damage the transverse crack density in the manufactured test coupon was 6 cm^{-1}. Progressive increase in load caused the transverse crack density in the [90] plies to increase to a CDS of 10 cm^{-1}. Increase in load also caused an increase in the number of vertical cracks appearing between the transverse cracks to increase and in the length of the pre-existing vertical cracks. Figures 4.14 – 4.16 are representative example of various modes of damage that occurred during the loading. These micrographs were taken from tests carried out at different temperatures. At all temperatures, delamination, fiber splitting and transverse cracking in [0] layers were observed. Figure 4.14 shows the micrograph of a transverse crack formed between two vertical cracks. Delamination between [0] and [90] layer is shown in Figure 4.15. Partial splitting of the [0] layer subsequent to fiber breakage is observed in Figure 4.16.

The tensile test results at constant strain rate and constant load rate on the [0/90/0] and $[0/90_2]_s$ laminates point to the fact that increase in thickness of [90] plies reduces the CDS.

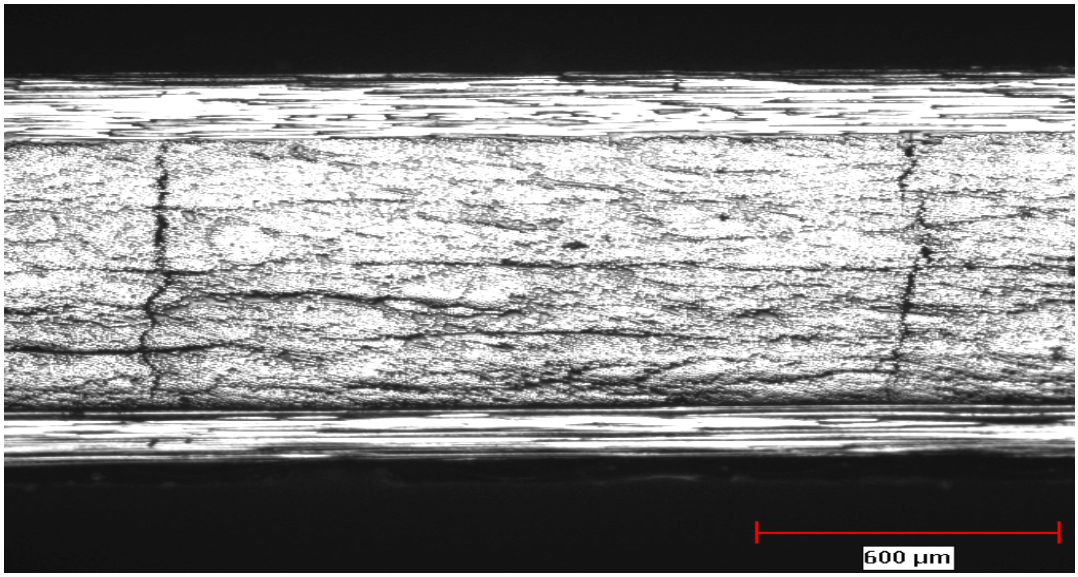

Figure 4.11: Edge of $[0/90_2]_s$ specimen after polishing, showing the disappearance of vertical crack

Table 4.3: Calculated residual stress values for $[0/90_m]_s$ laminate

Laminate type	**Residual Stress in 90^0 ply (MPa)**
[0/ 90/0]	86.5
$[0/ 90]_s$	85.5
$[0/ 90_2]_s$	82.0

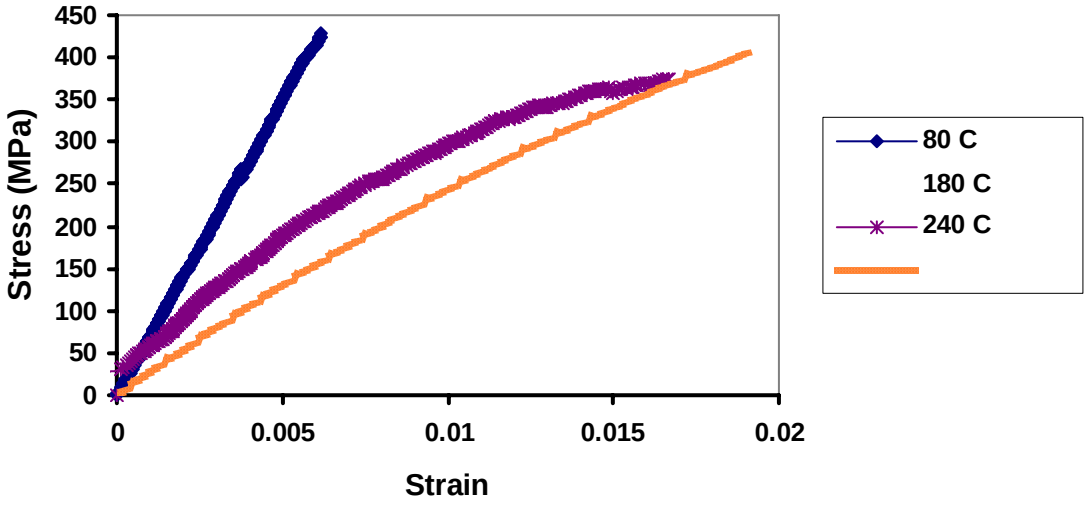

Figure 4.12: Stress-strain plot of $[0/90_2]_s$ at various temperatures

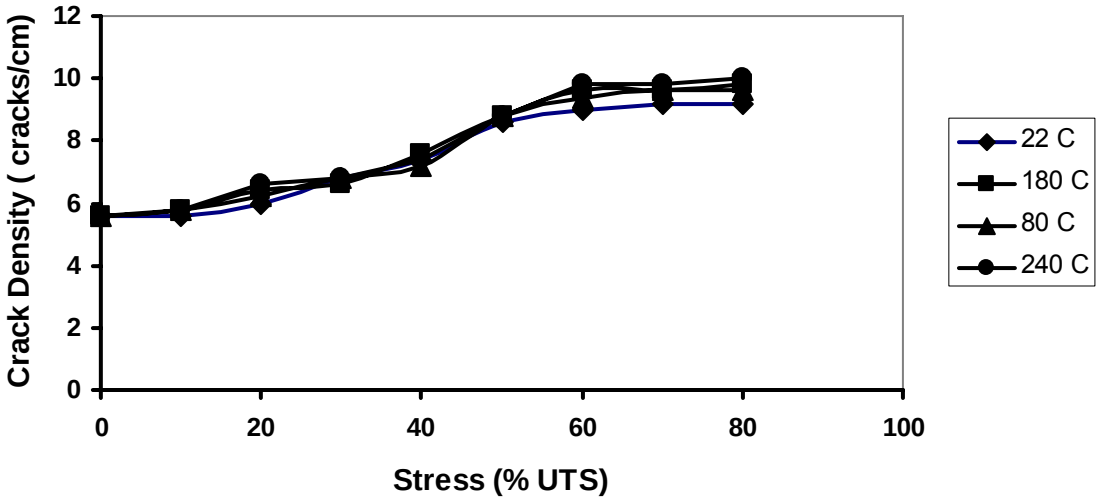

Figure 4.13: Crack density as a function of stress at various temperatures for $[0/90_2]_s$

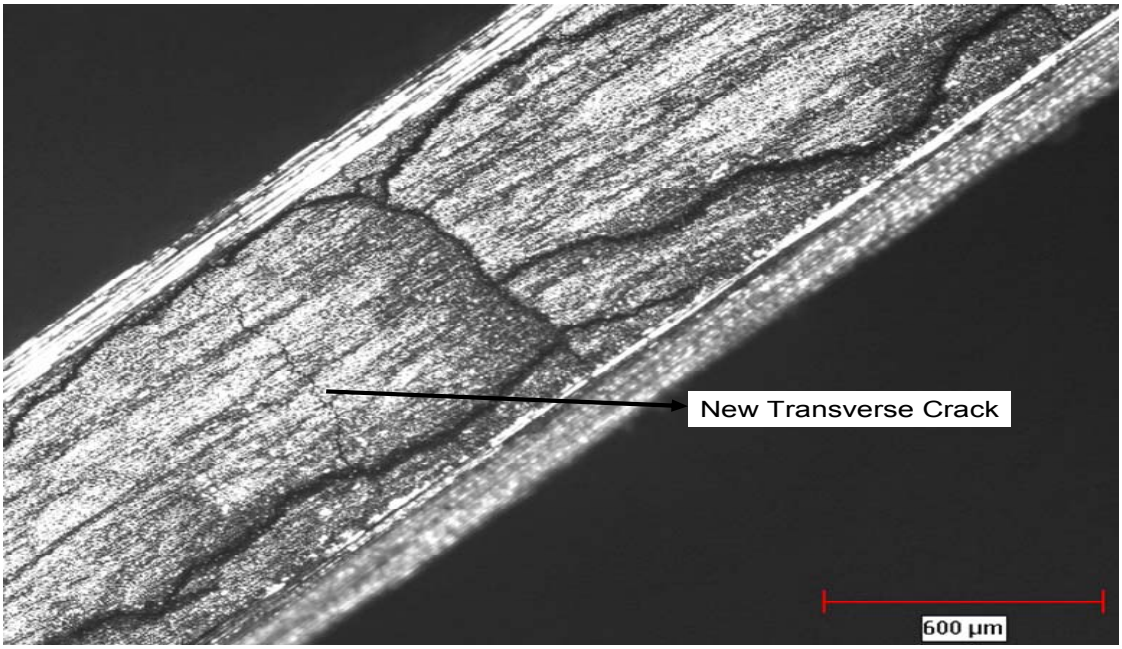

Figure 4.14: Micrograph showing the formation of new transverse crack between two vertical cracks at 50% UTS and 80^0C in a $[0/90_2]_s$ sample

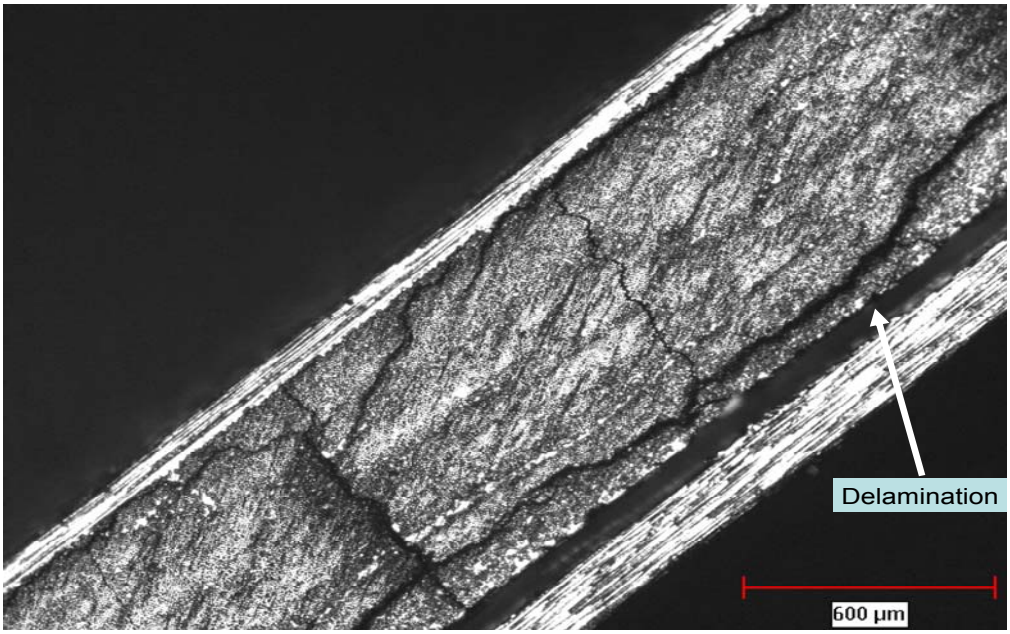

Figure 4.15: Micrograph showing delamination between [0] and [90] layer in $[0/90_2]_s$ sample at 60% UTS and 180^0C

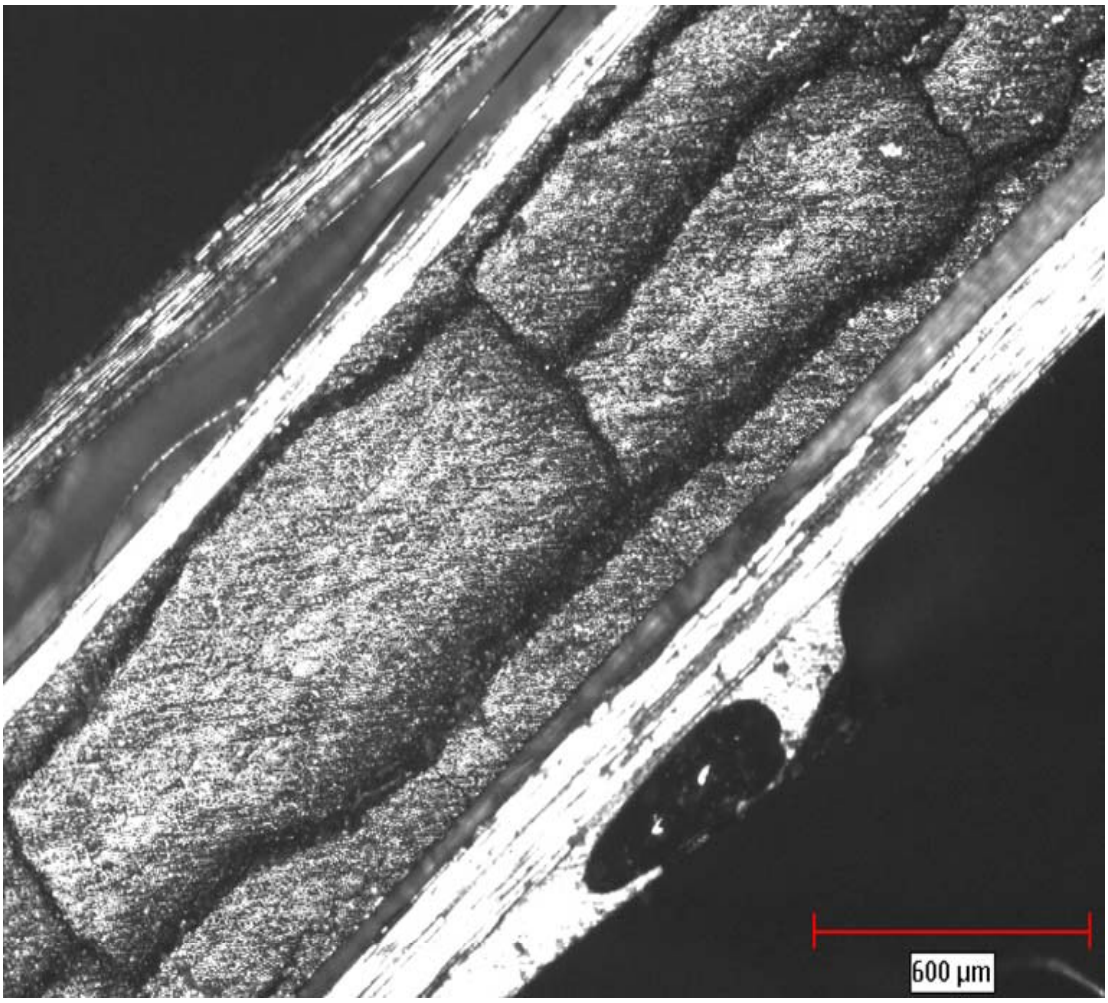

Figure 4.16: Micrograph of a partially split [0] ply in $[0/90_2]_s$ sample at 50% UTS and 240^0C

This can be clearly seen from the Figures 4.10 and 4.13, where the CDS values for the [0/90/0] laminate is around 16 cm^{-1}, while for the $[0/90_2]_s$ laminate it is around 9 cm^{-1}. Similar trend was also observed by Nairn [41] for three different cross-ply laminates, $[0/90]_s$ $[0/90_2]_s$ and $[0/90_4]_s$.

4.1.3 $[\pm 45/90_2]_s$ Laminate

Constant strain rate tensile tests were carried to obtain the UTS at various temperatures. The stress strain plot is shown in Figure 4.18, while the results are tabulated in Table 4.1. With increase in temperature from 80^0C to 240^0C the UTS decreased from 64 to 30 MPa.

FPF stresses were obtained by carrying out test at constant load rate. FPF stress values are tabulated in Table 4.2. At 80^0C, the FPF was 29 MPa. The first damage mode was the transverse crack in [90] ply, spanning the entire width of [90] layer shown in Figure 4.19. With increase in load to 50% UTS the transverse crack density increased while no damage was observed in any other ply. At 60% UTS the number of transverse crack increased to 15. A micrograph of the transverse crack is shown in Figure 4.20. Further increase in the stress to 70% UTS increased the number of transverse cracks to 28. At this load a vertical crack spanning the length of the specimen was observed in the [90] layer as shown in Figure 4.21. Additionally, the transverse crack at two locations in the [90] layer extended into [-45] layer, shown in Figure 4.22.

At 80% UTS the transverse crack density in [90] layer further increased, while there was no change in the [-45] layer. More vertical cracks appeared in [90] layer. Delamination between [45] and [-45] plies, shown in Figure 4.23, was observed over a

small region. Increasing the load to 90% UTS caused no further increase in the transverse crack density in the [90] layer. While a transverse crack in [-45] ply extended from the delaminated region in the interface between [45] and [-45] to cause delamination between [90] and [-45] plies as shown in Figure 4.23. The final fracture of the laminate was by separation through cracking of [45] and [-45] layers in the delaminated region.

Constant load rate tensile tests were also completed at 180^0C and 240^0C to obtain the FPF stress and the crack density data. FPF values at 180^0C ad 240^0C were 26 and 9 MPa respectively. Figure 4.24 shows the plot of crack density as a function of stress at various temperatures. This plot shows that with change in temperature the CDS values show a slight variation between 6 and 7 cm^{-1}. Additionally, there was no specific trend with increase in temperature from 80 ^{0}C to 240 ^{0}C. Damage modes at 180^0C and 240^0C were similar to those observed during testing at 80^0C, but they appeared at lower stress levels. Figures 4.25 and 4.26 show representative micrographs of various damage modes at 180^0C and 240^0C respectively.

4.1.4 Comparison of Time-Independent Damage Evolution in the Three Tested Laminates

A comparison of the crack density data for $[0/90_2]_s$ and $[\pm45/90_2]_s$ suggests that a decrease in outer-ply constraint would cause a decrease in the CDS. The constraint here is the modulus of the outer lying layer. It is generally seen that more the modulus of the outer lying layer, more is the constraint to the deformation of the inner layer. In this study [0] and [+45] are the outer layers with [0] layer having the higher modulus. The CDS values for all the three laminates at various temperatures are tabulated in Table 4.4.

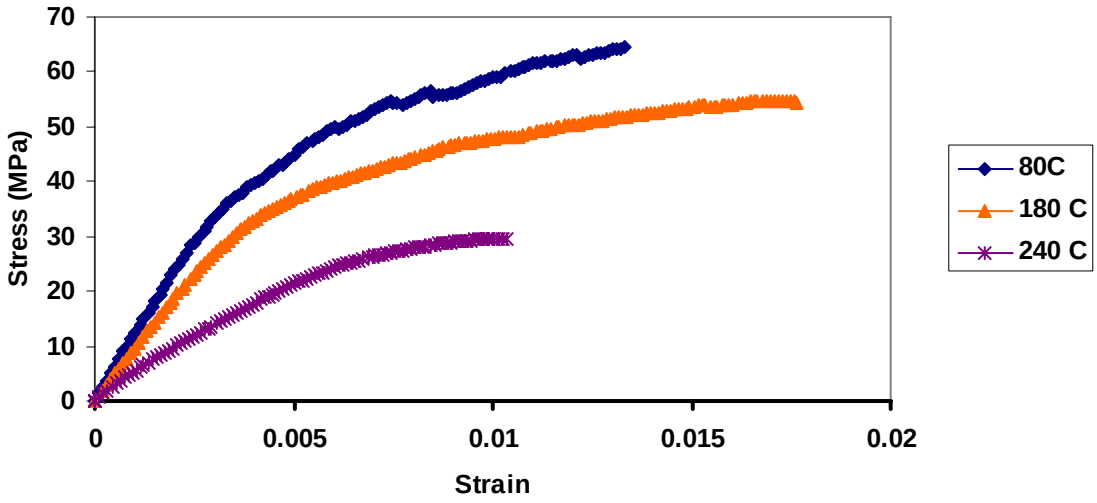

Figure 4.17: Stress strain plot of $[\pm 45/90_2]_s$ at various temperatures

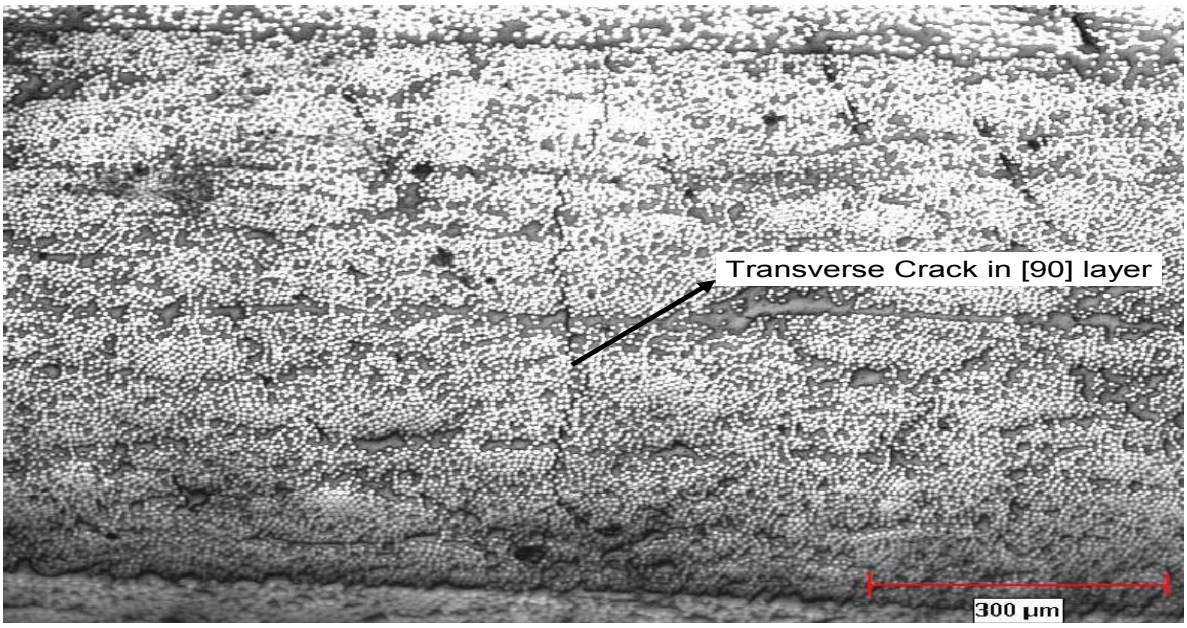

Figure 4.18: Micrograph of the first damage mode in $[\pm 45/90_2]_s$ specimen tested at 80^0C

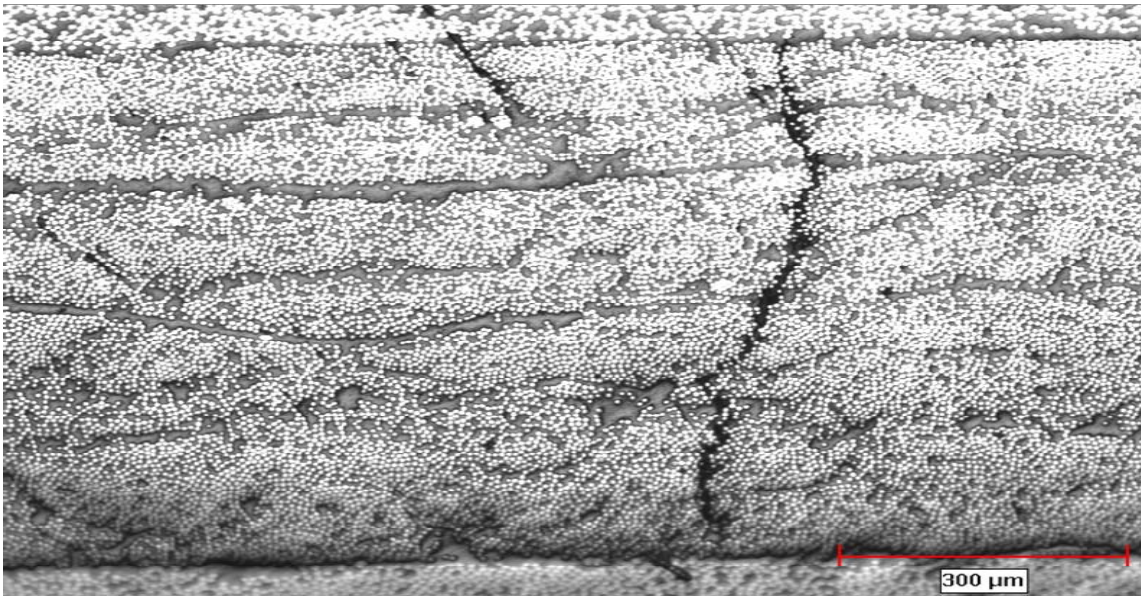

Figure 4.19: Micrograph of the transverse crack in [90] ply at 80^0C and 60% UTS in a $[\pm 45/90_2]_s$ sample

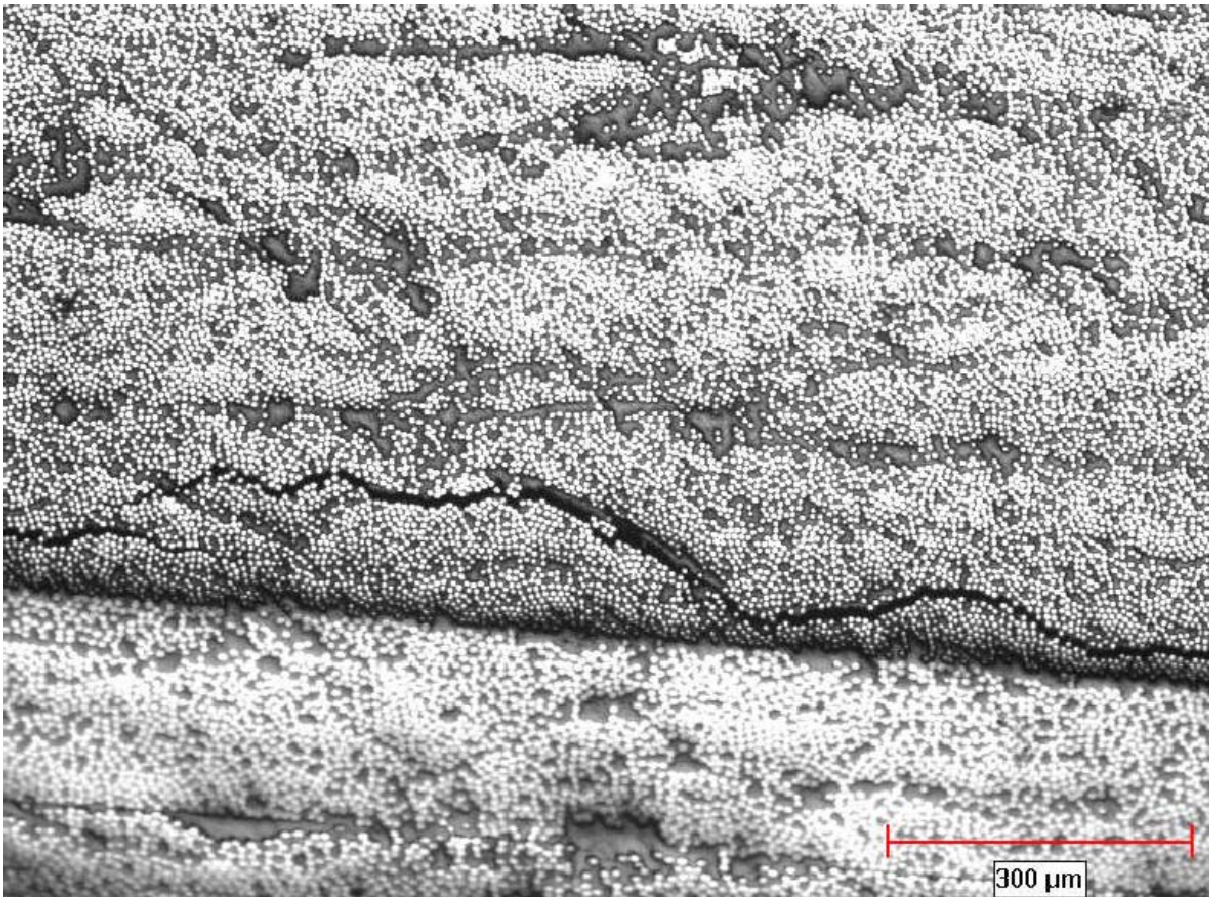

Figure 4.20: Micrograph showing vertical cracking in [90] ply at 80^0C and 70% UTS in a $[\pm 45/90_2]_s$ sample

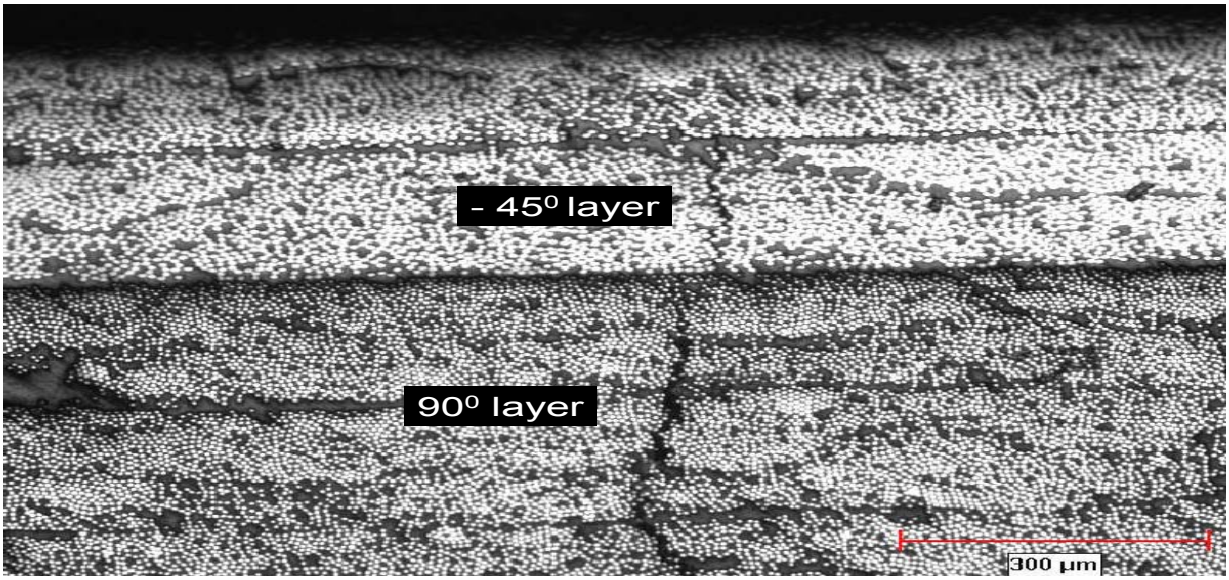

Figure 4.21: Micrograph showing transverse crack in the [-45] and [90] layer for a $[\pm 45/90_2]_s$ sample tested at 70% UTS and 80^0C

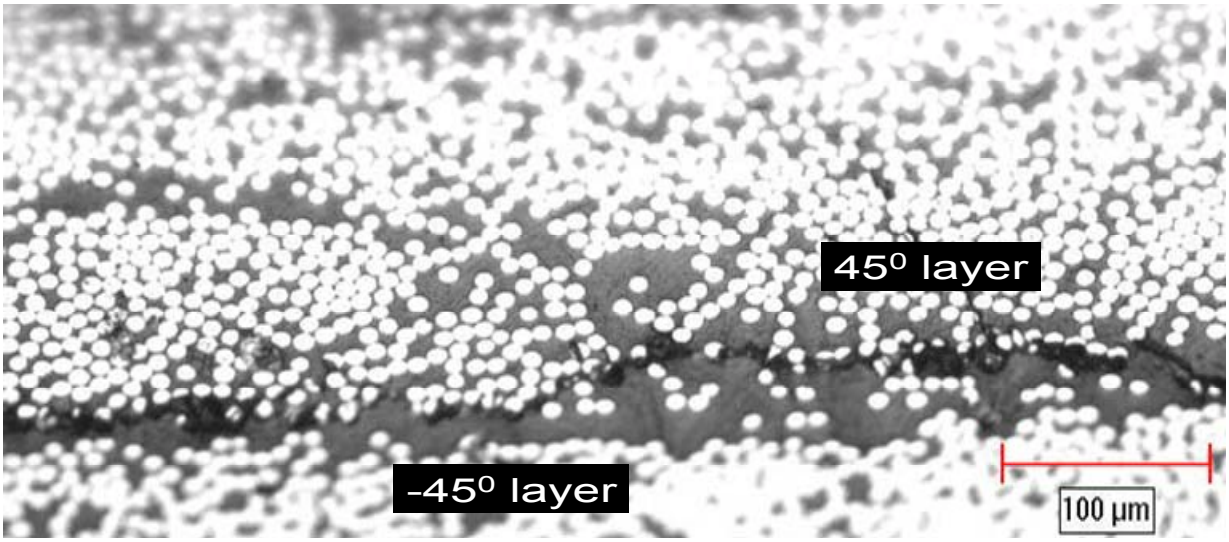

Figure 4.22: Micrograph showing the delamination between [45] and [-45] layers for $[\pm 45/90_2]_s$ sample tested at 80% UTS and 80^0C

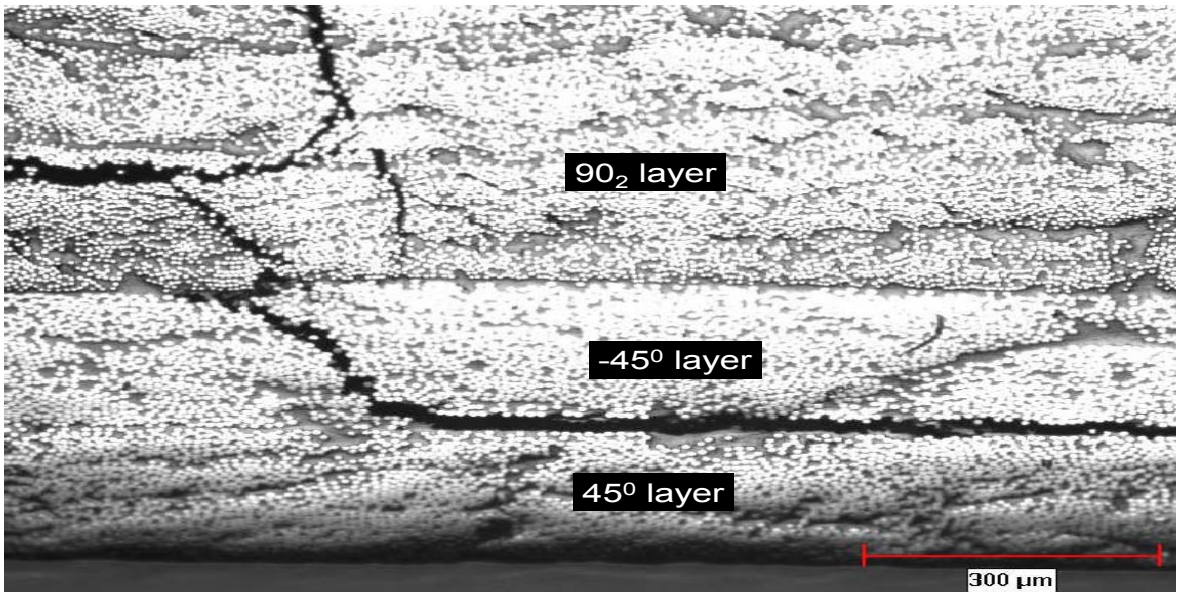

Figure 4.23: Micrograph showing delamination between various layers in $[\pm 45/90_2]_s$

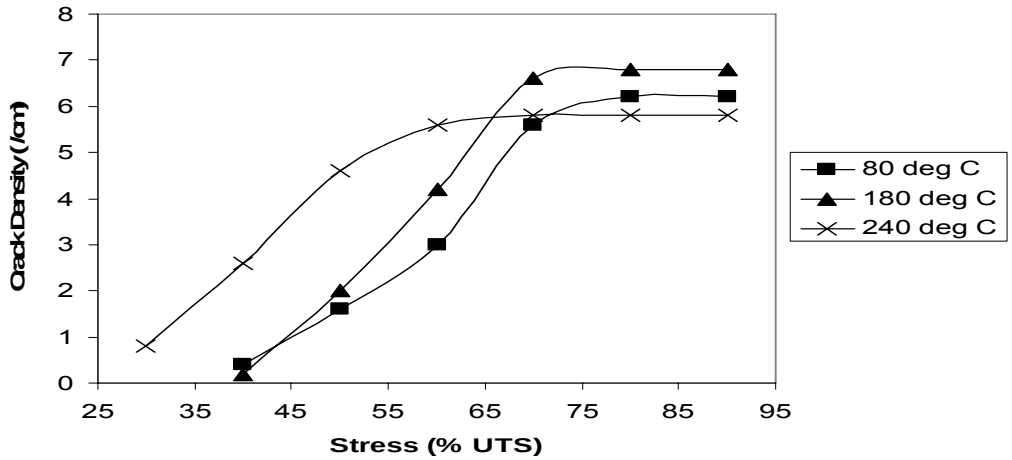

Figure 4.24: Plot of crack density as a function of stress at various temperatures for $[\pm 45/90_2]_s$ samples

Table 4.4: CDS values for all the laminates at different temperatures

LAMINATE	TEMPERATURE (^{0}C)	CDS (cm^{-1})
[0/90/0]	80	14
	180	16
	240	15
$[0/90_2]_s$	80	9
	180	9
	240	10
$[\pm45/90_2]_s$	80	6.5
	180	7
	240	6

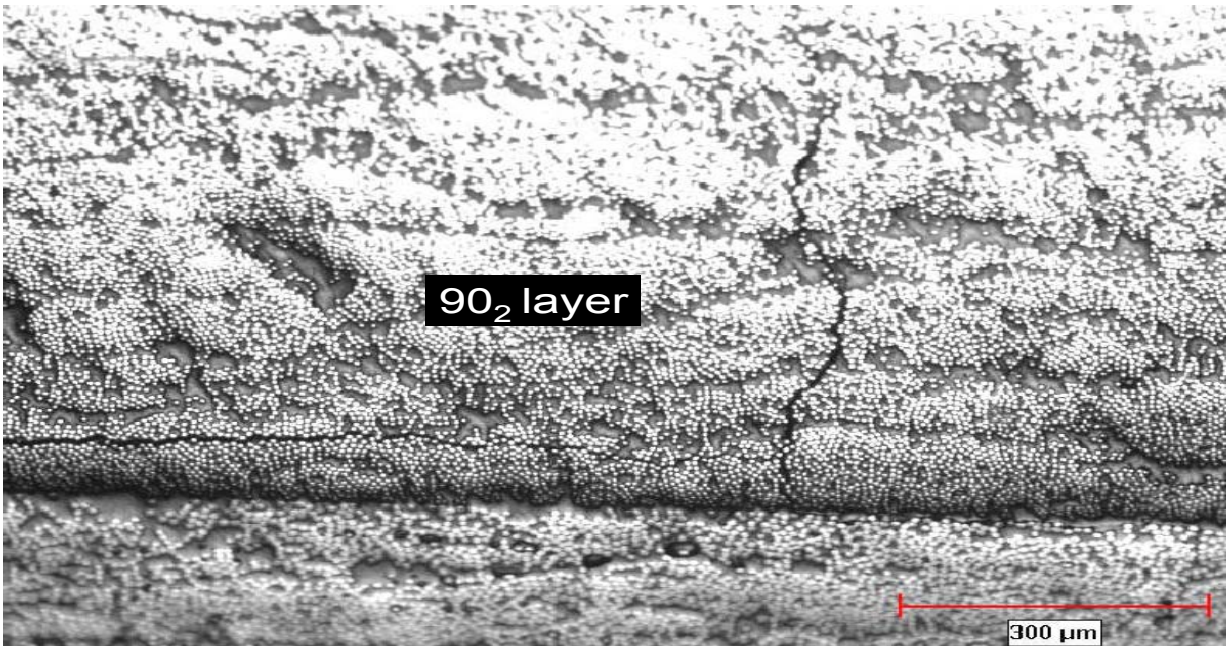

Figure 4.25: Micrograph showing transverse and vertical crack in the [90] layer tested at 60%UTS and 180^{0}C on a $[\pm 45/90_2]_s$ sample

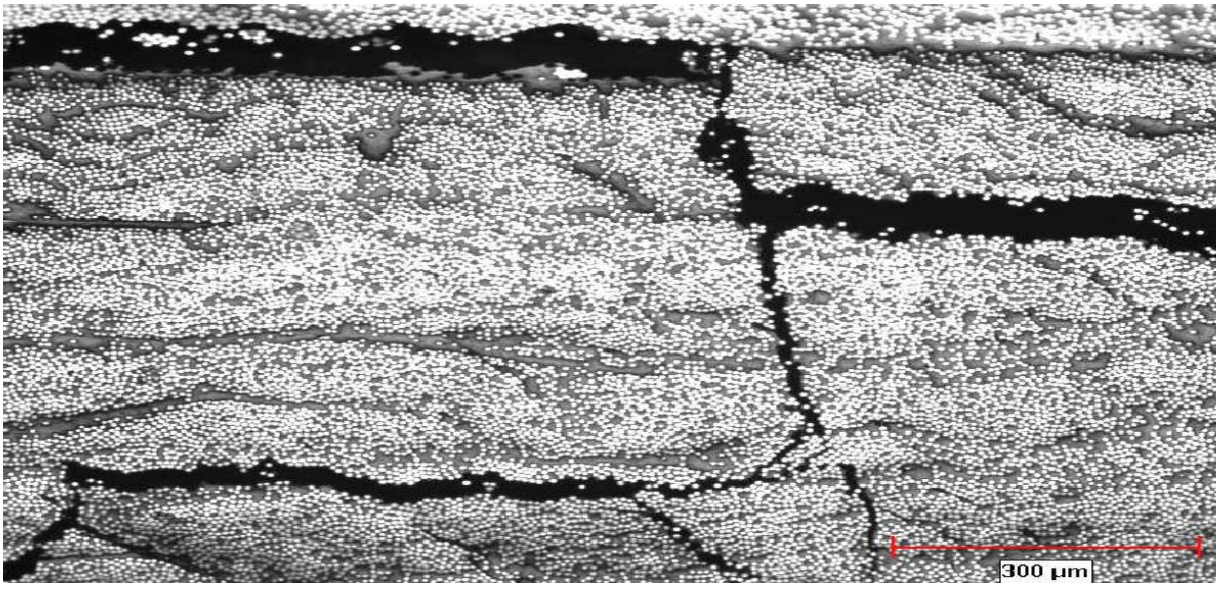

Figure 4.26: Micrograph showing various damage modes in $[\pm 45/90_2]_s$ tested at 90% UTS and 240^{0}C

In the present work the CDS decreased from above 10 to 7 cm^{-1}. The results also indicate the tendency for time independent transverse cracking to decrease and that of vertical cracking to increase with decrease in thickness of [90] plies and increase in outer ply constraint. This is in good agreement with the results obtained by Nairn et al. [42].

4.2 CREEP RUPTURE TEST RESULTS

4.2.1 [0/90/0] Laminate

Creep rupture tests were carried out at constant stress to determine the time to failure of the sample as well as to study the time dependent evolution of various damage modes. Figure 4.27 shows the rupture time of [0/90/0] composite as a function of applied stress at various temperatures. With increase in stress and temperature the rupture time decreased. Hence, temperature and stress accelerated the failure of the composite. It can be observed that at 80^0C, under a stress level of 85% UTS the rupture time of the composite was 212 hrs, whereas under a stress level of 95% UTS the creep rupture time reduced substantially to 74 hrs. At 240^0C, under a stress level of 70% UTS the rupture time was 85 hrs, while under a stress level of 90% UTS the creep rupture time reduced to 22 hrs. At all temperatures the final failure of the sample was caused by a broom like fracture in [0] ply, as shown in Figure 4.28.

4.2.2 $[0/90_2]_s$ Laminate

Figure 4.30 shows the rupture time of $[0/90_2]_s$ composite as a function of applied stress at various temperatures. There is a significant difference between the rupture times for

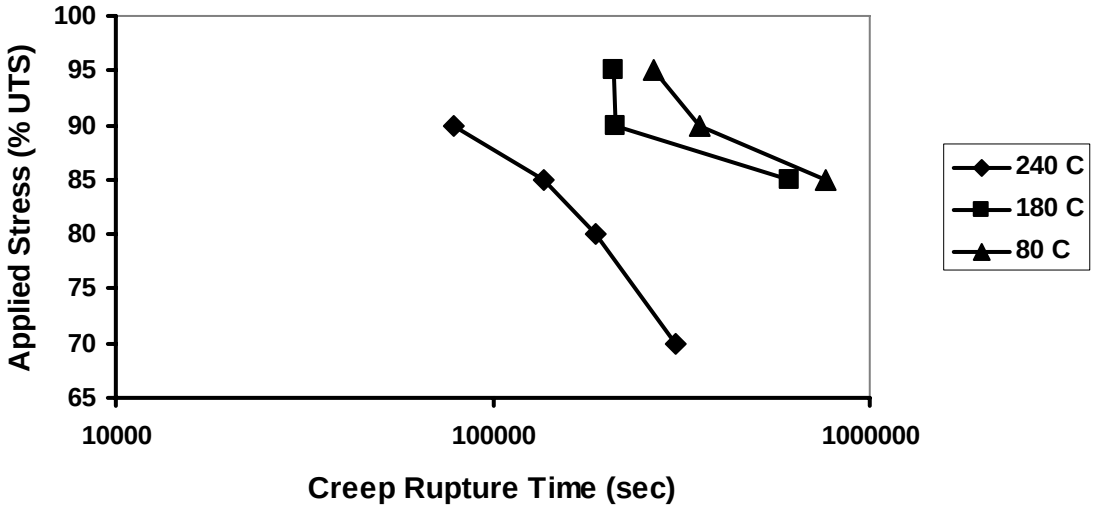

Figure 4.27: Creep rupture time of [0/90/0] samples at various stress levels and temperatures

Figure 4.28: Fractured [0/90/0] sample after creep rupture testing at 85% UTS and 240^0 C

samples tested at 80^0C and other two temperatures, whereas the difference between the rupture times at 180^0 C and 240^0 C is not noticeable. The reason for this anomaly could be the presence of process induced damage, causing the various damage modes to interact differently at higher temperatures when tested over a long period of time. At 180^0 C at a stress level of 40% UTS the rupture time of the $[0/90_2]_s$ composite was 7800 minutes, whereas at a stress of 90% UTS the creep rupture time was 16 minutes. At 240^0 C, creep rupture tests beyond 85% UTS was not possible due to fracture of samples immediately upon loading caused by the presence of process induced damage. The decrease in the thickness of the [90] layer caused an increase in the creep rupture time at all temperatures. This is clearly observed in Figures 4.27 and 4.29.

The final failure at all temperatures was the broom like fracture in the [0] ply, with pieces of [90] layer held between the split segments of [0] ply, as shown in Figure 4.30.

4.2.3 $[\pm 45/90_2]_s$ Laminate

The rupture time of $[\pm 45/90_2]_s$ composite as a function of applied stress at various temperatures is shown in Figure 4.31. The plot shows a decrease in the creep rupture time with increase in stress and temperature. This trend is similar to the trend observed in the [0/90/0] samples, while the $[0/90_2]_s$ samples showed no conclusive trend at high temperatures.

The final fracture, shown in Figure 4.32, at all temperatures was by separation through transverse cracking of [-45] and [+45] layers in the [90] and [-45] delaminated region.

The creep rupture results for individual laminates are reported in Figures 4.33 – 4.35 comparing the three laminates at one constant temperature. For a given % UTS, $[0/90_2]_s$ specimens fractured in the shortest time and [0/90/0] specimens were the last to fail. Creep rupture times for $[\pm 45/90_2]_s$ were between the creep rupture times for the other two laminates.

4.3 TIME DEPENDENT DAMAGE PROGRESSION

4.3.1 [0/90/0] Laminate

When a [0/90/0] sample was loaded to 20% UTS and 240^0 C, the (vertical cracking) FPF was observed after 112 hrs despite the fact that FPF stress measured during tensile testing at 240^0 C was 28% UTS. This type of delayed transverse cracking of the [90] ply has been reported by Raghavan and Meshii [30]. However, delayed vertical cracking of the [90] ply is reported here for the first time. Hence it would be appropriate to conclude that the FPF by any damage mode and the corresponding stress is time dependent.

For creep rupture stress levels beyond 20% UTS damage modes observed in this laminate were the vertical crack spanning the entire gage length and a few transverse cracks in the [90] ply at all temperatures. Prior to starting the test at 80^0 C the samples were crack free. Tests were carried out at three different stress levels of 85, 90 and 95% UTS. During loading to the desired stress level a vertical crack spanning the entire gage length was introduced into the [90] plies. Transverse cracks were also introduced and the initial transverse crack density was around 2.8 cm^{-1} for 85 and 90% UTS, while it was

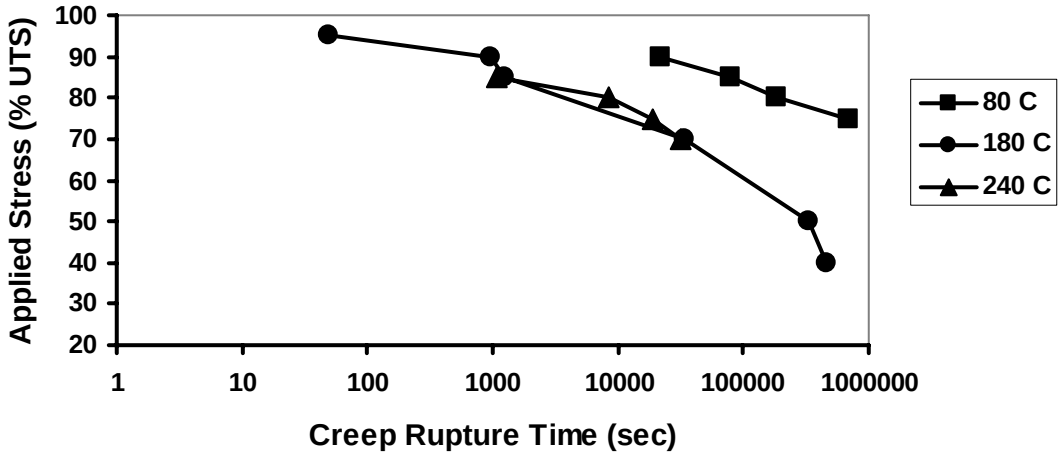

Figure 4.29: Creep rupture time of $[0/90_2]_s$ samples at various stresses and temperatures.

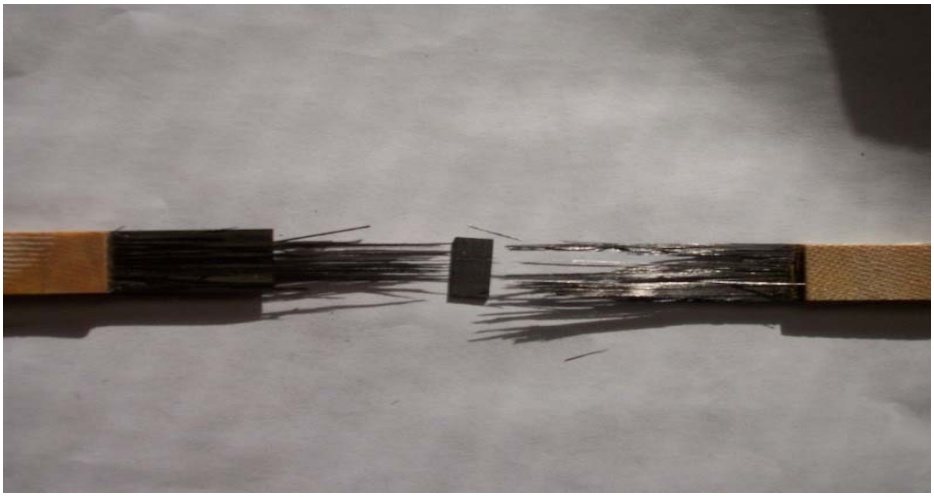

Figure 4.30: Fractured $[0/90_2]_s$ sample after creep rupture testing at 80^0C and 85% UTS

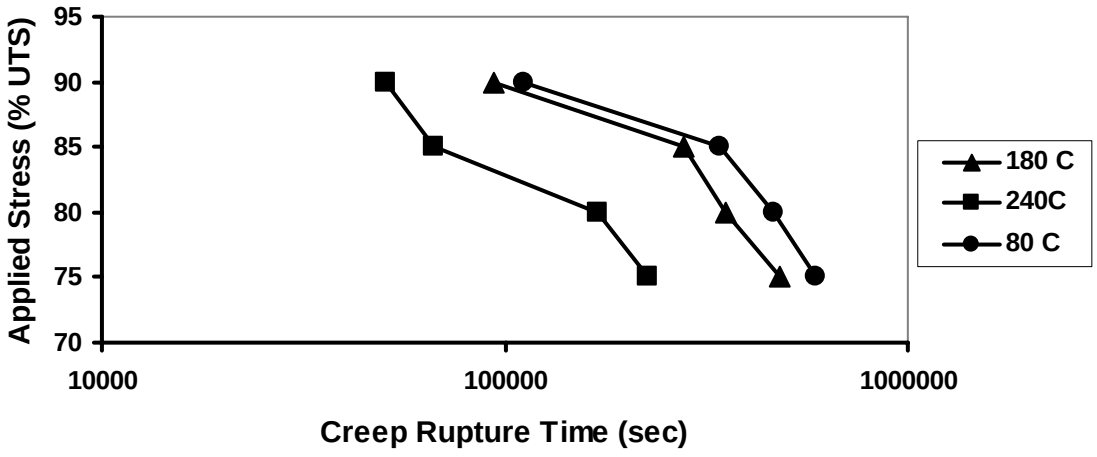

Figure 4.31: Creep rupture time of $[\pm 45/90_2]_s$ samples at various stresses and temperatures.

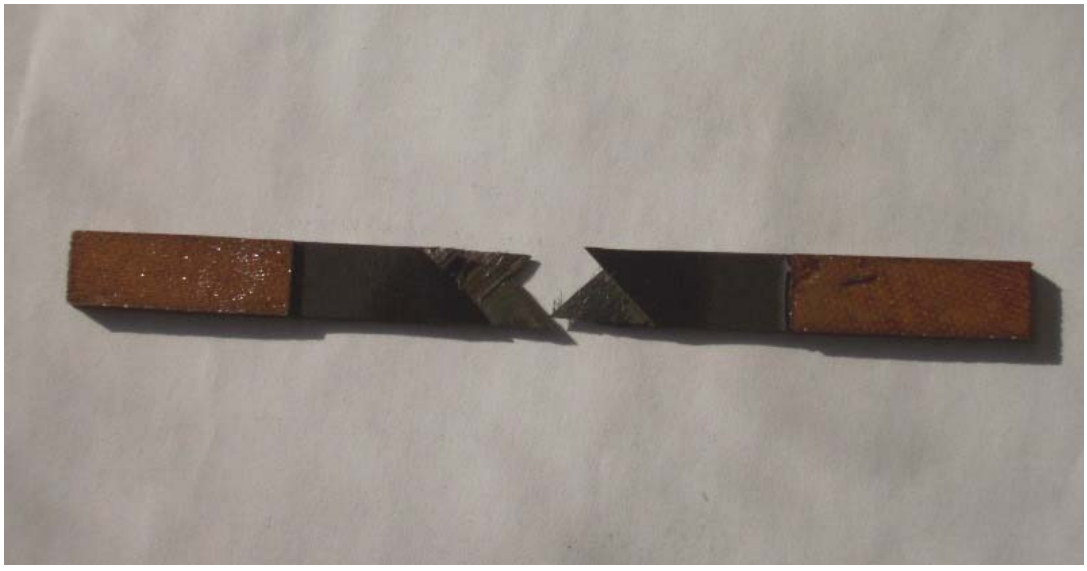

Figure 4.32: Fractured $[\pm 45/90_2]_s$ sample after creep rupture testing at 180^0C and 90 % UTS

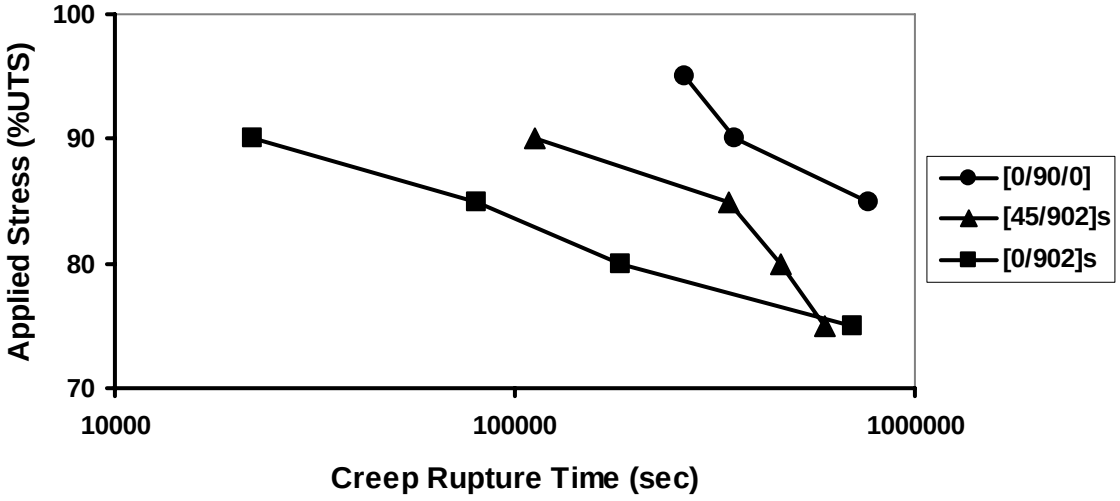

Figure 4.33: Creep Rupture data for three laminates at 80^0 C

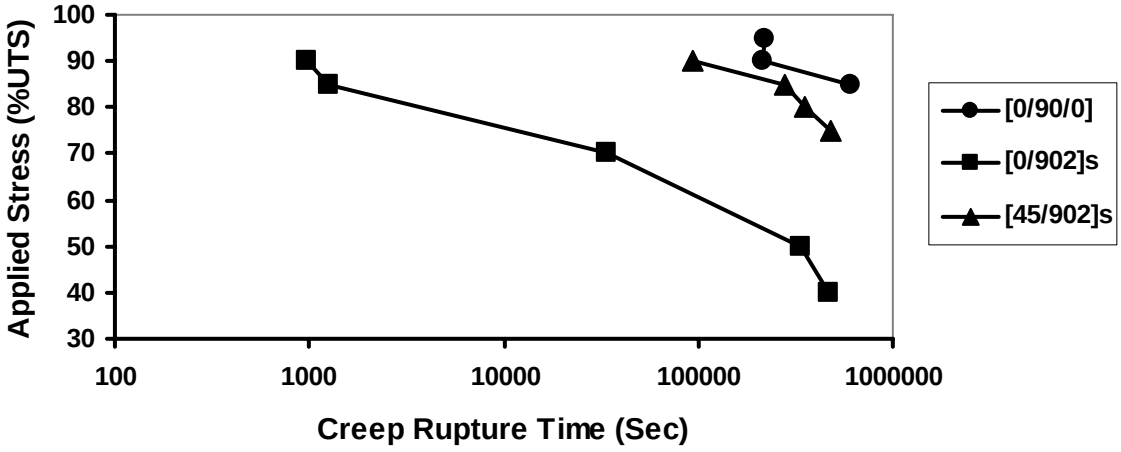

Figure 4.34: Creep rupture data for three laminates at 180^0 C

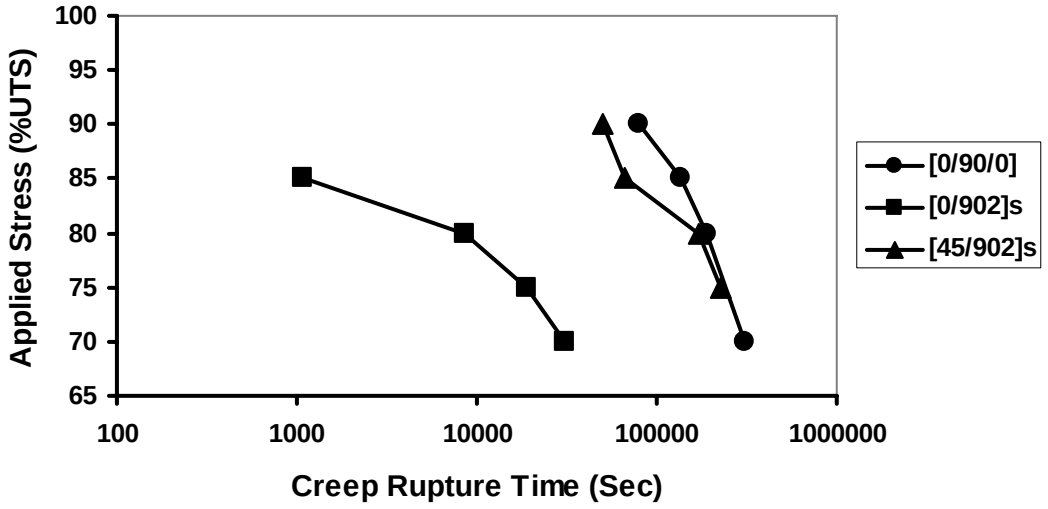

Figure 4.35: Creep rupture data for three laminates at 240^0 C

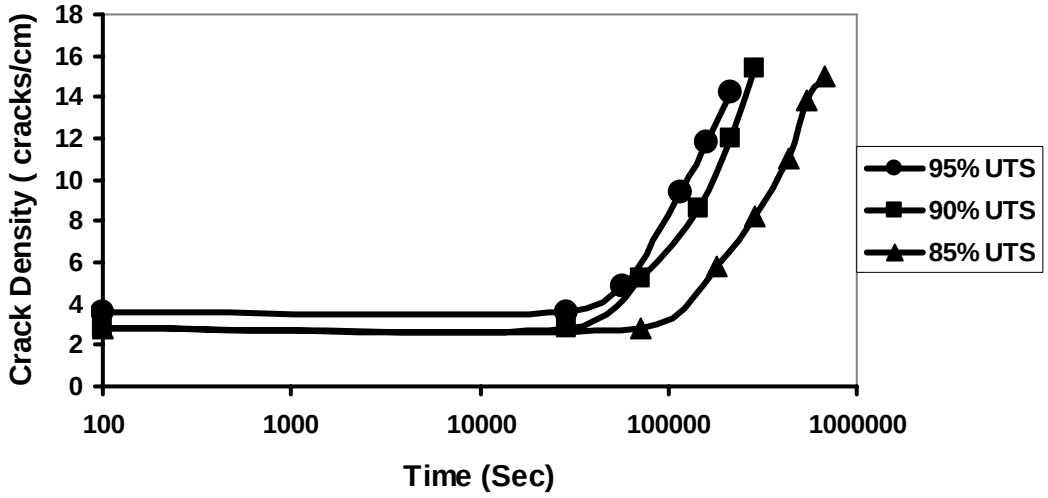

Figure 4.36: Time dependent evolution of transverse crack density in [0/90/0] at 80^0 C

around 3.6 cm^{-1} for 95% UTS. With increase in time at each stress level the transverse crack density increased. A plot of the increase in transverse crack density with time for the three stress levels at 80^0 C is shown in Figure 4.36. Samples were initially unloaded for damage observation after 8 hours and thereafter approximately every 8 hours. At a stress level of 85% UTS the sample was tested for more than 190 hours, while at 90% UTS the sample was tested for more than 80 hrs. At a stress level of 95% UTS the sample was tested for the least amount of time, approximately 66 hrs. At the time of fracture all the samples had reached the CDS value of around 16 cm^{-1}.

At the first point of observation (approx. after 8 hrs) vertical cracks along with the transverse cracks were observed, similar to Figures 4.3 and 4.4. At the second and the third point of observation (16 and 24 hrs) the transverse crack density increased. Around the third observation point more than one vertical crack was seen similar to Figure 4.5. A micrograph of the damage seen in the sample after testing for 80 hrs at 85% UTS is shown in Figure 4.37. The transverse crack density increased with time and reached the CDS measured during tensile testing. The evolution of various damage modes with time was very similar to that observed during tensile testing.

At 180^0 C tests were carried out at 85, 90 and 95% UTS. Similar to tests 80^0 C the first mode of damage was the vertical crack spanning the length of gage length, with some transverse cracks. The initial transverse crack density (measured after 100 sec) was around 3.6 cm^{-1} at a stress level of 85% UTS, 6.4 at 90% UTS, while it was around 5.6 cm^{-1} at 95% UTS. A plot of the changing crack density with time for the three stress levels at 180^0 C is shown in Figure 4.38. The specimen failed after 78 hrs at 85 % UTS after reaching the CDS of approximately 16 cm^{-1}. At 90% UTS the CDS was reached

after about 36 hours, while at 95% UTS the CDS was reached after 48 hours. A possible reason for this counter intuitive behavior may be the lower starting crack density for the 95% UTS sample when compared to the 90% UTS sample. Similar to the damage evolution at 80^0 C, transverse crack density increased with time and so also the vertical crack. A micrograph of the damage after 56 hrs of testing at 85% UTS is shown in Figure 4.39.

At 240^0 C tests were carried out at 70, 80, 85 and 90% UTS. A plot of the crack density with time is shown in Figure 4.40. At 70, 80 and 85% UTS the samples failed after reaching the CDS of 17 cm^{-1}. At 90% UTS the sample failed at a transverse crack density of 14 cm^{-1}, which is thought to be due to premature failure of the sample.

The reported CDS values for the creep rupture tests are an average of the values obtained at each temperature for different stress levels. The CDS values obtained during the creep rupture tests are compared with those obtained during the tensile testing in Table 4.5 for various test temperatures. Since both values are similar it can be concluded that (a) ultimate failure mode of the laminate is same in both constant load rate and constant strain rate conditions. (b) CDS of the sample may be used in predicting the creep rupture time.

In addition to transverse cracking, delamination between the [0] and [90] plies, as shown in Figure 4.8, was also observed before the final fracture. Also seen was the fiber fracture in the [0] ply, as shown in Figure 4.41. The fiber fracture in the [0] ply along with partial delamination appeared after 8 hrs in the sample loaded to a stress level of 95% UTS. For the sample loaded to 85% UTS fiber fracture and partial delamination appeared after 16 hrs of testing. It took 18 and 30 hrs for these two damages (fiber fracture and partial

Table 4.5: Comparison of the Tensile and Creep rupture CDS values

LAMINATE	TEMPERATURE (^{0}C)	Tensile CDS (cm^{-1})	Creep Rupture CDS (cm^{-1})
[0/90/0]	80	14	15
	180	16	17
	240	15	16
$[0/90_2]_s$	80	9	9
	180	9	9
	240	10	9
$[\pm45/90_2]_s$	80	6.5	7
	180	7	7
	240	6	6

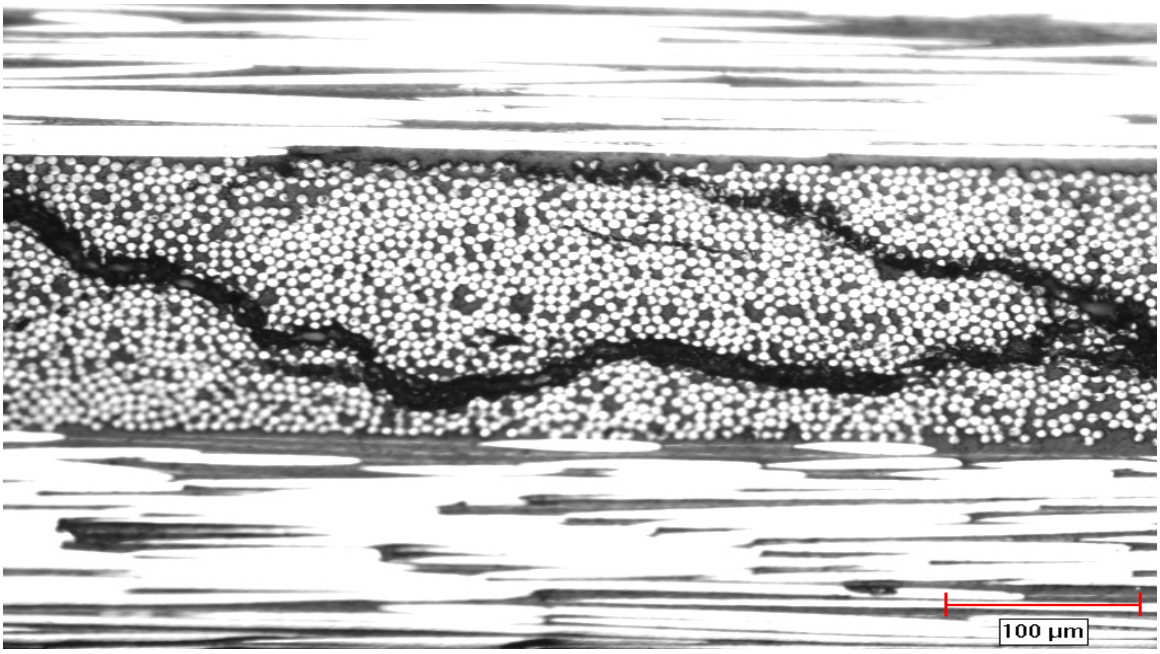

Figure 4.37: Damage in the [0/90/0] sample tested at 80^0C and 85% UTS after 80 hrs

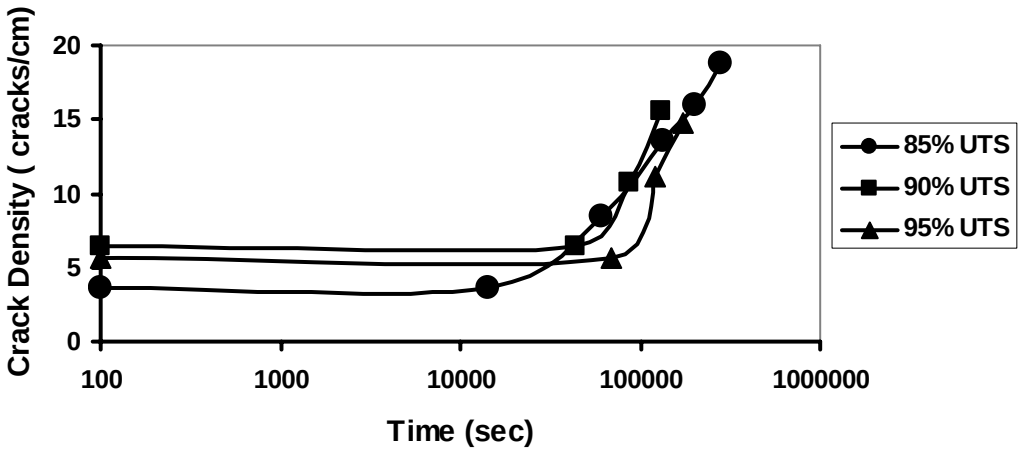

Figure 4.38: Time dependent evolution of transverse crack density in [0/90/0] at 180^0 C

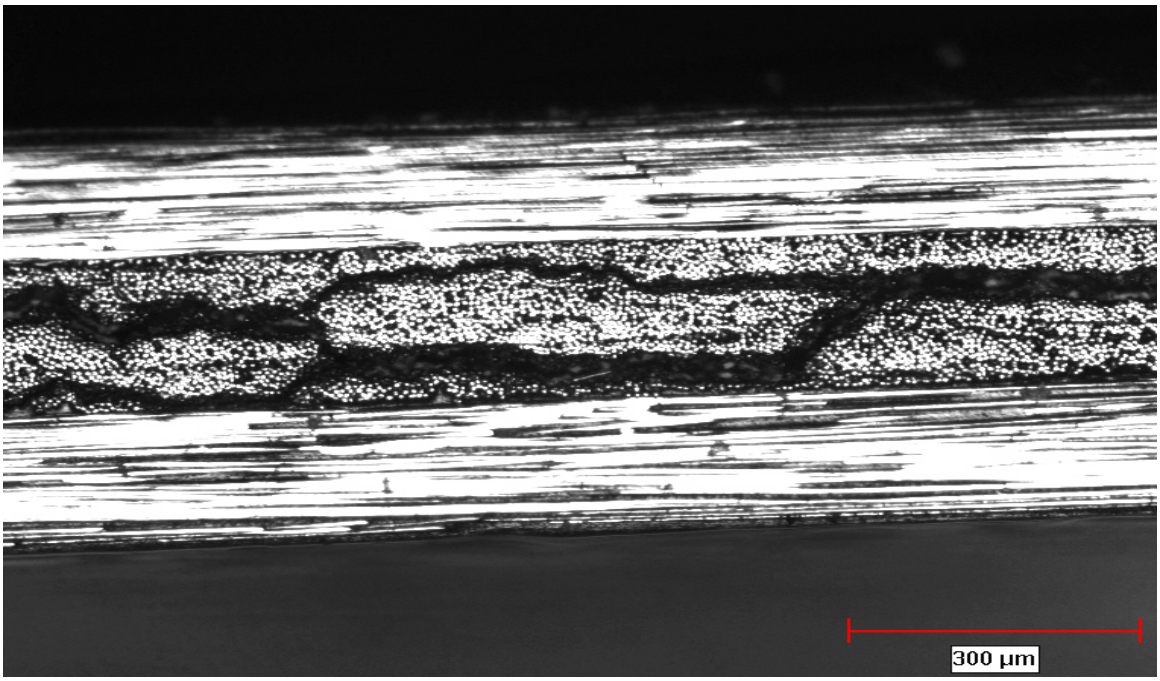

Figure 4.39: Damage in [0/90/0] sample tested at 180^0 C and 85 % UTS after 56 hrs

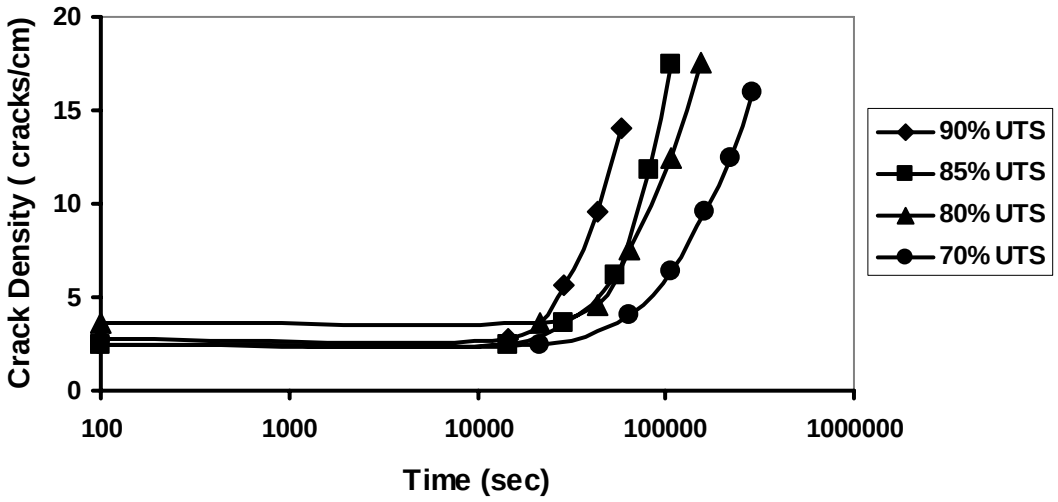

Figure 4.40: Time dependent evolution of transverse crack density in [0/90/0] at 240^0 C

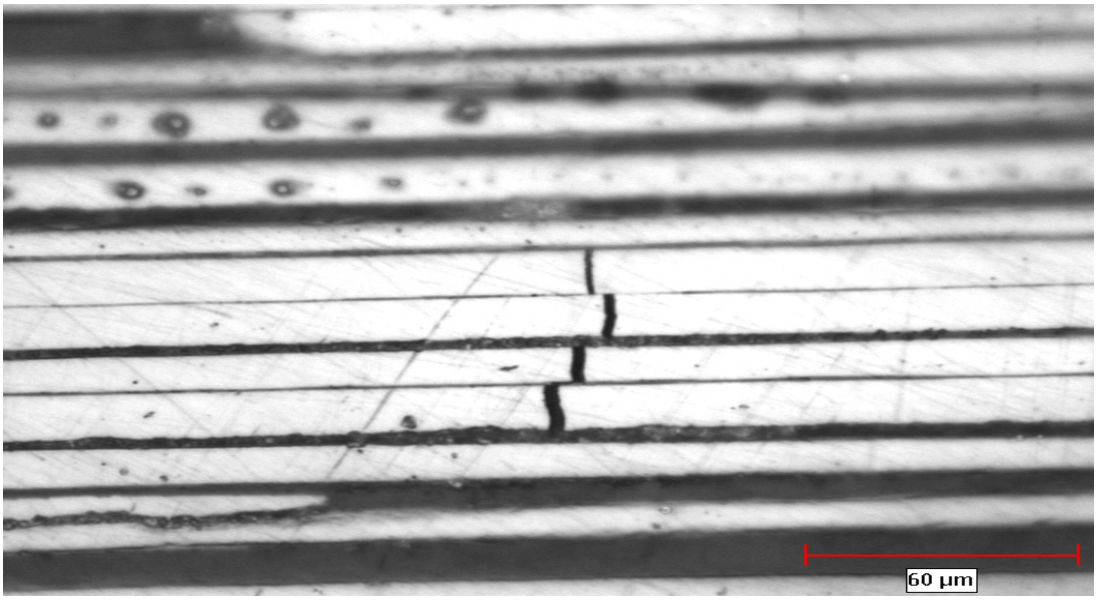

Figure 4.41: Fiber fracture in the [0] ply at 80 % UTS and 240^0 C after testing for 18 hrs in a [0/90/0] sample

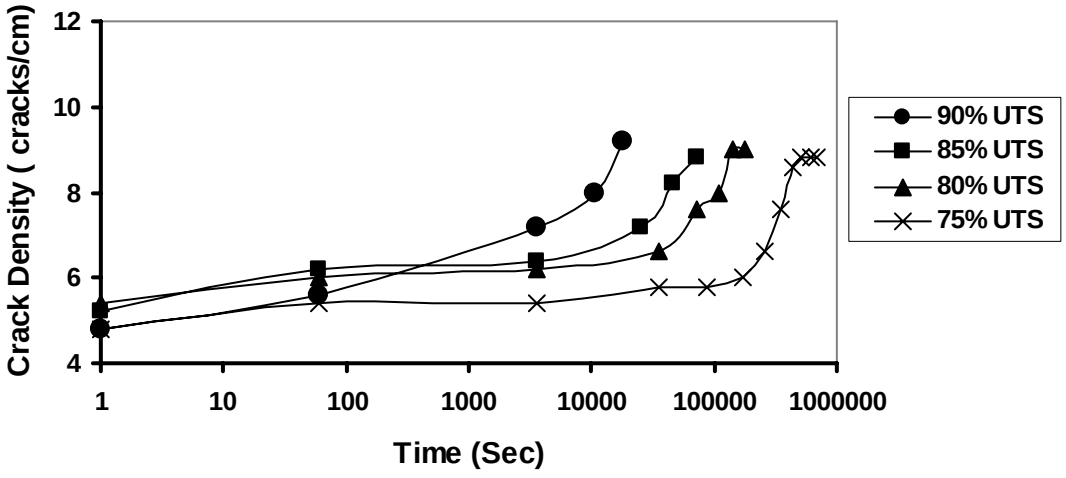

Figure 4.42: Time dependent evolution of transverse crack density in $[0/90_2]_s$ at 80^0 C

delamination) to appear for the sample loaded to 80 and 70% UTS respectively.

4.3.2 $[0/90_2]_s$ Laminate

At 80^0 C tests were carried out at 75, 80, 85 and 90% UTS. Prior to testing these samples had transverse and vertical cracks caused during processing, with a transverse crack density of around 5 cm^{-1}. With progress in time at all stress levels, the transverse crack density increased, similar to the trend observed in the [0/90/0] samples. A plot of the crack density versus time at 80^0 C is shown in Figure 4.42. The sample loaded to 75% UTS reached the CDS value of approximately 10 cm^{-1} after nearly 120 hours. But the final fracture occurred after 190 hours of testing. The reason for this behavior is not understood at the moment.

At a stress level of 80% UTS the CDS value was reached after 50 hours of testing. The sample failed after some time. For samples tested at 85 and 90% UTS the CDS values were reached at 20 and 5 hours respectively. From Figure 4.42 it is apparent that the CDS value obtained during creep testing was around 10 cm^{-1}, which is comparable to the CDS value of 9 cm^{-1} obtained during tensile testing.

At all stress levels with increase in transverse crack density the number of vertical cracks appearing between the transverse cracks as well as the length of the vertical cracks increased. Other modes of damage observed were delamination between the [0] and [90] plies, partial splitting of [0] layer, shown in Figure 4.43. Delamination on one side of the sample and fiber splitting in [0] layer occurred after 10 hours in samples tested at 75 and 80% UTS. The delamination on the other side occurred after 28 hours. For samples tested at 85% UTS delamination and fiber splitting occurred after 7 hours of testing.

At 180^0 C samples were tested at 40, 50, 70, 85 and 90% UTS. At 40, 50 and 70% UTS the CDS value (10 cm^{-1}) was reached after 108, 84 and 7 hours of testing respectively. The samples at 85 and 90% UTS fractured before attaining CDS. A plot of the crack density evolution with time is shown in Figure 4.44. Similar to 80^0 C, various damage modes like vertical cracking in the [90] ply, delamination between [0] and [90] ply and partial splitting of [0] layer was observed. At 50% UTS partial delamination between [0] and [90] ply and splitting of [0] layer was observed after 10 hours of testing, while delamination on the other side was observed after 36 hrs of testing. At 70% UTS partial delamination was observed after 2 hrs of testing, as shown in Figure 4.45. Delamination on the other side of the sample was observed after 5 hours of testing.

At 240^0 C samples were tested at 70, 75, 80 and 85% UTS. A plot of the crack density evolution with time is shown in Figure 4.46. The CDS values for 70, 75 and 80% UTS samples were reached after 7, 4 and 1 hour respectively. Similar to results at 80^0 C and 180^0 C damage modes such as vertical cracking, delamination between [0] and [90] ply and splitting of the [0] layer were also observed in samples tested at 240^0 C. At 70% UTS delamination between [0] and [90] layer on both sides of the sample was observed after 4 hours of testing, partial splitting of the [0] ply was also observed at this point of observation. Similar damage mode evolution was observed after 2 hrs at a stress level of 75% UTS.

The CDS values observed during the creep rupture testing was similar to those obtained during tensile testing for all temperatures. It was around 9 cm^{-1} in both the cases, as shown in Table 4.5.

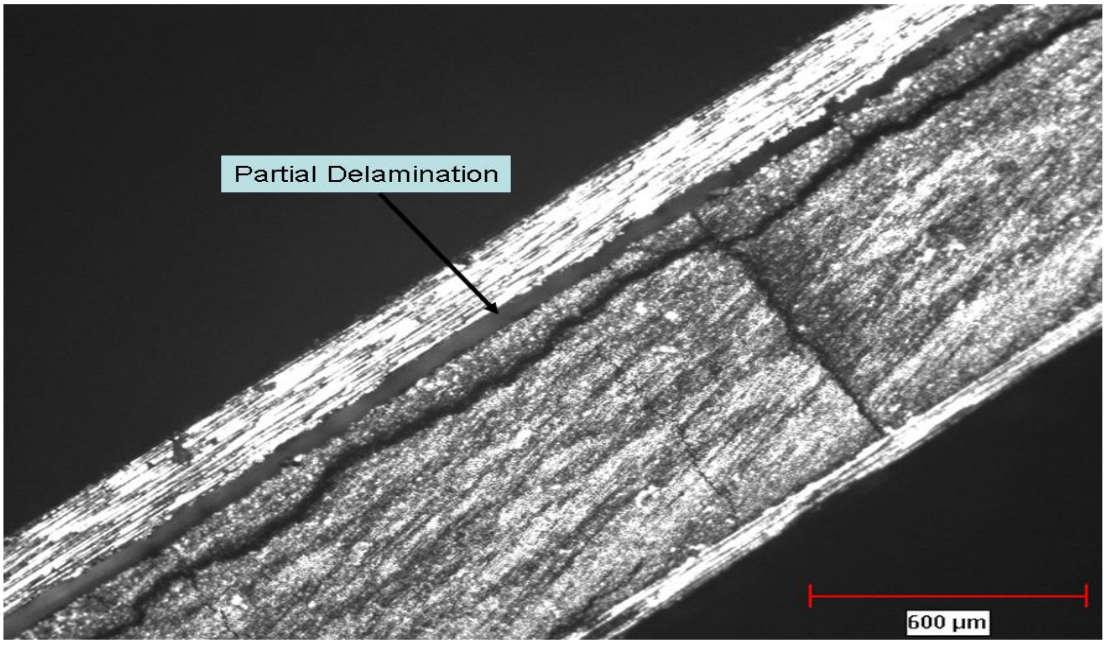

Figure 4.43: Partial delamination between [0] and [90] layer of $[0/90_2]_s$ sample tested at 80 ^{0}C and 85% UTS after 7 hours

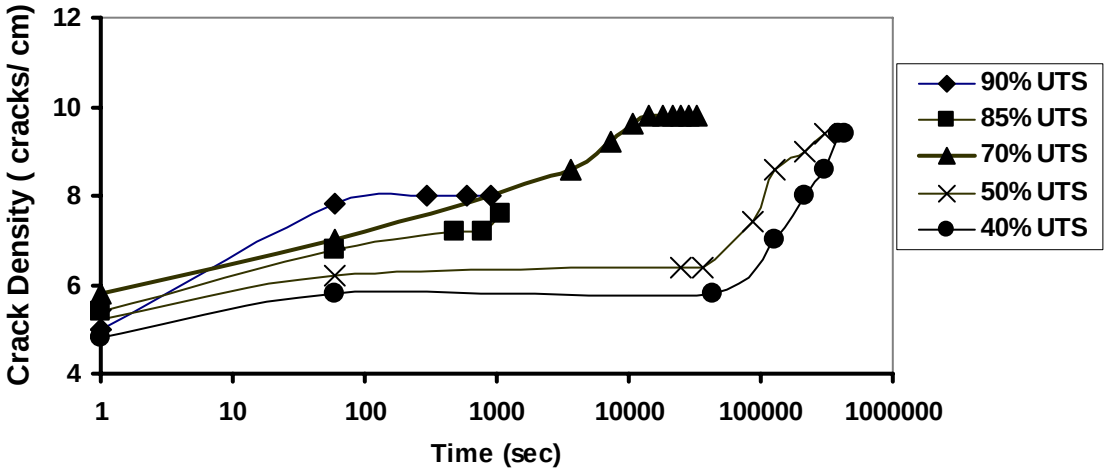

Figure 4.44: Time dependent evolution of transverse crack density in $[0/90_2]_s$ at 180^0 C

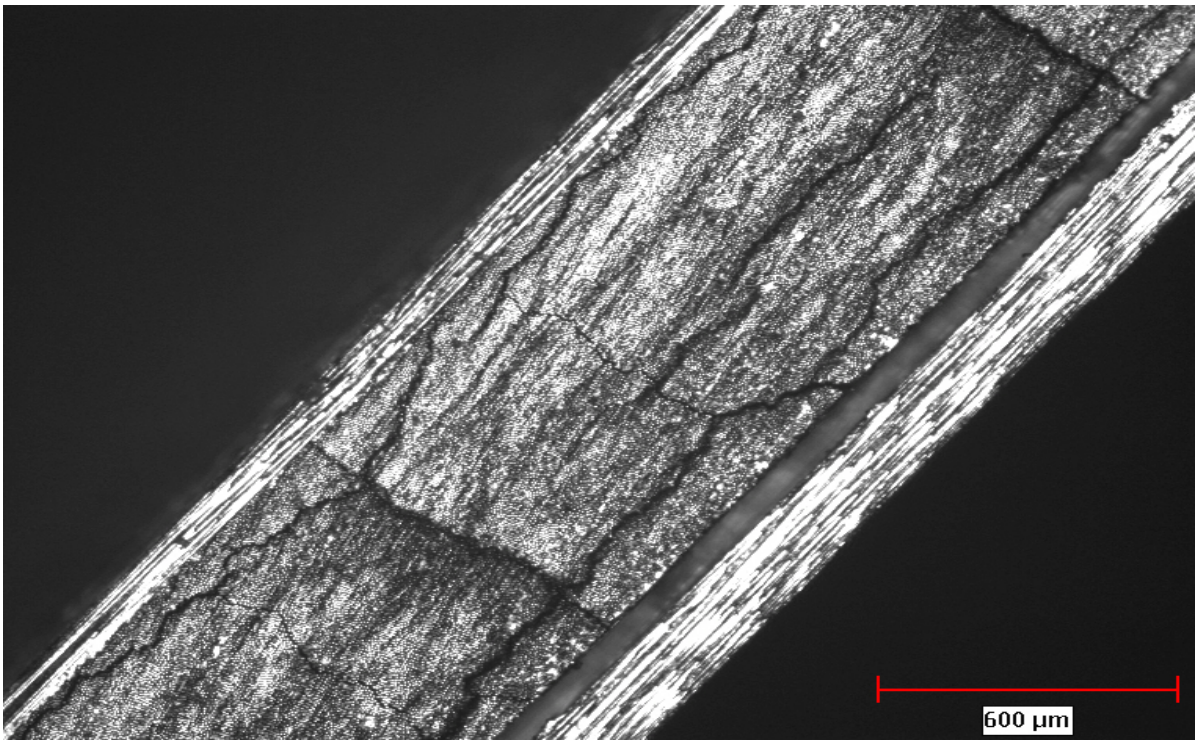

Figure 4.45: Various damage modes seen in $[0/90_2]_s$ sample tested at 70% UTS and 180^0C after 2 hours.

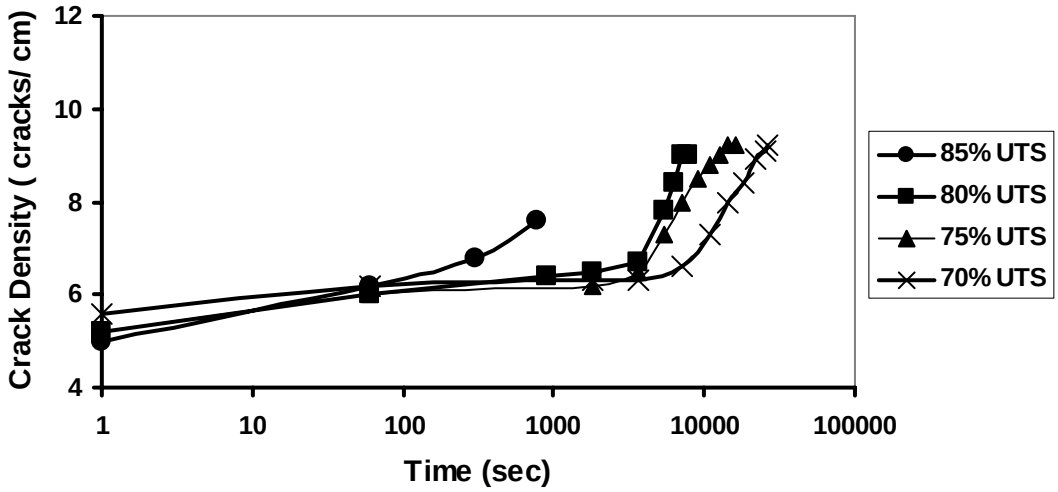

Figure 4.46: Time dependent evolution of transverse crack density in $[0/90_2]_s$ at 240^0 C

4.3.3 $[\pm 45/90_2]_s$ Laminate

Test specimens had no damage prior to testing at all temperatures and stresses. Samples were tested at 75,80, 85 and 90% UTS at each temperature (80, 180 and 240^0 C).

When the samples were loaded to the desired stress level at 80^0 C, few transverse cracks were introduced in the [90] ply. With time the initial transverse crack density increased as shown in Figure 4.47. At 75% UTS, it took nearly 100 hours for the sample to attain the CDS of 7 cm^{-1}. Vertical cracks in the [90] layer was observed after 24 hrs. Also observed at this time was the presence of transverse crack in the [-45] layer. With progress in time other modes of damage were observed; delamination between [+45] and [-45] layer after 48 hrs of testing and delamination between [-45] and [90] layer after 72 hrs. Transverse cracking in the [90] and [-45] layers, with vertical cracking in [90] ply is shown in Figure 4.48. At 80 and 85% UTS, the CDS was reached after 80 and 70 hrs respectively. Damage progression was very similar to that observed during testing at 75% UTS, but occurred at shorter time intervals.

At 180^0 C the transverse crack density increased with time as shown in Figure 4.49. The CDS at 75% UTS was reached after 102 hrs. At 80 and 85% UTS it took about 80 and 50 hrs respectively for the samples to attain the CDS. At 90% UTS the specimen broke after 19 hrs, before CDS could be reached. Various damage modes observed at 80^0 C were also seen at 180^0C. For specimen tested at 75% UTS, the vertical crack in the [90] ply as well as the transverse crack in the [-45] ply were observed after 30 hrs of testing. Delamination between [+45] and [-45] as well as between [-45] and [90] plies were observed after 80 hrs of testing. For specimens tested at 80 and 85% UTS the damage modes observed were similar to those observed at 75% UTS and the order of appearance

was also the same, except for the time interval which became shorter as the stress increased.

Crack density measurements were carried out on specimens tested at 240^0 C, a plot of the changing crack density with time is shown in Figure 4.50. At 75 and 80% UTS the specimens reached CDS values after 50 and 40 hrs respectively. At 85 and 90% UTS the specimen failed before attaining CDS values. Vertical damage at 75% UTS was observed after 12 hrs. Delamination between [+45] and [-45] as well as between [-45] and [90] plies were observed after 36 hrs of testing. Similar damage modes were observed at 80% UTS, but at shorter time intervals.

The CDS values observed during the creep rupture testing was similar to those obtained during tensile testing for all temperatures. It was around 7 cm^{-1} in both the cases, as shown in Table 4.5.

4.3.4 Interaction Among Various Damage Modes

In summary, various time dependent damage modes observed during creep rupture testing of all the laminates were transverse cracking, delamination, vertical cracking and fiber fracture.

The transverse crack density in [90] plies of all laminates continued to increase with time despite the formation of other damage modes. It approached CDS at lower stress levels and higher temperatures, for which transverse cracking was the dominant damage mode for the major portion of creep rupture testing. The width of the vertical crack marginally increased with time suggesting slow propagation of vertical cracks across the width of the specimen, i.e. perpendicular to thickness. However, the vertical

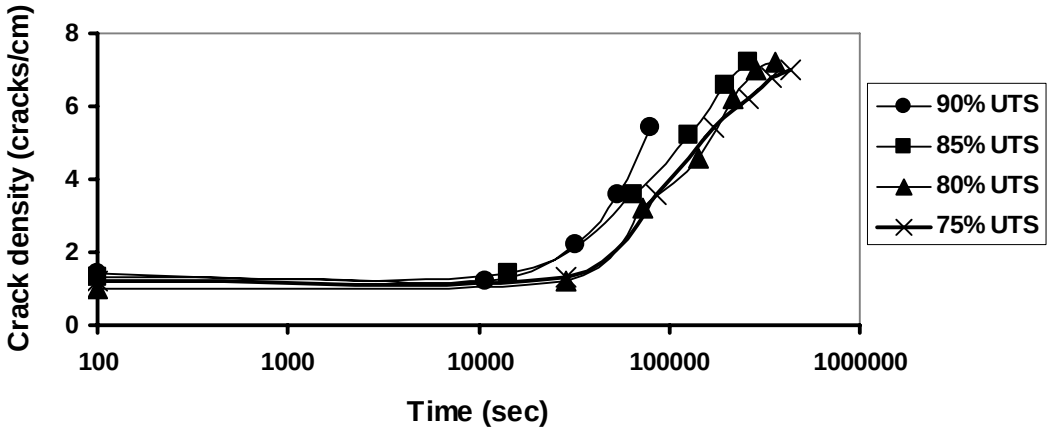

Figure 4.47: Time dependent evolution of transverse crack density in $[\pm 45/90_2]_s$ at 80^0 C

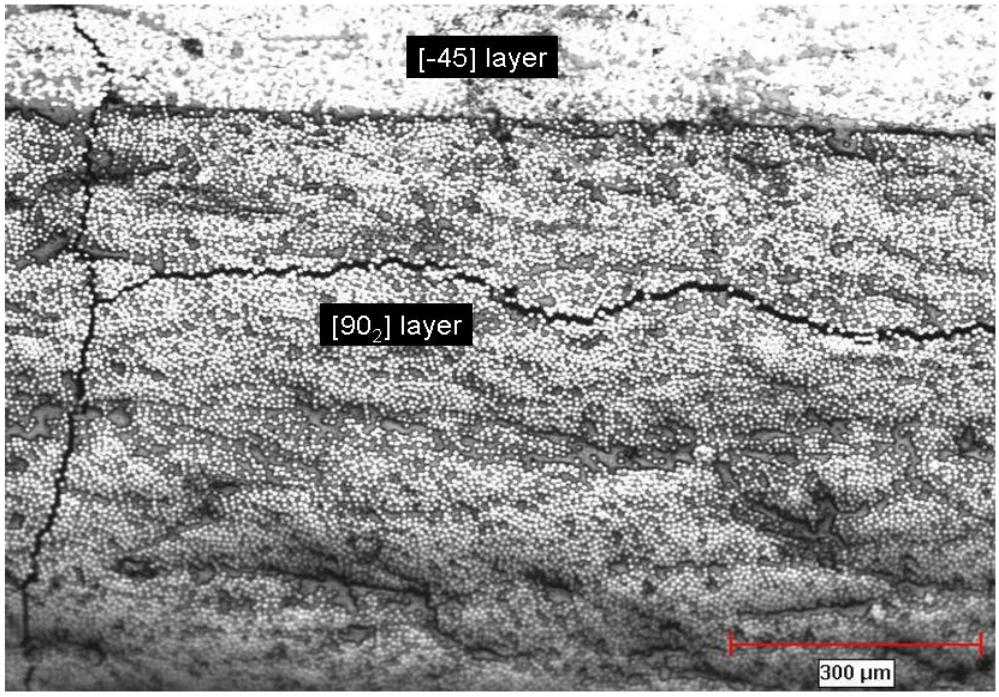

Figure 4.48: Various damage modes in $[\pm 45/90_2]_s$ at 80^0C and 75% UTS after testing for 48 hrs

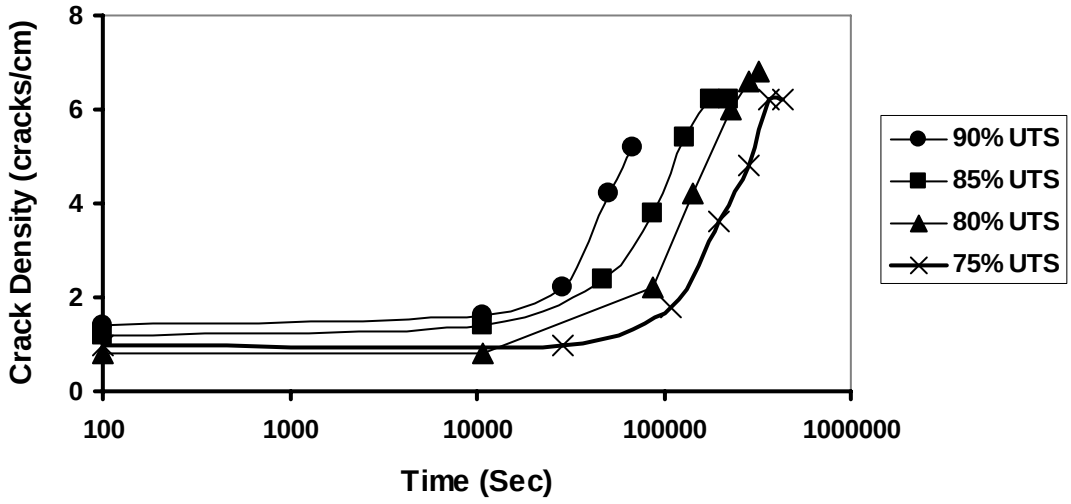

Figure 4.49: Time dependent evolution of transverse crack density in $[\pm 45/90_2]_s$ at 180^0 C

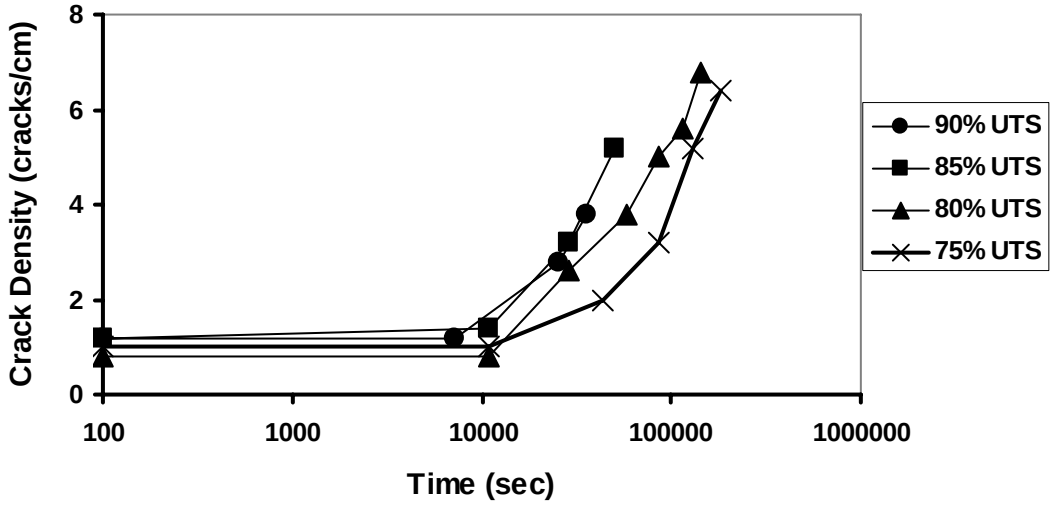

Figure 4.50: Time dependent evolution of transverse crack density in $[\pm 45/90_2]_s$ at 240^0 C

crack was not observed to transverse the entire width. The length of the vertical crack formed in [90] plies of [0/90/0] specimen spanned the entire gage length of the sample. However, the length of the vertical crack formed in $[\pm 45/90_2]_s$ sample gradually increased with time when they jumped from one transverse crack to another, connecting them.

Time dependent transverse cracking of [-45] plies in $[\pm 45/90_2]_s$ samples followed the transverse cracking in [90]. Delamination between [+45] and [-45] or [-45] and [90] plies was the next mode of damage to appear following the vertical and transverse cracking. The delamination area gradually increased with time allowing the portion of [90] plies that remained bonded to outer plies to continue to share the load. Delamination led to final creep rupture of $[\pm 45/90_2]_s$ samples. However, in [0/90/0] and $[0/90_2]_s$, delamination was followed by splitting of [0] plies and fiber fracture in [0] plies, which led to final creep rupture.

Above FPF stress, a single mode of damage was observed only in $[\pm 45/90_2]_s$ samples, upon loading, for about 40-45% of the creep rupture time at s stress level of 75% of UTS at 80^0C and 180^0C and this time period reduced to about 24% at 240^0C. The time period, during which all the damage modes were active was about final 33% of the creep rupture time at 80^0C and 180^0C and 70% of the creep rupture time at 240^0C. To illustrate the interaction among damage modes, the rate of increase in transverse crack density in [90] plies at an applied stress of 75% of UTS is plotted in Figure 4.51 for $[\pm 45/90_2]_s$ samples as a function of crack density normalized using crack density corresponding to CDS. The rate of increase in crack density at 80^0C decreased

monotonically with increase in crack density and time. This is to be expected since the load shared by the [90] plies would decrease with increase in crack density. However, with increase in temperature to 180^0C and 240^0C, the rate is approximately constant suggesting the influence of other damage modes that might change the stress state and the creep rate of, and the damage evolution rate in [90] plies. Similar trend was also observed in [0/90/0] as shown in Figure 4.52. It is obvious from the above results that creep rupture time is influenced significantly by the time dependent evolution of various damage modes and interaction among them impacting one another's rate of evolution.

Therefore, creep rupture in multi-directional laminates is complex with contributions from a number of damage modes. Prediction of time dependence of FPF stress due to a single damage mode is relatively easy and it could be used in design. However, a low value of FPF stress obtained by static tensile tests (typically used in design) and possibility of this to decrease with time suggests that time dependent progressive damage is a distinct possibility in all multidirectional laminates. This study clearly demonstrates that accelerated creep rupture testing to predict creep rupture time in service conditions is invalid due to this complex contribution from various damage modes. In such cases, ability to predict time-dependent evolution of damage, degradation in modulus and strength, and creep rupture time is critical. This study suggests that such predictions are likely to be good approximations only due to the anticipated complexity in modeling the interactions among various damage modes.

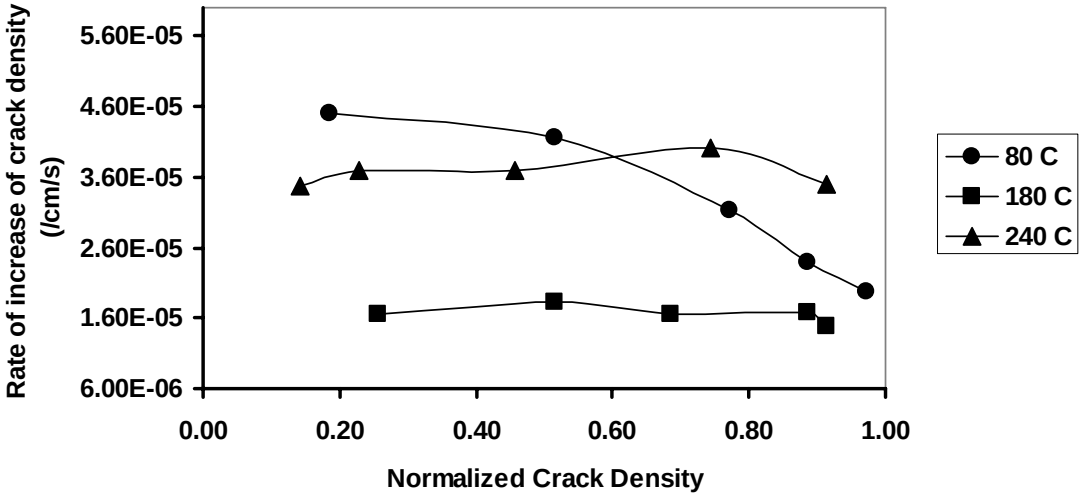

Figure 4.51: Rate of increase of transverse crack density in $[\pm 45/90_2]_s$ at 75% UTS

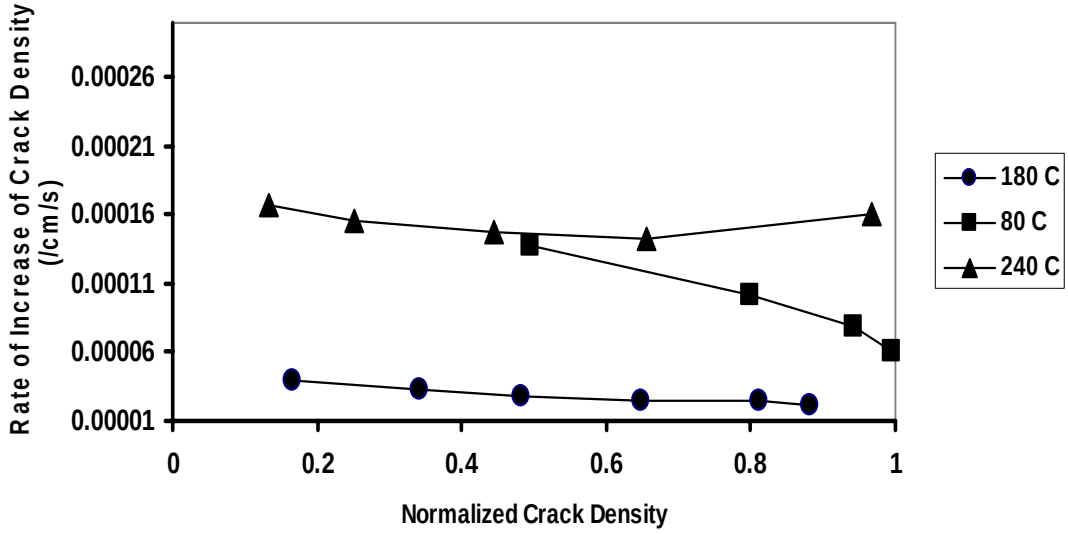

Figure 4.52: Rate of increase of transverse crack density in [0/90/0] at 85% UTS

5. CONCLUSIONS

Objectives of this thesis, listed in section 2.6, have been successfully realized through constant load creep rupture testing of three laminates over a wide range of temperature and stress. As discussed in 2.4.3, the time-dependent damage evolution is a reality in multi-directional composite laminates. More than one extrinsic damage modes develop with time under constant load owing to visco-elasticity of the polymer matrix and ply constraints.

Based on the results of these experiments, the following inferences and conclusions can be drawn on time dependent evolution of various damage modes in, and their impact on the creep rupture of, multidirectional composites.

- The various damage modes that can evolve with time in multi-directional polymer composites are transverse crack due to in-plane normal stress (σ_{22}), vertical cracks due to out-of-plane normal stress (σ_{33}), delamination due to interlaminar shear stress (σ_{23}), and fiber fracture.
- The FPF stress is time-dependent and decreases with time, i.e. time to FPF increases with decrease in applied stress. Therefore, time-dependent progressive damage is a distinct possibility in multidirectional composites even if the applied load is below the customarily used FPF stress determined using quasi-static constant load / deformation rate tests.

- The first mode of damage and the sequence of evolution of various damage modes with time depend on the laminate lay-up sequence.
- The rate of evolution of one damage mode varied significantly in the presence of other damage modes.
- Depending on the applied stress and temperature, one or more of these damage modes evolve simultaneously influencing one another's evolution rate and the creep rupture time. Hence, accelerated creep rupture testing, using stress and temperature levels higher than the service stress and temperature, to predict creep rupture time at the service conditions may be incorrect if the complex contributions from various damage modes are not properly accounted.
- Creep rupture predictions are likely to deviate from actual values due to the anticipated complexity in modeling the interactions among various damage modes.

Reference

1. Brinson, H.F., and Gates, T.S., "Viscoelasticity and aging of polymer matrix composites", Comprehensive Composite Materials Handbook, Elsevier Ltd. Burlington, USA, (2000), pp. 333-368

2. Iyer,V.C., Balachander, M.A. and Raghavan, J., " Long term durability of polymer composites" Proceeding of International conference SAMPE 2001, (2001), pp. 25-40

3. Yeow, Y.T., Morris, D.H. and Brinson, H.F., " Time temperature behavior of a unidirectional graphite/epoxy composite", ASTM special technical publications 674, ASME, (1979), pp. 263-281

4. Dillard, D.A., Morris, D.H., and Brinson, H.F., "Creep and Creep rupture of laminates graphite/epoxy composites", A report prepared for NASA, VPSU,Blacksburg, VA USA(1981).

5. Brinson, H.F., Morris, D.H. and Dillard, D.A., "Environmental effects and viscoelastic behavior of laminated graphite/epoxy composite", Proceedings of 2nd International conference on environmental degradation of engineering material, (1981), pp. 445 – 453

6. Gramoll, K.C., Dillard, D.A., and Brinson, H.F., "Thermo Viscoelastic characterization and prediction of Kevlar epoxy composite laminate", Composite Material Testing and Design, Vol. 9, (1990), pp. 477 – 493

7. Morris, D.H., Yeow, Y.T. and Brinson, H.F., "The viscoelastic behavior of the principle compliance matrix of a unidirectional graphite/epoxy composite" NASA contractor report, VPI-E-79-9, (1979)

8. Yeow, Y.T., " The time temperature behavior of graphite epoxy laminate", PhD dissertation, Virginia Polytechnic Institute and State University, VA, USA (1978)

9. Dillard, D.A, "Creep and creep rupture of laminated epoxy graphite composite" PhD dissertation, Virginia Polytechnic Institute and State University, VA, USA (1981)

10. Scott, D.W., Lai, T.S. and Zureick, A.H., "Creep behavior of fiber reinforced polymer composite", Journal of Reinforced Plastics and Composites, Vol.14, (1995), pp. 588 – 619

11. Brinson, L.C. and Gates, T.S., "Effect of physical aging on long term creep of polymer and polymer matrix composite", NASA Technical Memorandum, (1994), pp. 1-36

12. Raghavan, J. and Meshii, M., "Prediction of creep rupture of unidirectional carbon fiber reinforced polymer composites", Material Science and Engineering, A197, (1995), pp. 237 – 249

13. Griffith, W.I., "The accelerated characterization of viscoelastic composite materials", PhD dissertation, Virginia Polytechnic Institute and State University, VA, USA (1979)

14. Brinson, H.F. and Dillard, D.A., "The prediction of long term viscoelastic properties of fiber reinforced plastics", Proceedings of the 4th ICCM, (1982), pp.795 – 801

15. Yen, S.C. and Morris, D.H., "Accelerated characterization of a fiber composite using a strain energy failure criterion", Polymer Composites, Vol.10, (1989), pp.249 – 255

16. Fahmy, A.A. and Hurt. J.C., "Stress dependence of water diffusion in epoxy resin", Polymer Composites, Vol.1, (1980), pp. 77 – 80

17. Weistman, J., "Effect of fluids on polymeric composites – A review", Comprehensive Composite Materials Handbook, Elsevier Ltd., (2000), pp. 369-402

18. Woo, E.M., “Moisture temperature equivalency in creep analysis of a heterogeneous matrix carbon fiber/epoxy composites”, Composites, Vol. 25, (1994), pp. 425 430

19. Mohan, R. and Adams, D.F., “Non-linear creep recovery response of a polymer matrix and its composite”; Experimental mechanics; Vol.9, (1985) pp.262 -271

20. Raghavan, J. and Meshii, M., “Creep rupture of polymer composites”, Composite Science and Technology, Vol. 57, (1997), pp. 375 – 388

21. Charles, E.B., “The mechanism of elevated temperature property losses in high performance structural epoxy resin matrix materials after exposure to high humidity environment”, Polymer Engineering and Science, Vol.18, (1978), pp. 16-24

22. Balachander, M.A., “ On prediction of creep in multidirectional polymer composites”, M Sc Thesis, University of Manitoba, Canada, (2001)

23. McKenna, G.B., “On the physics required for prediction of long term performance of polymers and their composites”, Journal of Research of the National Institute of Standards and Technology, Vol. 99, (1994), pp. 169 – 189

24. Pasricha, A., Dillard, D.A., Tuttle, M., "Effect of physical aging and variable stress history on the strain response of polymer composites", Composite Science and Technology, Vol.57, (1997), pp. 1271 – 1279

25. Kennedy, T.C. and Wang Min, "Three-dimensional non-linear viscoelastic analysis of laminated composites", Journal of Composite Materials, Vol. 28, (1994), pp. 902 – 925

26. Gower, M.R.L and Sims, G.D., "Characterization of defects in composite material system", National Physical Laboratory report MATC 158, Project MMS 13, (2004), pp. 1 – 19

27. Keiji, O. and Hyoung –soo Kim, "Creep deformation of cross-ply laminate with constant transverse crack density", Materials Science Research International, Special Technical Publication, (2001), pp. 261 – 265

28. Keiji, O and Smith, P.A., "Modeling creep and recovery behavior of a quasi-isotropic laminate with transverse cracking", Advanced Composite Materials, Vol.11, (2002), pp.81 – 93

29. Akshantala, N.V. and Brinson, L.C., "Experimental study of viscoelastic effects and aging on elevated temperature damage and failure in polymer composites", Mechanics of Time Dependent Materials, Vol. 7, (2003), pp. 1-19

30. Raghavan, J. and Meshii, M., "Time dependent damage in carbon fiber reinforced polymer composites", Composites (A), Vol. 27 A, (1996), pp.1223 -1227

31. Manson, J.E. and Seferis, J.C., "Process simulated laminate, A methodology to internal stress characterization in advanced composite materials", Journal of Composite Materials, Vol.26, (1992), pp.403 – 431

32. Joh, D., Byun, K. and Hu. J., "Thermal residual stresses in thick graphite / epoxy composite laminate – uniaxial approach", Experimental Mechanics, Vol. 33, (1993), pp. 70 – 76

33. Hayer, M.W., "Calculation of room temperature shapes of unsymmetric laminates", Journal of Composite Materials, Vol. 5, (1981), pp. 296 – 310

34. Unger, W.J. and Hansen, J.S., "The effect of thermal processing on residual strain development in unidirectional composite", Journal of Composite Materials, Vol. 27, (1993), pp. 59 – 81

35. Herakovich, C.T. and Hayer, M.W., "Damage induced property changes in composites subjected to cyclic thermal loading", Engineering Fracture Mechanics, Vol. 25, (1985), pp. 779 -791

36. Keiji, O., “Influence of thermal history on transverse cracking in a carbon fiber reinforced epoxy composite”, Advanced Composite Materials, Vol. 11, (2003), pp. 265 – 275

37. Penn, L.S., Chou, R.C.T, Wang, A.S.D and Binienda, W.K., “The effect of matrix shrinkage on damage accumulation in composites”, Journal of Composite Materials, Vol. 23, (1989), pp. 570 – 586

38. Ogi. K. and Takao, Y., “Modeling a creep behavior of cross-ply laminates with progressive transverse cracking”, Advanced Composite Materials, Vol. 8, (1999), pp. 189 – 203

39. Ogi, K. and Shiraishi, T., “Viscoelastic shear lag analysis of a cross ply laminate with transverse cracking”, Proceedings of CREEP 7, Japan Society of Mechanical Engineers, (2001), pp. 277 – 280

40. Moore, R.H. and Dillard, D.A., “Time dependent matrix cracking in cross-ply laminates”, Composite Science and Technology, Vol. 39, (1990), pp. 1 – 12

41. Nairn, J.A., “Matrix Microcracking in Composites”, Comprehensive Composite Materials Handbook, Elsevier Ltd., (2000), pp. 403 – 432

42. Nairn, J.A, Hu, S. and Bark, J.S., " A critical evaluation of theories for predicting microcracking in composite laminate", Journal of Material Science, Vol. 28, (1993), pp. 5099 – 5111

43. Guedes, R.M., Jose, M., Marques, A. and Albert, C., "Prediction of long term behavior of composite materials", Computers and Structures, Vol. 76, (2000), pp. 183 – 194

44. Corum, J.M., Battiste, R.L., Liu, K.C., and Ruggles, M.B., "Basic properties of reference cross-ply carbon fiber composite" Oak-Ridge National Laboratory report, ORNL/TM – 2000/29, (2000), pp. 27 – 35

45. Corum, J.M., Battiste, R.L., Deng, S., Liu, K.C., Ruggles, M.B. and Weistsman, Y.J., "Durability based design properties of reference cross-ply carbon fiber composite", Oak-Ridge National Laboratory report, ORNL/TM – 2000/322, (2001), pp. 10-1 – 10-9

46. Guedes, R.M., "An energy criterion to predict delayed failure of multidirectional polymer matrix composite based on non-linear viscoelastic model", Composites (A), Vol. 35, (2004), pp. 559 – 571

47. Kobayashi, S, Ogihara, S. and Takeda, N., "Experimental characterization of the effect of stacking sequence on the transverse crack behavior in quasi-isotropic laminates", Advanced Composite Material, Vol. 9, (2000), pp. 241 – 251

48. Crossman,F.W., Warren, W.J., Wang, A.S.D. and Law, G.E., "Initiation and growth of transverse cracks and edge delamination in composite laminates – Experimental correlation", Journal of Composite Materials Supplement, Vol. 14, (1980), pp. 88 - 108

APPENDIX - A

Factors Influencing Creep and Creep Rupture of Composites

A comprehensive early work on the effect of temperature on creep of unidirectional and multidirectional composites can be found in the works of Brinson et al. [1] Yeow et al. [3], Gramoll et al. [6], Dillard et al. [4], and Brinson et al. [5]. It was observed that the compliance remains the same at various stress levels for a particular temperature in the linear creep region. An increase in temperature results in acceleration of the creep rupture time, demonstrated convincingly by various researchers [2, 4, 5, 9].

Similar to the temperature effect, increase in stress causes an increase in the creep compliance of the composite material. Researchers [1, 3, 4, 5, 6] have carried out numerous studies to show the effect of stress on creep of composite and found the compliance to increase with stress. The effect of stress on the creep rupture of composites results in acceleration of the creep rupture [2, 4, 5, 9, 12, 20]. These researchers have also shown that the combined effect of temperature and stress causes an increase in the creep compliance and also decrease in the creep rupture time.

Moisture absorption accelerates the time dependent response of the polymer composites. This is due to plasticization of the matrix. The presence of moisture in polymer lowers the glass transition temperature (T_g), causing a reduction in modulus [16, 17, 18, 19, 43]. The effect of moisture can be related by the time-moisture superposition principle. Accordingly, the moisture shift factor $a_H(m)$ can be used to represent the effect

of moisture. The combined effect of moisture and temperature modifies the shift factor to the form $a_{TH}(TM)$.

Creep rupture studies [2, 16, 21, 22] on moisture conditioned coupons have recorded a decrease in the rupture time when compared to the coupons in dry condition. Iyer et al. [2] and Balachander [22] observed a decrease in creep rupture time for moisture conditioned samples when compared to the creep rupture time of specimens subjected to different conditions (post cured, physical aging and physical aging with moisture) at 80^0 C and any given stress level. They also reported that the influence of moisture on creep rupture time increases with increase in time. Fahmy and Hurt [16] observed a more pronounced influence of moisture on creep when the composite was under stress.

The process of physical aging in a polymer occurs when it is cooled rapidly to a temperature below its T_g (glass to rubber transition temperature). The material evolves towards thermodynamic equilibrium as shown in Figure A1. This evolution causes a change in the enthalpy and entropy of the system, producing a significant change in the mechanical properties [23]. Physical aging process is thermoreversible by heating the material above its T_g and subsequently quenching the material.

Researchers have carried out extensive studies on the creep of physically aged polymer composites [10, 11, 23, 24]. It has been found that polymer composites are affected by aging in a manner similar to homogenous polymers and techniques used to

deal with aging of polymers can be applied on composites as well. They found that the magnitude and rate of creep decreased with increase in physical aging time. The creep characterization of the aging composite is usually done at short intervals. Typically creep test duration is less than one-tenth that of the aging time before the start of the test to avoid significant aging during creep test. The creep curves of aging experiments are superposable, pointing to the fact that effect of aging is to retard the creep and shift the creep curves to longer times. Thus a single parameter can be used to characterize the susceptibility of a composite to age.

The shift factor for aging is given by

$$a_{tc} = \left(\frac{t_{ref}}{t_e}\right)^{\mu}$$

where

t_{ref} is the reference aging temperature

t_e is the aging time

μ is the shift rate

Published literature [11, 23, 24] shows that physical aging has no effect on S_{11} (Compliance along principal fiber direction) or S_{12} (Compliance along transverse coupling direction) while S_{22} (transverse direction compliance) and S_{66} (in-plane shear compliance) are affected by aging. However the aging shift factors for transverse creep and shear creep are different.

Chandra [2] observed a reduction is rupture time for the transverse direction due to the progressive embrittlement of the polymer matrix with physical aging.

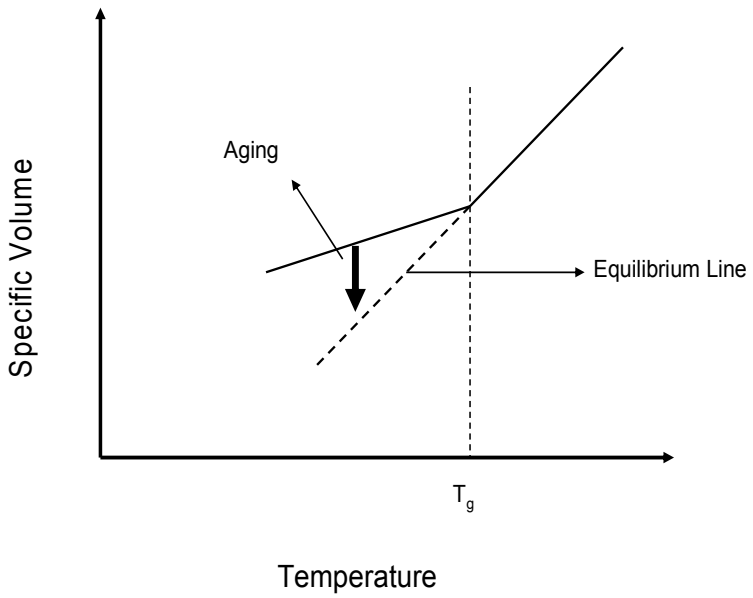

Fig. A1: Schematic of physical aging

Bala [22] also saw a similar trend of decrease in rupture time for a physically aged sample when compared to the post cured sample at a given stress level. Dillard's work [9] on the creep rupture of physically aged samples was contradictory to the findings of Bala and Chandra. Dillard [9] observed an increase in creep rupture time with increase in aging time. He also reported an increase in the strength of the composite. Based on the strength increase, the possible reason for the increase in creep rupture time may be due to the post curing of laminates.

2.2.4 Accelerated Characterization of Creep Behavior

Accelerated procedures have been used to characterize the viscoelastic behavior in a composite system. Two widely accepted methods are Time Temperature Superposition Principle (TTSP) and Time Temperature Stress Superposition Principle (TTSSP).

TTSP assumes that the creep curves at various temperatures during static loading of PMC have similar shape but are shifted with respect to time. A schematic illustration is shown in Figure A2. The master curve generated by TTSP represents the compliance of the material at a particular temperature over a long period of time.

The temperature shift factor (a_T) above the glass transition temperature (T_g) can be obtained using the WLF (Williams, Landel, Ferry) equation:

$$\log a_T = \frac{-c_1^0 (T - T_0)}{c_2^0 + (T - T_0)}$$

Below T_g the temperature shift factor can be obtained using the Arrhenius equation:

$$a_T = \exp \frac{\Delta H}{R}[\frac{1}{T} - \frac{1}{T_0}]$$

Where,

T is the temperature of interest,

T_0 is the reference temperature at which the creep curve is available,

c_1 & c_2 are constants,

ΔH is the activation energy

R is the gas constant.

Once the temperature shift factor is determined, creep compliance at any temperature can be calculated using:

$$S_T(t) = S_{T0}(a_T t)$$

Yeow [8] has demonstrated that TTSP is valid in the linear viscoelastic region for polymer composites. Existing literature points to the fact that TTSP is not valid for non-linear viscoelastic region [2, 9-12]. The reason put forth for the invalidity of TTSP was the change in shape of the creep curve with stress levels.

TTSSP factors into account effect of stress as well as temperature. This is a useful method to clearly understand the effect of stress on the creep compliance of a laminate. TTSSP came into existence through a combination of TTSP and TSSP (Time Stress Superposition Principle). TSSP assumes that increase in stress accelerates creep, much like temperature. Griffith [13] combined the latter two approaches to come up with

TTSSP. Figure A3 schematically illustrates the TTSSP technique. Figure 2.6a shows creep curves at several temperatures and stress levels. By employing TTSP, the creep curves were shifted to obtain a master curve for the σ_1 stress level. Figure A3b represents the master curves generated for T_1 reference temperature at all the stress levels. Due to the above mentioned two steps, the temperature shift factor a_T for varying stress levels are obtained. Using the Time Stress Superposition Principle (TSSP) the creep curves at various stress levels are shifted to obtain the master curve for temperature T_1. Following the same procedure master curves were obtained for temperature T_1 through T_4 the stress shift factor a_σ and its corresponding temperature dependence, illustrated in figure A3c & A3d. The master curves obtained in A3b and A3d were shifted to get the unified master curve. This master curve was valid through all the temperatures and stress levels within the data range.

Yen and Morris [15] carried out creep tests at four different stress levels and temperatures for duration of 200 minutes. The results from these tests were used to form a master curve at reference temperature of 23^0 C. These results were used in conjunction with Findley's power law model and compared with the results of a 1000 minute creep experiment. The excellent agreement of the model with the experimental result led to the conclusion that TTSSP in conjunction with theoretical model can produce reliable results for the prediction of long term performance of FRP composites.

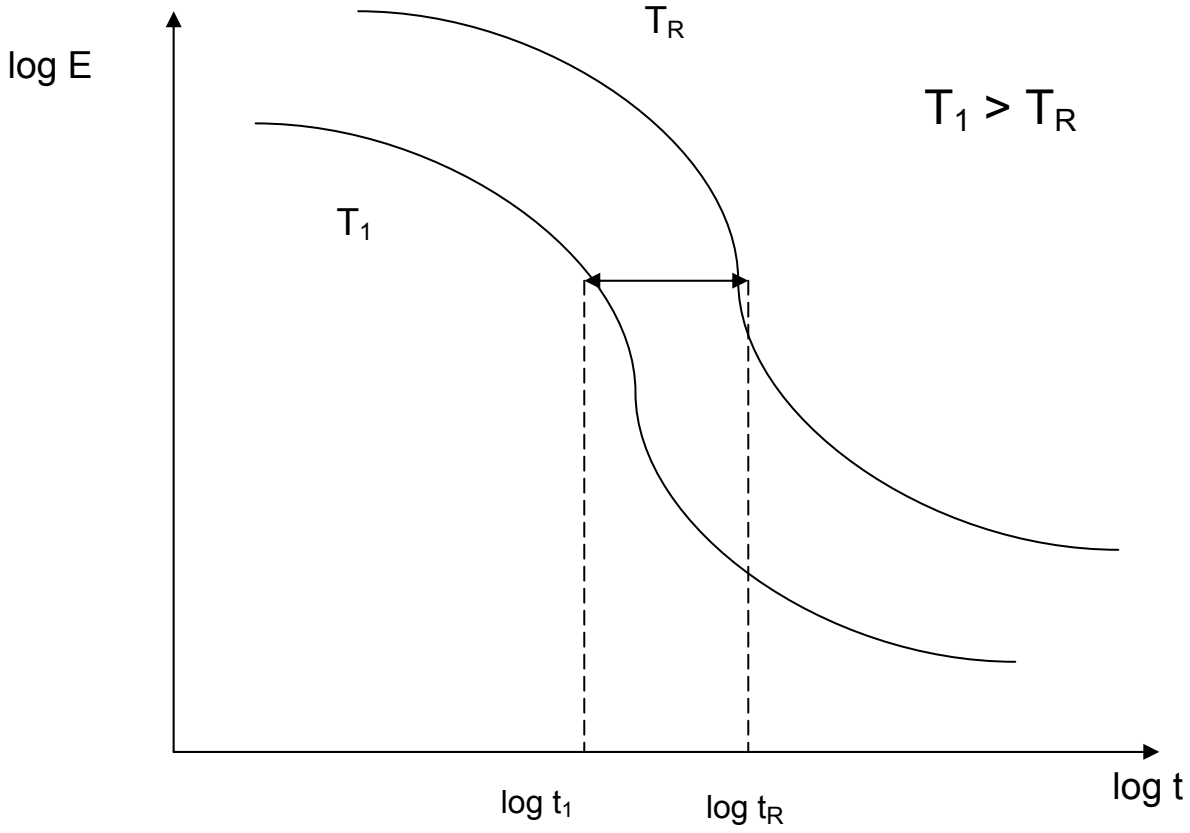

Fig. A2: Schematic Illustration of Time Temperature Superposition Principle

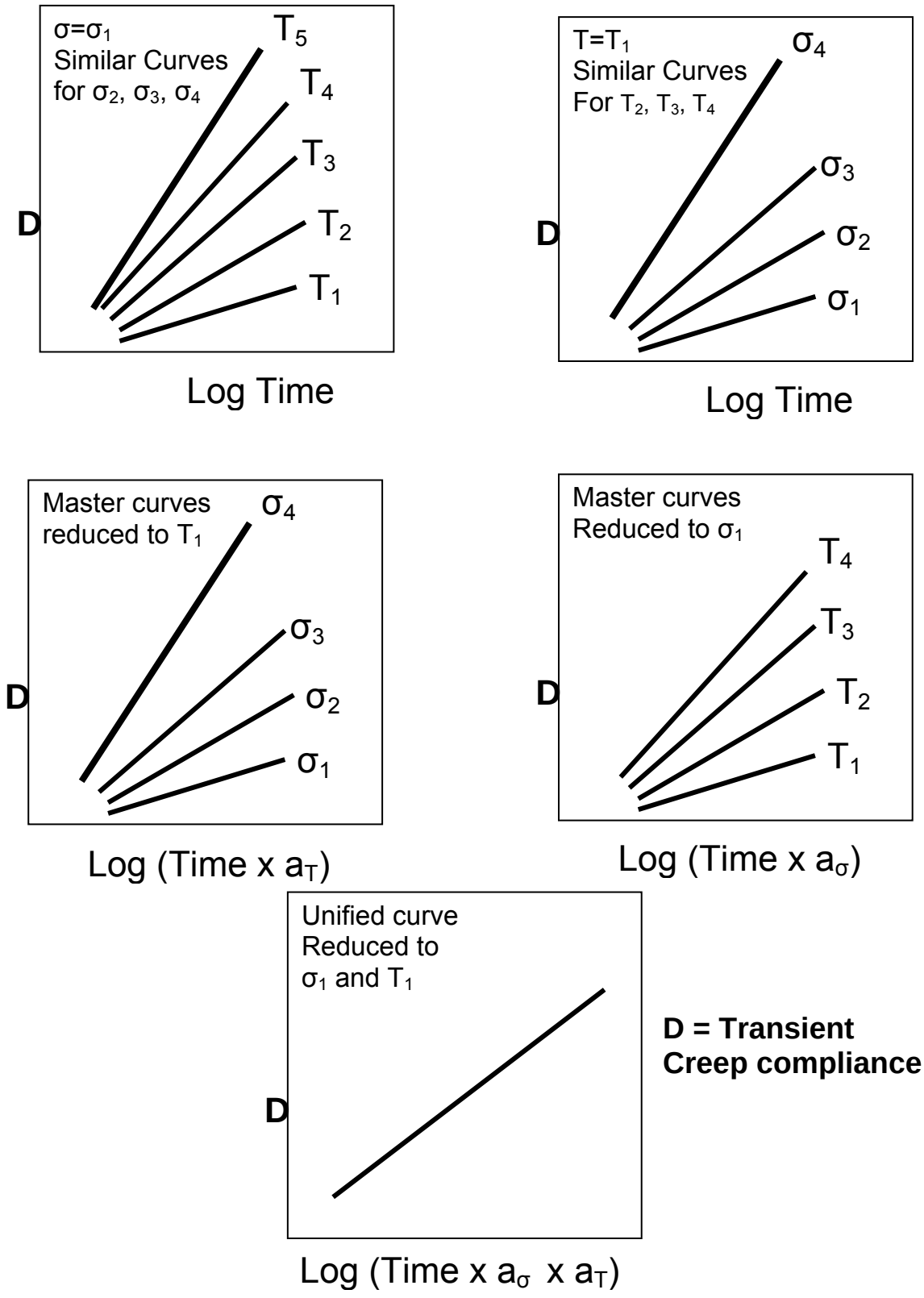

FigureA3: Schematic Illustration of TTSP Technique

APPENDIX – B

The existing literature indicates that the magnitude of the residual stress in a composite is not sufficient enough to induce damage to the laminate during processing. But thermal residual stresses are capable of causing damage when the laminate is subsequently loaded either thermally or mechanically. Herakovich and Hyer [35] studied damage in the form of transverse cracks resulting from thermal loading. Graphite epoxy specimens were subjected to cyclic thermal loading in the temperature range of -250^0 F (-157^0 C) to 250^0 F (121^0 C). Tests were conducted on $[0/90_3]_s$ and $[0_2/90_2]_s$ laminates. They concluded that the transverse crack density increased with thermal cycling, in most cases approaching a limiting value. These cracks also significantly reduce the coefficient of thermal expansion (CTE) of the laminate. At lower temperatures (-250^0 F) fiber splitting was observed. Ogi [36] showed through his experiments on $[0/90_3]_s$ laminate that thermal residual stress decreases the onset stress of transverse cracking. He concluded that with increase in temperature from 150^0 C to 200^0 C and duration of thermal history from 4 hrs to 100 hrs an increase in residual stress due to shrinkage occurs.

The effect of residual stress on damage accumulation was studied by Penn et al. [37]. By addition of chemical additives they reduced the residual stress of the laminate with the intention of delaying the transverse cracking. However, they found that the onset of cracks and the saturation crack density were same for the treated and untreated specimens. They concluded that the chemical additive despite the beneficial effect in terms of the reduction in residual stress increased the fracture sensitivity, leading to the lack of difference in damage accumulation between the two specimens.

Thermal residual stresses are inherently difficult to measure and characterize. Ply sectioning technique [31, 32] is one of the methods used to measure the residual stress. In this process, the laminate is sectioned by machining or embedding a separating film inside the laminate. Upon removal of the ply, the unbalanced stresses created out-of-plane deformation. Residual stresses were then calculated using the lamination theory and curvature of the laminate.

Another method used is the measurement of warpage of an unsymmetrical composite laminate. Hayer [33] manufactured an unsymmetrical laminate and on cooling warpage was observed. He used the classical lamination theory to relate the curvature to the moment resultant on the laminates and from the stress-strain relationship, the residual stresses were calculated. Strain gages are also used for obtaining the residual stress. Unger and Hansen [34] implanted strain gages into the laminate and allowed them to go through the manufacturing procedure while monitoring the strain change.